UNIVERSITY OF CALIFORNIA, SAN DIEGO

HCCI Engine Control and Optimization

A dissertation submitted in partial satisfaction of the
requirements for the degree
Doctor of Philosophy

in

Engineering Sciences (Mechanical Engineering)

by

Nicholas J. Killingsworth

Committee in charge:

Miroslav Krstić, Chair
Salvador Aceves
Steven Buckley
William Helton
Tara Javida
Forman Williams

2007

The dissertation of Nicholas J. Killingsworth is approved, and it is acceptable in quality and form for publication on microfilm:

_____

_____

_____

_____

_____

_____
Chair

University of California, San Diego

2007

TABLE OF CONTENTS

ABBREVIATIONS

AFR	Air to Fuel Ratio
AM	Amplitude Modulation
ATDC	After Top Dead Center
BTDC	Before Top Dead Center
CA1	Crank angle where 1% of the energy has been released
CA10	Crank angle where 10% of the energy has been released
CA50	Crank angle where 50% of the energy has been released
CA90	Crank angle where 90% of the energy has been released
CAD	Crank Angle Degrees
CK	Chemical Kinetics
CI	Compression Ignition
CO	Carbon Monoxide
CO_2	Carbon Dioxide
DEM	Discrete Event Model
EGR	Exhaust Gas Recirculation
ES	Extremum Seeking
EVC	Exhaust Valve Closing
EVO	Exhaust Valve Opening
FTM	Fast Thermal Management
HCCI	Homogeneous Charge Compression Ignition
IAE	Integrated Absolute Error
IFT	Iterative Feedback Tuning
IMC	Internal Model Control
ISE	Integrated Square Error
ITAE	Integrated Time Absolute Error
ITSE	Integrated Time Square Error
IVC	Inlet Valve Closing
IVO	Inlet Valve Opening
IMEP	Indicated Mean Effective Pressure
LPG	Liquid Petroleum gas
LQG	Linear Quadratic Gaussian
MPC	Model Predictive Control
MVM	Mean Value Model
NO_x	Nitrogen oxides
PI	Proportional Integral controller
PID	Proportional Integral Derivative controller
PWM	Pulse Width Modulation
RPM	Revolutions Per Minute
SI	Spark Ignition
SOC	Start Of Combustion

TDC	Top Dead Center
UHC	Unburned Hydrocarbons
VCR	Variable Compression Ratio
VVA	Variable Valve Actuation
VVT	Variable Valve Timing
ZN	Ziegler-Nichols

LIST OF SYMBOLS

$\Delta\theta$	Burn duration
α	Perturbation amplitude
β	Ratio of mass flow from hot and cold manifolds
γ	Specific heat ratio, adaptation gain in ES algorithm
η_c	Combustion Efficiency
θ	Crank angle, input parameters in ES algorithm
ρ	Density
ϕ	Fuel/air equivalence ratio
ω	Modulation frequency
A	Area
a	Crank radius, constant that determines modulation frequency
B	Engine bore
b_1, b_2, b_3, b_4	Constants
c_p	Specific heat at constant pressure
c_v	Specific heat at constant volume
e	Error
i	Inert gas fraction
J	Cost function
k	Proportional gain
L	Engine stroke
l	Connecting rod length
m	Mass
n	Constant exponent used in ignition correlation
n_c	Polytropic exponent during compression
n_e	Polytropic exponent during compression
p	Pressure
R	Universal gas constant
Q	Heat
Q_{LHV}	Lower heating value of a fuel
h	High pass filter constant
h_c	Convective heat transfer coefficient
T	Temperature
T_d	Derivative time
T_i	Integral time
T_w	Cylinder wall temperature
t	Time
U	Extensive internal energy
u	Specific internal energy, control signal
V	Volume
V_c	Clearance volume

Vd	Displacement volume
w	Average cylinder gas velocity
W	Mechanical work

LIST OF FIGURES

LIST OF TABLES

ACKNOWLEDGEMENTS

This dissertation is the product of the work and support of many people and I am extremely grateful to all who have had an influence throughout the years. First, I would like to express my gratitude to my advisor Professor Miroslav Krstić for his wonderful guidance and trusting me to go in a research direction of great personal interest.

Without my mentor Dr. Salvador Aceves at Lawrence Livermore National Laboratory (LLNL) this would not have been possible, he provided invaluable technical guidance as well as numerous other incites into the research world. Dr. Dan Flowers also played an integral role in this dissertation, and I am grateful to him for providing supervision and essential technical guidance.

I am very thankful to the members of my committee for reading this manuscript and their valuable comments, especially Professor Steven Buckley.

I would like to thank my former and current fellow graduate students Dr. Lawrence Yuan, Dr. Eugenio Schuster, Dr. Rafael Vazquez, Marco Luethi, Antranik Siranosian, Jennie Cochran, and Nima Ghods for provided a very fun and positive research environment and for the many helpful discussions.

Furthermore, I would like to thank my colleagues at LLNL Tim Ross and Francisco Espinosa-Loza for all the extra time they put in running experiments and for their feedback, which helped guide this dissertation. I would also like to thank Dr. Joel Martinez-Frias, Dr. Jonas Edman, and Dr. Roy Ognik for many fruitful discussions and creating such a friendly atmosphere. I would also like to thank Professor Robert Dibble at UC Berkeley and his past students Dr. Jason Souder, Dr. Parag Mehresh, and Dr. Hunter Mack for very useful advice and providing much of the research in which this dissertation is based on.

I am grateful to Professor Ralph Aldrege at UC Davis for encouraging me to pursue a master degree and eventually a Ph.D and teaching me much about research and combustion. Furthermore, I would like to thank Professor Zuhair

Munir, Dr. Vahid Vaezi and Dr. Olivia Graeve for teaching me about research and sparking my initial interest in it.

I am very grateful for the financial support of the NSF Alliances for Graduate Education and the Professoriate (AGEP) and the National Consortium for Graduate Degrees for Minorities in Engineering and Science, Inc. (GEM) for providing funding for my first two years at UCSD. The Student Employee Graduate Research Fellowship (SEGRF) program has been great allowing me to carry out the last two and half years of my research at LLNL with access to a world class team of researchers working on HCCI and experimental facilities.

Finally, my most profound thanks go to my parents Fitz and Denise for always having faith in me and for always being there to support me. I would also like to thank my sister Adri for her unending support and friendship.

This dissertation includes reprints or adaptations of the following papers:

N. J. Killingsworth and M. Krstić, "Auto-tuning of PID controllers via extremum seeking," *In Proceedings of the American Control Conference*, Portland, OR, June 2005. (Chapter 6)

D. L. Flowers, J. Martinez-Frias, F. Espinosa-Loza, N. J. Killingsworth, S. M. Aceves, R. Dibble, M. Krstic, and A Bining, "Development and testing of a 6-Cylinder HCCI engine for distributed generation," *In Proceedings of ASME ICEF – 2005*,Ottawa, Canada, pp. 465–473, 2005.(Chapter 2)

N. J. Killingsworth and M. Krstić, "PID tuning using extremum seeking: online, model-free performance optimization," *IEEE Control Systems Magazine*, vol. 26, no. 1, pp. 70–79, 2006.(Chapters 4, 6)

N. J. Killingsworth, S. M. Aceves, D. L. Flowers, and M. Krstić, "A simple HCCI engine model for control," *In Proceedings of the IEEE International Conference on Control Applications*, Munich, Germany, October 2006.(Chapter 3)

N. J. Killingsworth, S. M. Aceves, D. L. Flowers, M. Janković, and M. Krstić, "A model of gasoline HCCI engine combustion for control," *In Proceedings of the 5th US Combustion Meeting*, San Diego, CA, 2007.(Chapter 3)

N. J. Killingsworth, S. M. Aceves, D. L. Flowers, and M. Krstić, "Extremum seeking tuning of an experimental HCCI engine combustion timing controller," *In Proceedings of the American Control Conference*, New York, NY, June 2007.(Chapter 7)

N. J. Killingsworth, S. M. Aceves, D. L. Flowers, F. Espinosa-Loza, and M. Krstić, "HCCI engine combustion timing control: optimizing gains and fuel consumption via extremum seeking," submitted to *IEEE Transactions on Control Systems Technology*, 2007.(Chapters 5, 7)

VITA

2000	B. S., in Mechanical and Materials Science Engineering, University of California, Davis
2002	M. S., in Mechanical and Aeronautical Engineering, University of California, Davis
2007	Ph. D., in Engineering Sciences (Mechanical Engineering), University of California San Diego

PUBLICATIONS

N. J. Killingsworth and M. Krstić, "Auto-tuning of PID controllers via extremum seeking," *In Proceedings of the American Control Conference*, Portland, OR, June 2005.

D. L. Flowers, J. Martinez-Frias, F. Espinosa-Loza, N. J. Killingsworth, S. M. Aceves, R. Dibble, M. Krstic, and A Bining, "Development and testing of a 6-Cylinder HCCI engine for distributed generation," *In Proceedings of ASME ICEF – 2005*,Ottawa, Canada, pp. 465–473, 2005.

N. J. Killingsworth and M. Krstić, "PID tuning using extremum seeking: online, model-free performance optimization," *IEEE Control Systems Magazine*, vol. 26, no. 1, pp. 70–79, 2006.

N. J. Killingsworth, S. M. Aceves, D. L. Flowers, and M. Krstić, "A simple HCCI engine model for control," *In Proceedings of the IEEE International Conference on Control Applications*, Munich, Germany, October 2006.

N. J. Killingsworth, S. M. Aceves, D. L. Flowers, M. Janković, and M. Krstić, "A model of gasoline HCCI engine combustion for control," *In Proceedings of the 5th US Combustion Meeting*, San Diego, CA, 2007.

N. J. Killingsworth, S. M. Aceves, D. L. Flowers, and M. Krstić, "Extremum seeking tuning of an experimental HCCI engine combustion timing controller," *In Proceedings of the American Control Conference*, New York, NY, June 2007.

N. J. Killingsworth, S. M. Aceves, D. L. Flowers, F. Espinosa-Loza, and M. Krstić, "HCCI engine combustion timing control: optimizing gains and fuel consumption via extremum seeking," submitted to *IEEE Transactions on Control Systems Technology*, 2007.

ABSTRACT OF THE DISSERTATION

HCCI Engine Control and Optimization

by

Nicholas J. Killingsworth

Doctor of Philosophy in Engineering Sciences (Mechanical Engineering)

University of California San Diego, 2007

Miroslav Krstić, Chair

Homogeneous charge compression ignition (HCCI) engines have the benefit of high efficiency with low emissions of NO_x and particulates. These benefits are due to the autoignition process of the dilute mixture of fuel and air during compression. However, because there is no direct ignition trigger, control of ignition is inherently more difficult than in standard internal combustion engines. This difficulty necessitates that a feedback controller be used to keep the engine at a desired (efficient) setpoint in the face of disturbances. Because of the nonlinear autoignition process, the sensitivity of ignition changes with the operating point. Thus, gain scheduling is required to cover the entire operating range of the engine. Controller tuning can therefore be a time intensive process. With the goal of reducing the time to tune the controller, we use extremum seeking (ES) to tune the parameters of various forms of combustion timing controllers. Additionally, in this dissertation we demonstrate how ES can be used for the determination of an optimal combustion timing setpoint of an experimental HCCI engine. The use of ES has the benefit of achieving both optimal setpoint (for maximizing the engine efficiency) and controller parameter tuning tasks quickly.

The lack of a direct combustion trigger makes control of combustion timing during transients especially challenging. To aid in HCCI engine control during

transients, we have developed a model that can be used to derive a controller for a thermally-managed, gasoline and natural gas fueled HCCI engine. The model uses an ignition threshold derived from detailed chemical kinetic simulations of HCCI engine combustion to provide an estimate for the combustion timing. The ignition threshold is a function of both temperature and pressure. An estimate of the residual gas fraction from the previous cycle can also be obtained, which is essential information due to the strong temperature sensitivity of HCCI ignition. This model allows the synthesis of nonlinear control laws, which can be utilized for control of an HCCI engine during transients.

Chapter 1

Introduction

This dissertation focuses on solving specific barriers for an advanced engine combustion technology. Advanced energy technologies are necessary for combating future environmental challenges. The heavy use of fossil fuels has lead to a number of serious consequences that we must all face. Chief among these effects is global warming, which has already had environmental and economic impacts. Global warming is largely attributed to an increase in greenhouse gases. These gases absorb radiation from the earth, trapping heat within the earth's atmosphere and contributing to an increase in the earth's average temperature. Unfortunately, one of the major by-products of complete combustion is carbon dioxide CO_2, a greenhouse gas. The only way to reduce the amount of net CO_2 that a combustion process produces is to reduce the amount of fossil fuel it consumes or replace the fossil fuel with a low carbon (or carbon neutral) equivalent. Additionally, because the US imports the majority of its fossil fuels we are dependent on the countries that produce fuels. As a result, a decrease in the use of fossil fuels also carries important political implications. Fortuitously, the solution to both of these issues is the same: reduce the amount of fuel consumed through improved efficiency or through use of alternative low carbon fuels.

The transportation sector accounted for 33% of the CO_2 emissions in 2005 and is the largest of the residential, commercial, and industrial sectors in the US [4]. Accordingly, an increase in vehicle efficiency has a profound effect on the total CO_2 emissions in the US. While incremental progress still occurs improving

both spark ignition (SI) and diesel compression ignition (CI) engines, both are fairly mature technologies so the room for improvement is limited. Fortunately, an alternative internal combustion engine technology exists that has the potential to substantially improve efficiency and reduce vehicle emissions, the homogeneous charge compression ignition engine (HCCI).

This dissertation will address the solution of some of the key technical barriers currently keeping HCCI engines from series production.

1.1 Background

Before describing HCCI engines, the operation of spark ignition (SI) and compression ignition (CI) engines is discussed to establish a baseline and context for HCCI. Figure 1.1 shows a four-stroke cycle for any type of engine (SI, CI, HCCI). For an SI engine a homogeneous mixture of fuel and air is drawn into the cylinder during the intake stroke. This fuel-air mixture is compressed during the compression stroke. A spark is then introduced, triggering the gas to ignite and causing a premixed flame to propagate outward, consuming the fuel-air mixture. The intake gases expand during this combustion process and push the cylinder down resulting in the power stroke. The piston then travels up, pushing the exhaust gas out of the cylinder through the exhaust valve.

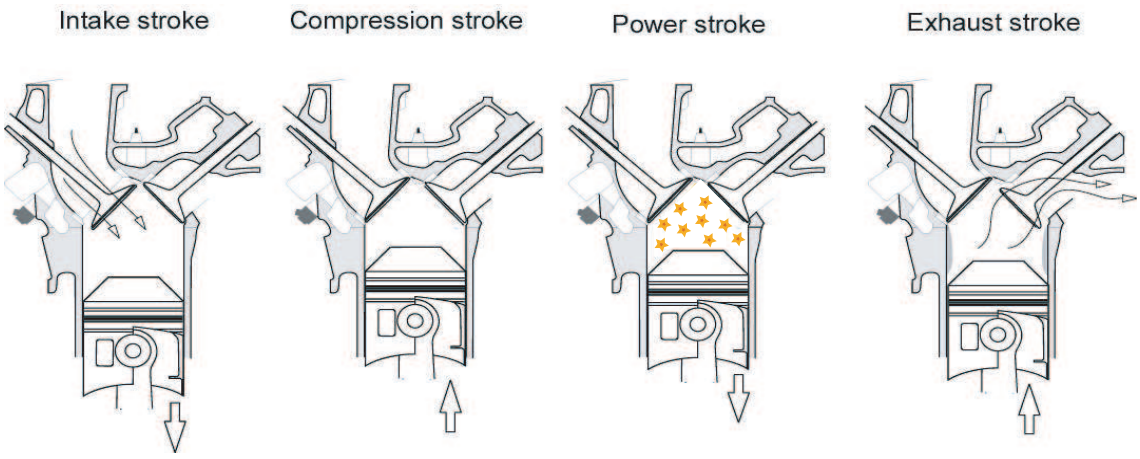

Figure 1.1: Four stroke engine cycle. With permission, from Ford Motor Company.

A CI engine differs in that the intake "charge" (the gas inducted into the engine during the intake stroke) consists of only air. The air inducted is then compressed, and combustion is triggered by injection of fuel into the cylinder. Because the air is at such high pressure and temperature due to compression, the air and injected fuel simultaneously mix and react resulting in a non-premixed flame around the injected fuel jet. The high efficiency of CI engines results from a high compression ratio. In contrast, SI engines cannot be run at such high compression ratios, because they will undergo a process called knock, in which the premixed fuel and air auto-ignites ahead of the propagating flame. During knock, part of the mixture reacts at once, releasing a great deal of energy in a short amount of time and resulting in very high pressures that can potentially damage the engine. With regard to emissions, CI engines produce significant particulate emissions, a great deal more than SI engines due to the non-premixed flame. Additionally, the flame temperature in both of these engines is very close to the adiabatic flame temperature and results in high production of nitrogen oxides (NO_x). Aftertreatment effectively reduces NO_x in SI engines, but is yet to be commercially viable and widespread in CI engines

The HCCI engine contains attributes of both the SI and CI engine. HCCI engines use an intake charge that is a homogeneous mixture of fuel and air as in a SI engine, but the mixture is compression ignited, as in a CI engine. In contrast to both SI and CI engines, an HCCI engine does not contain a direct trigger to start the combustion process like the other two engines, but depends on the thermochemical path of the mixture being compressed. Thus, ignition depends on the temperature and pressure history of the gas mixture.

The HCCI autoignition process is very much like knocking in SI engines, except that HCCI occurs homogeneously throughout the cylinder, not ahead of a flame front [92]. The high compression ratios needed to auto-ignite the mixture can yield efficiencies similar to that of CI engines, provided that the indirectly controlled ignition starts at the right time. Moreover, HCCI engines can be run very lean, meaning that the intake charge contains significantly more air than is needed for complete combustion. This excess air dilution lowers the flame temper-

ature, resulting in low NO_x production. So, in effect HCCI engines have desirable properties of SI and CI engines, but add the difficult task of controlling the start of combustion. Table 1.1 summarizes the attributes and issues with SI, CI, and HCCI engines.

Table 1.1: Internal Combustion Engine Comparison

Engine	Efficiency	Emissions	Combustion Timing
SI	knock limited	low	spark discharge
CI	high	high NO_x and particulates	fuel injection
HCCI	high	high CO and UHC	indirect: temperature pressure history

1.1.1 Autoignition

Autoignition is the rapid reaction of fuel and oxidizer without the aid of an external ignition source, such as a flame or a spark, often referred to as an "explosion". There are two mechanisms that can explain explosions: chain branching and thermal. Complex chemical kinetics play the dominant role in chain branching explosions. Many species are formed as the fuel is oxidized, and thus there are many intermediate reactions between many species formed as the reactants convert to products. Moreover, these reactions occur simultaneously and interdependently. The chain reactions that take place during oxidation of the fuel can be broken down into the *initiating* reaction in which radicals and intermediate species are created from the stable reactants (fuel and oxygen). Another class of reactions are, *propagation* reactions, where the radicals and intermediates react further such that one radical is created for each that is consumed, continuing the chain reaction. The process slows or ends due to *termination* reactions in which radicals react to create stable molecules, removing radicals from the system. In *chain branching* reactions two radicals are created for each radical consumed, such that a few branching reactions in sequence cause a large increase in the number of radicals. When the rate of chain branching exceeds the rate of termination reactions an increase in radicals results, leading to an explosion. The build up of these

radicals is often called the induction period.

Explosions involving exothermic reactions can also be explained using an argument based on an energy balance. When the energy released due to chemical reactions is higher than the heat losses of the system, the temperature will rise. Because reaction rates have an exponential dependence on temperature, a rapid increase in temperature quickly results, causing a thermal explosion.

HCCI ignition is autoignition by chain branching explosion mechanism, ignition occurs as chain branching reactions accelerate due to compression heating.

1.1.2 Combustion Timing

Stable and efficient operation of HCCI engines requires that the combustion timing be tightly controlled to the proper setpoint. At high loads, early combustion can yield unacceptable pressure rise rates ($dp/d\theta$) or unacceptable peak cylinder pressure, causing excessive noise, and potentially damaging the engine. Additionally, NO_x tends to increase as ignition advances [57]. On the other hand, late combustion timing leads to incomplete combustion and increasing emissions of carbon monoxide (CO) and unburned hydrocarbons (UHC) [57, 1]. Combustion becomes unstable and can fail to occur (misfire) as the combustion timing is delayed even further [57, 24]. Thus, the proper choice of the combustion timing at each operating point is crucial for HCCI engines.

There is no way to directly actuate the combustion timing in an HCCI engine (i.e. no sparkplug or fuel injection event to start combustion). Feedback is thus required to control the combustion timing. The combustion timing can be defined based on several different criteria [11]. The point at which combustion starts or a certain percentage of fuel burned can be used, such as 10 or 50 percent. Additionally, it can be defined as the point of peak pressure or peak pressure rise ($dp/d\theta$) in the cylinder.

There are a number of ways to measure the combustion timing. The in-cylinder pressure can be measured using piezoelectric pressure transducers, and the percent mass fraction burned can be obtained by performing a heat release analysis on the pressure data. However, piezoelectric pressure transducers are impractical for

production due to their high cost and short life time (< 100 hours). Another means to obtain the combustion timing is to use knock sensors or microphones on the engine block. One of the most promising technologies is inexpensive ion current sensors. However, the ability of ion sensors to detect combustion under a range of in-cylinder conditions is still an ongoing research topic [81].

1.1.3 Actuation of Combustion Timing

Without a direct means to control the combustion timing, we must resort to actuating other engine parameters to indirectly control combustion. The rates at which chemical reactions proceed determine when the intake charge will auto-ignite and are dependent on the gas temperature, pressure, and composition: percentages of fuel, air, and recirculated exhaust gas. There have been many investigations to determine the proper engine parameters to actuate combustion. They can be broken into the following four categories, of which all in some way affect the chemical kinetics and thus the start of combustion: gas density(pressure), gas temperature, gas composition, and mixture homogeneity [90].

Table 1.2 lists the different methods available to actuate the combustion timing of HCCI engines. There are many methods available. However, the time response and the ability to implement different approaches on a production engine may make some options more favorable.

1.2 Related Work

HCCI engine research first appeared in the literature in 1979 by Onishi et al. [58] and Noguchi et al. [54] and has become an active area of research [92]. While much technological progress has been made towards commercialization of HCCI engines, control remains a barrier. This section provides an overview of research in the area of HCCI engine control.

Table 1.2: Methods of Actuating Combustion Timing

Method	Actuator	References
Intake temperature	electric air heater exhaust heat exchanger	[49],[29],[36],[90]
Trapping exhaust gas	EGR valve exhaust rebreathing lift variable valve timing exhaust throttles	[15] [5] [77]
Variable compression ratio	geometric — VCR engine effective — VVT	[28] [31] [5]
Mixture reactivity	equivalence ratio dual fuel fuel reformer pilot injection	[55] [56] [57]
Temperature during compression	water/steam injection wall temperature	[19]
Intake pressure	turbocharger/supercharger	

1.2.1 HCCI Models for Control

Control of HCCI engines during transients requires feedforward control. The use of process models provides an effective means to generate a feedforward controller through model-based control methods. Model-based control requires the generation of an HCCI engine model from first principles or through system identification. It is a nearly impossible task to fully characterize the many complex processes that occur in HCCI engines in a model efficient enough to be useful in a real-time engine controller. Moreover, because the goal of the model generation is to provide a model that can be used to derive control laws, these models need only contain those subsystems that affect the behaviors we would like to control. Thus, it is desirable to develop simple models of the HCCI engine that allow us to extract the main system dynamics.

The dynamics of HCCI combustion can be modeled using either a mean value model (MVM) or discrete event model (DEM). A MVM is continuous and depicts only the average behavior of an engine. On the other hand, in a DEM all engine events correspond to the actual points in the cycle in which they occur, and thus, this type of model characterizes the reciprocating nature of the engine cycle.

Furthermore, time is the independent variable in a MVM whereas the crankshaft angle is the independent variable for a DEM.

Several HCCI control-oriented models have been developed and most are DEM. Shaver et al. [74] derive a model including the effects of residuals induced by variable valve actuation, the authors find that modeling ignition of the propane-air mixture using an integrated Arrhenius rate expression provides better results than using a temperature threshold or knock integral. The interaction within the intake and exhaust manifolds between cylinders in a multi-cylinder engine is addressed by Souder et al. [78], who use a knock integral to capture ignition. The two stage ignition inherent in diesel fuel combustion is characterized in the paper by Canova et al. [14]. The initiation of the first stage is modeled using an integrated Arrhenius rate expression and the second stage by a temperature threshold that is a function of EGR and the air to fuel ratio (AFR). An HCCI engine running on ethanol fuel is modeled by Sun et al. [82] using a two-step reaction mechanism. Bengtsson et al. [10] model HCCI combustion using a shell model for hydrocarbon fuels containing five species and eight reactions. They compare this model to experimental results, and an integrated Arrhenius rate threshold. CA50 predicted by the integrated Arrhenius rate threshold is found to deviate from the experimental results with changes in inlet temperature.

Mean value models are more typical in spark ignited and diesel control-oriented models. Rausen et al. [65] considered a MVM for HCCI. The model has eight states and includes an exhaust gas recirculation valve and exhaust rebreathing lift. A set of algebraic equations is used to relate the in-cylinder conditions at intake valve close to the conditions at exhaust valve close. A similar cycle-by-cycle model was developed by Shaver et al. [71] for an HCCI engine with variable valve actuation, except this model does not include flow to and from the exhaust and intake manifolds and assumes constant combustion phasing. This model is expanded in [73] by Shaver et al.. Combustion phasing is calculated with an integrated Arrhenius rate expression. Furthermore, this model [73] provides an expression that relates the current cycle's peak pressure and combustion phasing to the inlet and past cycle conditions.

Although these DEMs and MVMs have made great strides in simplifying the complex physics that take place in an HCCI engine, they are still rather complicated, making it either impossible to derive control laws or yielding control laws that are too computationally intensive for real-time implementation. There has been success linearizing some of them to obtain models that are tractable for the generation of control laws [71], [15], [75]. However, these linearized models are only valid around the operating point where they are linearized.

1.2.2 HCCI Control Techniques

The first closed-loop control of an experimental HCCI engine appeared in [56] by Olsson et al.. Gain-scheduled proportional integral derivative (PID) controllers were used to control the combustion timing of each cylinder by effectively regulating the octane number of fuel going to each cylinder. Two fuels with different octane numbers (n-heptane and isooctane) were mixed to vary the octane number, and thus reactivity, of the fuel. Strandh et al. [80] used system identification to construct a model of the dual fuel HCCI engine mentioned above. This model is used to derive a linear quadratic Gaussian (LQG) control law as well as a first order feedforward filter. The performance of the LQG and PID controllers was compared both with and without the feedforward filter. The feedforward filter was found to increase the bandwidth of the controller, allowing cycle-by-cycle control. While the duel fuel method proves effective, it is not seen as a practical method of control for a production engine.

Haraldsson et al. [31] use the compression ratio of a novel variable compression ratio (VCR) engine with a PID controller to control the mean combustion timing of all five cylinders. Additionally, the cylinders are individually balanced with PID controllers actuating the air to fuel ratio for each cylinder. The VCR method of control is compared to a fast thermal management (FTM) actuation system by Haraldsson et al. in [29]. The FTM system consists of a stream of ambient air and and a hot stream of air that has passed through an exhaust heat exchanger. The two air streams are combined to regulate the intake air temperature. The FTM system is used to control the mean combustion timing and PID controllers are

again used with gains that depend on the engine speed. The authors [29] find that changes in RPM alter the amount of heat transfer and thus the wall temperature. Additionally, they find that closed-loop control with the FTM system has a time constant 57% faster than the closed-loop system employing VCR. The FTM system discussed above is later modified to allow individual cylinder control of the intake air temperature in a paper by Hyvonen et al. [36]. Haraldsson et al. [30] use the modified FTM system combined with VCR and the amount of fuel to control the VCR engine during the European EC2000 drive cycle. A combination of LQG and PID controllers are used, and it is found that the LQG controller performed well within the range for which it was designed, but poorly outside of this range [30]. Model predictive control (MPC) is used to control a heavy duty HCCI engine with variable valve actuation (VVA) by Bengtsson et al. [12]. They use MPC to simultaneously minimize the fuel consumption and emissions while satisfying constraints on the maximum in-cylinder pressure.

Souder [77] also performs system identification on a four cylinder engine; however, the actuators in this case are throttles on each of the exhaust manifold runners. Actuating in this manner increases (decreases) the back pressure and causes more (less) residual gas to be retained in the cylinder thus increasing (decreasing) the temperature of the charge. While this setup may not be practical because of throttling losses, it is similar in effect to using variable exhaust valve timing, which is considered a practical approach. The linear model obtained using system identification is used to construct a LQG controller, however this controller has poor performance because of slowly varying unmodeled disturbances such as changes in the cylinder wall temperature [77]. Integrator action is added to the LQG controller to solve this problem. Souder [77] derives a plant model of the experimental engine using spectral analysis. This model allows the derivation of a μ-synthesis controller and a H_∞ controller, which are found to have better robustness than the LQG based controllers when applied to the experimental engine [77].

Shaver et al. [72, 74] present a nonlinear model of the HCCI engine cycle with VVA and a linearized version of this model is used to construct a linear-quadratic regulator (LQR) control law [71]. Subsequently, they develop a control algorithm

based on dynamic feedback linearization [73]. Shaver et al. [75] demonstrate control of both the in-cylinder pressure as well as the combustion timing using a decoupled control scheme with two time scales on the VVA engine. The in-cylinder pressure is controlled on a cycle-by-cycle basis while the combustion timing is controlled on a slower time scale.

Chiang and Stefanopoulou [15] use a mean-value model of a HCCI engine with exhaust rebreathing lift for the purpose of control design based on the model presented by Rausen et al. [65]. This model is linearized, used to design a two-input two-output controller, and the controller is simulated with the nonlinear model. In [16] Chiang and Stefanopoulou use an extended version of the MVM model [65] and explore the stability of various equilibria. Additionally, based on simulations they determine that a static feedforward controller can cause instability during the transition from high to low load, but that a dynamic feedforward controller can provide stability during this transition [16].

Agrell et al. [5] use a PI controller with the combustion timing averaged over five cycles as the input and the valve timing on a single-cylinder engine with variable valve timing as the output. They use one of two different valve strategies depending on the operating conditions: one strategy changes the inlet valve closing to vary the effective compression ratio and the other is negative valve overlap, which traps more residual gas, increasing the temperature of the charge. A feedforward controller is added to the PI controller in [6]. The feedforward controller consists of an ignition model that is a nonlinear map covering a number of operating conditions and based on a knock integral.

All these studies show the potential for transient operation of HCCI engines, however none of these methods are feasible in production. Most methods utilize linear models only valid over a narrow operating range of the engine. A number of linear models spanning the operating range of the engine must then be determined and interpolated. Such a scheme was used to control an HCCI engine with VVA over a range of operation regimes using MPC by Bengtsson et al. [12]; however, this method is computationally intensive thus not implementable on current engine control units (ECU). The authors of this study point out that the development of

nonlinear models would improve the controllers performance [12]. The development of a nonlinear model of HCCI combustion valid over the entire operating range of an engine that can be used to generate control laws thus holds the potential of bringing HCCI engines into series production.

1.3 Thesis Overview

This section provides an outline of the contents of this thesis.

In **Chapter 2** the experimental HCCI engine used in this thesis is described, including the modifications made to the stock engine to run HCCI mode as well as the real-time control system. The use of intake temperature to control the combustion timing of a multi-cylinder engine is demonstrated.

In **Chapter 3** a controls-oriented model of natural gas fueled HCCI engine combustion is developed. This model uses an ignition line that is a function of in-cylinder motored temperature and pressure to capture start of combustion. The use of this simple correlation allows the use of this model in the development of feedforward control algorithms. A feedforward controller based on this model is simulated on a zero dimensional model of an HCCI engine. Furthermore, this model is extended to gasoline fueled HCCI engine combustion and validated against experimental engine data.

Chapter 4 gives a simple tutorial that gives some insight into how extremum seeking works.

In **Chapter 5** the use of extremum seeking to speed up the mapping process of an engine is outlined. Specifically, the use of ES to minimize the fuel consumption of an HCCI engine by determining the optimal combustion timing is experimentally shown.

In **Chapter 6** an online model based method of tuning PID controller gains using extremum seeking is presented. This tuning method is demonstrated on a series of four process models and compared to three widely used PID tuning methods. Extremum seeking tuning is found to yield controllers that provide similar if not better performance than the other tuning methods.

In **Chapter 7** extremum seeking is used to tune the combustion timing PID controller on an experimental HCCI engine. Moreover, ES is used to tune a PI controller plus a constant feedforward term for improved setpoint response. ES proves to be a quick means to determine optimal PID parameters while the engine is running.

In **Chapter 8** the work presented in this thesis is summarized and future directions of research are shared.

Chapter 2

Experimental Engine

A Caterpillar 3406 Natural Gas Spark Ignited engine has been converted to run in HCCI mode. The main characteristics of this engine are listed in Table 2.1. The stock engine has 6 cylinders, 14.6 liters displacement and 10:3:1 compression ratio. Figure 2.1 shows a picture of the modified engine.

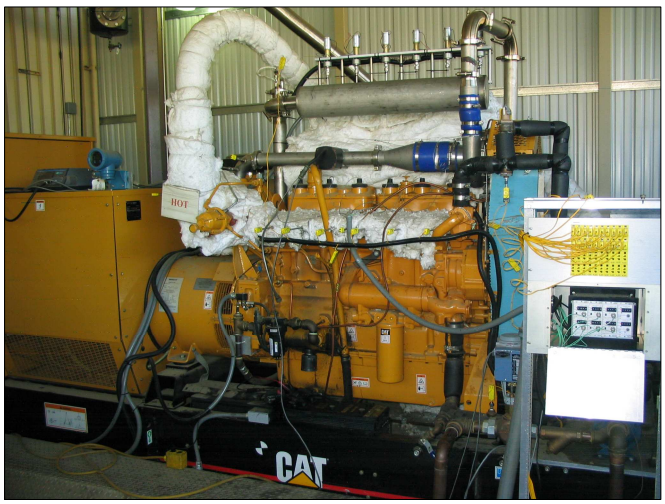

Figure 2.1: Engine used in HCCI experiments, 14.6 L, 6 cylinder natural gas engine setup for stationary power generation.

Many modifications were made to convert the engine to a natural gas HCCI engine. The first modification to the engine was to replace the stock low compression ratio (10:1) pistons with pistons typically used in the higher compression ratio

(16:1) diesel version of the Caterpillar 3406. This modification was necessary to improve the thermal efficiency of the engine and to promote the natural gas fuel ignition. Spark plugs were replaced by pressure sensors (one for each cylinder) occupying the spark plug holes. Other modifications were conducted in all the major engine systems and these are described in the following sections of this chapter.

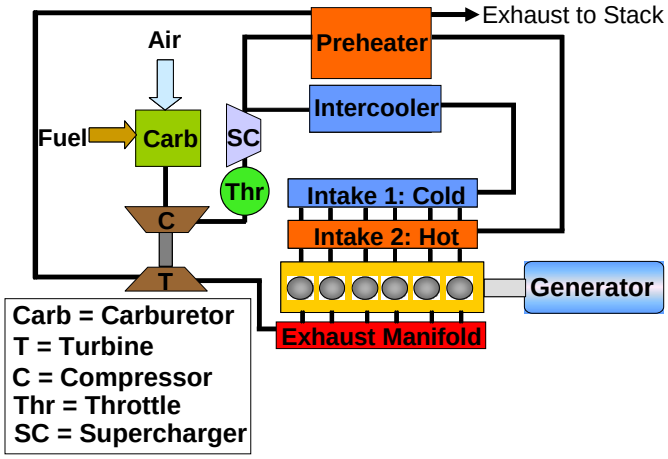

Figure 2.2: Schematic of the experimental HCCI engine thermal management system. On each cylinder a valve regulates the blend of hot and cold fuel-air mixture, controlling the intake temperature.

2.1 Thermal Management

The thermal management system, shown in Figure 2.2, controls the combustion timing of the engine on a cylinder-by-cylinder basis, by controlling the temperature of gases inducted into each cylinder, which in turn controls the autoignition process. Inducted air flows through the carburetor where natural gas fuel is added, then travels through the turbocharger, throttle and supercharger. Then after the supercharger, the fuel-air mixture splits into two streams, one "hot" and one "cold". The hot side passes through an exhaust-to-intake heat exchanger, while the cold side travels through an aftercooler. The hot and cold streams are delivered to two separate manifolds (Figure 2.3). Each cylinder has a temperature mixing valve

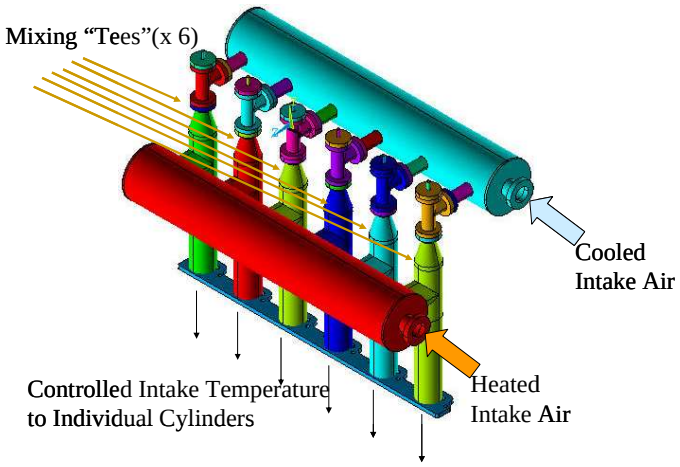

Figure 2.3: Schematic of dual manifold intake system used for cylinder-by-cylinder engine control. Control valve motors, not shown, go on top of the mixing tees.

where cold intake charge is blended with the charge from the hot manifold, regulating intake temperature to each cylinder, similar to controlling the temperature of a morning shower. Each temperature control valve is computer-controlled using an electric servo motor. The length of the intake runners results in about a one cycle transport delay before a change in the valve input affects the intake mixture entering the cylinder. This thermal management system allows the intake temperature of each cylinder to be quickly adjusted for cylinder-by-cylinder control of the combustion timing.

Table 2.1: Caterpillar 3406 Engine Parameters

number of cylinders	6
total displacement	14.6 L
compression ratio	16:1
cylinder bore	137 mm
connecting rod length	330 mm
stroke	164 mm

2.2 Starting System

HCCI engines are often difficult to start. At cold start, the compressed gas temperature in an HCCI engine is reduced because the charge receives no preheating from the intake manifold and the compressed charge is rapidly cooled by heat transfer to the cold combustion chamber walls. Without some compensating mechanism, the low compressed charge temperatures could prevent an HCCI engine from firing. A common approach has been to start the engine in spark ignition or diesel mode and transition to HCCI mode after warm up. However, successful transition typically requires advanced engines equipped with variable compression ratio (VCR) or variable valve timing (VVT), which may be expensive or difficult to implement for heavy duty engines. Furthermore, operation in SI mode requires operation at high equivalence ratio (> 0.7), which is high enough to damage the engine if thermal autoignition or knock occurs during the transition.

Instead of attempting to start the engine in SI mode and transition to HCCI mode, we used a brand new approach: start the engine directly in HCCI mode by preheating the intake with a gas fired burner. This was easy to implement by adding a burner to the preheater (Figure 2.4). The burner is run for a period of time (20 minutes) until the preheater reaches a high temperature (300 C). At this condition, running the intake charge through the preheater while simultaneously spinning the engine with an air starter is enough to achieve HCCI ignition. After ignition, combustion is self sustaining and the burner can be turned off, as the intake gases are heated by the hot exhaust.

2.3 Fueling System

The fueling system presents several challenges, because HCCI combustion is extremely sensitive to equivalence ratio. Just a few cycles of HCCI combustion at high equivalence ratio (> 0.5) are enough to cause physical damage to the engine. Therefore, the fueling system has to guarantee that no equivalence ratio excursions will occur beyond a "safe" equivalence ratio (~ 0.45) under any circumstances. It may also be desirable to run at low equivalence ratio for low load operation.

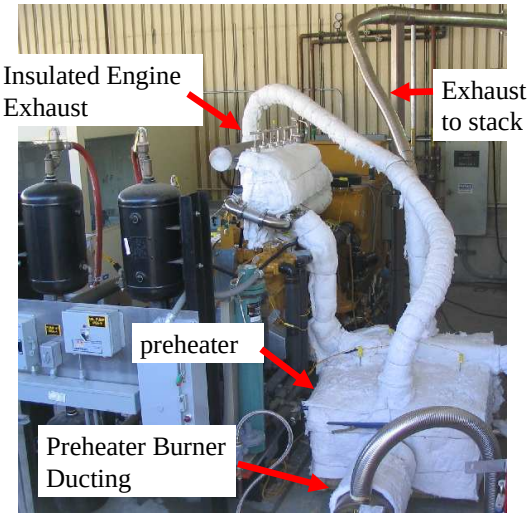

Figure 2.4: Picture of the engine showing the main components of the thermal management system.

These difficult requirements were met with a clever solution: the stock carburetor tuned for natural gas was replaced with a carburetor tuned for liquid petroleum gas (LPG). Considering that the average composition of natural gas is $C_{1.2}H_{3.5}$ and that the average composition of LPG is $C_{3.5}H_{8.5}$, a carburetor tuned for operating at equivalence ratio 0.9 on LPG will run at $\phi = 0.4$ when fueled with natural gas. This is ideal for HCCI, as the carburetor is quite efficient at maintaining the established equivalence ratio. The equivalence ratio is reduced below 0.4 with an electronic control valve that reduces the pressure in the natural gas line supplying the carburetor (Figure 2.5).

2.4 Boosting System

HCCI engines operate at low equivalence ratio ($\phi \leq 0.45$) to avoid damage due to knock. This high level of fuel dilution results in low power output, and intake boosting (up to 3 bar absolute pressure) is necessary to obtain appropriate levels of power ($\sim$ 10 bar BMEP or more).

The engine is delivered with a turbocharger. However, the engine originally was designed to run in spark-ignited mode at high equivalence ratio ($\sim$ 1) and with a

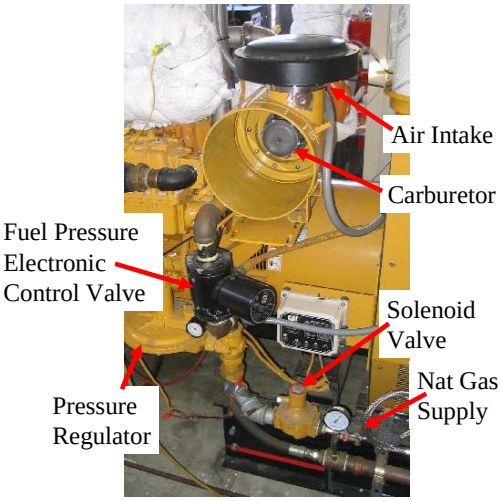

Figure 2.5: picture showing the fueling system components.

low compression ratio (10.3:1). The stock turbocharger is not sized appropriately for HCCI operation. HCCI exhaust temperature is very low compared to the stock SI engine exhaust, thus the enthalpy of the HCCI exhaust is insufficient to provide more than 1.2 to 1.3 bar boost. Since more boost is desired, a mechanical supercharger was added in series following the turbocharger. The engine was fitted with a custom supercharger from Vortech Engineering (Model V24XC), which achieves a 3:1 pressure ratio at 55,000 RPM.

2.5 Control System

It is typically considered that combustion control is the most challenging problem for widespread commercialization of HCCI engines. Compared to conventional engines the HCCI process gives up two important control aspects: 1) the timing of the start of ignition is not directly controlled by any external event such as the direct fuel injection, as in a diesel engine, or the sparking of the spark plug, as in a SI engine, and 2) the heat release rate is not controlled by either the rate and duration of a direct fuel injection process, as in a diesel engine, or by the finite turbulent flame propagation time, as in a SI engine. Instead, HCCI ignition is

determined by the charge mixture composition and its temperature history (and to a lesser extent, its pressure history). Changing the power output of an HCCI engine requires a change in the fueling rate and, hence, the charge mixture. As a result, the temperature history must be adjusted to maintain proper combustion timing. Similarly, changing the engine speed changes the amount of time for the autoignition chemistry to occur relative to the piston motion. Again, the temperature history of the mixture must be adjusted to compensate. These control issues become particularly challenging during rapid transients.

Multi-cylinder engines pose an additional challenge, since there are always small cylinder to cylinder differences in charge pressure and temperature at intake valve closing, due to cylinder-by-cylinder differences in volumetric efficiency or coolant temperature. In addition to this, there may be differences in compression ratio between cylinders due to geometric tolerances. These differences are small enough to be negligible in SI and diesel engines. However, HCCI combustion is controlled by thermal autoignition, and is extremely sensitive to temperature. A very small temperature difference can result in a considerable difference in ignition timing. It is therefore necessary to develop a controller that can detect cylinder to cylinder differences in ignition timing and adjust conditions in the individual cylinders so that optimum combustion timing can be achieved in all cylinders under all operating conditions.

Several potential control methods have been proposed to provide the compensation required for changes in speed and load. These include varying the amount of hot EGR introduced into the incoming charge, using a fuel additive to enhance ignition, using a variable compression ratio (VCR) mechanism to alter TDC temperatures, and using variable valve timing (VVT) to change the effective compression ratio or the amount of hot residual retained in the cylinder, or both. VVT appears most promising for transportation applications, because its time response could be made sufficiently fast to handle rapid transients.

For stationary applications, HCCI combustion control is not nearly as challenging, because a stationary engine runs predominantly at a constant speed and the load changes relatively slowly. Under these conditions, combustion control becomes

much more tractable, and can be accomplished without advanced engine technology such as VVT or VCR. In this application, combustion control is achieved by regulating the intake charge temperature. The intake temperature is modified by blending the intake from the cold and hot manifold system shown in Figures 2.3 and 2.6. The relative amount of intake from each manifold is controlled by throttling the intake from the cold manifold into each cylinder. This control system has the additional advantage of being able to independently regulate the intake temperature of each cylinder, producing optimum ignition timing in all cylinders.

Figure 2.6: Dual manifold intake system implemented in the Caterpillar engine for HCCI combustion control. The figure shows the cold manifold, the hot manifold (insulated with white material), and the mixing valves actuated by servo motors (top of the picture).

2.5.1 Hardware

Automatic control of the temperature valves is achieved using servo motors to regulate the position of each valve, as shown in Figure 2.6. A Globe Motors IM-15 DC permanent magnet planetary gearmotor is teamed with a Novotechnik GL hollow-shaft angular position sensor. The real-time control software sends a pulse width modulated (PWM) signal to a MNIH-0050 H-bridge, which regulates the direction and current to each electric motor. The position is scheduled by the

feedback controller such that a desired combustion timing setpoint is met.

The combustion timing feedback signal is derived from in-cylinder measurements of the pressure. A BEI H25 optical encoder on the camshaft hardware triggers acquisition from a Kistler 6052B piezoelectric pressure transducer every 0.5 crank angle degrees. A net heat release analysis of the pressure measurements determines the combustion timing in each cylinder [11]. We define the combustion timing to be the crank angle at which 50% of the heat (fuel chemical energy) has been released in the cycle ($CA50$). Finally, the calculated combustion timing is used as a feedback, allowing control of the combustion timing by means of the temperature control valves.

2.5.2 Real-Time Controller

Labview 8 based software handles all data acquisition and control tasks. The time-critical portions of the control software reside on a dedicated desktop PC (the "target") running Labview Real-Time. Another PC, the "host," is the user interface and displays pressure traces along with other data such as the combustion timing for each cylinder. Furthermore, the host allows the operator to adjust the combustion timing setpoint for each cylinder. Data is transferred from the target to the host via an ethernet cable. Figure 2.7 shows a schematic of the real-time controller hardware and how the hardware interacts.

The target contains three National Instruments data acquisition boards (see Figure 2.7). The analog signals from all six pressure transducers are sampled by a NI PCI-6221 M-series data acquisition board. The optical encoder on the camshaft has two outputs sending a pulse every revolution of the camshaft (two rotations of the crank shaft), as well as 1440 pulses per revolution of the camshaft, resulting in a pulse every 0.5 crank angle degrees. These two signals are read using counter timer channels on the above NI board and are shared among the other data acquisition boards using the RTSI bus. The other NI PCI-6221 M-series data acquisition board was used to measure the angular position of all six temperature control valves. A PID controller was used to regulate angular position of each valve and send a PWM signal to the H-bridge for each electric motor using the

counter timer channels on a NI PCI-6602 counter timer board.

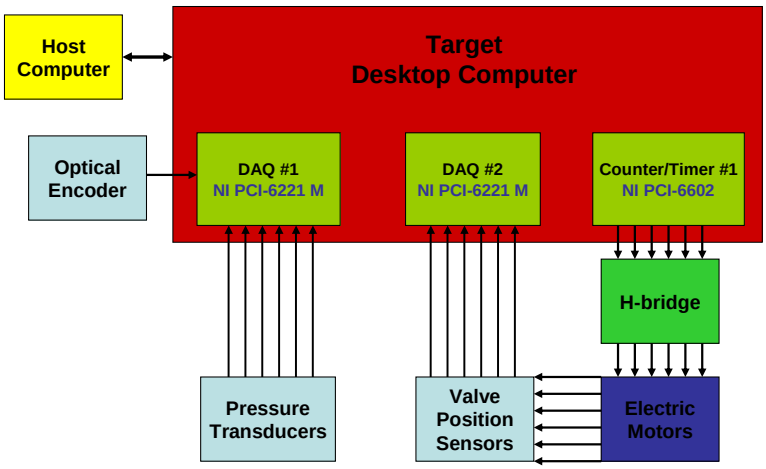

Figure 2.7: Schematic of the real-time HCCI engine controller.

2.6 Heat Release Analysis

A robust metric of the combustion timing must be determined that can be calculated quickly to be used as a feedback signal. The crank angle degree at which 50% of the fuel heat (chemical energy) is released in the cycle (CA50) turns out to be a robust indicator of combustion timing. CA50 is less sensitive than other metrics, for example CA10 or other percentages of heat release, because the slope of the heat release with crank angle degree is highest at this point. An error in percentage heat release only results in a small error in the crank angle degree. A study by Bengtsson et al. [11] showed that using a net heat release analysis resulted in the best correlation to CA50 calculated using a full heat release when compared to using maximum pressure, the Rassweiler & Withrow method for 50% mass fraction burned [89], and maximum heat release rate.

2.6.1 Net Heat Release

In this work we used CA50 determined from a net heat release calculation. The net heat release is approximate because of the many simplifying assumptions used in the analysis, but gives acceptable results for control. The net release comes from applying the first law of thermodynamics to a single zone model of the combustion chamber [33]

$$dU{=}\delta Q - \delta W. \tag{2.1}$$

The extensive internal energy, U, is assumed to be a function of temperature $U = mu(T)$, the product of specific internal energy u and the mass of gas m inside the cylinder, which is assumed to behave like an ideal gas

$$dU = mdu + udm = mdu = mc_V dT, \tag{2.2}$$

with c_V the constant-volume specific heat. Note that mass is constant. The work performed by the system is $\delta W = pdV$. Neglecting heat transfer losses, we assume that all heat generated is due to the chemical energy released during combustion, equation (2.1) becomes

$$\delta Q{=}mc_V dT + pdV. \tag{2.3}$$

We can then differentiate the ideal gas law $pV = mRT$ to find dT, where R is the specific gas constant. Furthermore, we use the relationship $c_V/R = 1/(\gamma - 1)$ (where we assume the ratio of specific heats $\gamma = \frac{c_p}{c_V}$ is constant) to arrive at

$$\frac{dQ}{d\theta}{=}\frac{\gamma}{\gamma - 1}p\frac{dV}{d\theta} + \frac{1}{\gamma - 1}V\frac{dp}{d\theta}. \tag{2.4}$$

The cylinder volume as a function of the crank angle can be found using the slider crank equation [33]

$$V(\theta) = V_c + \frac{\pi B^2}{4}\left(l + a - a\cos\theta - \sqrt{l^2 - (a\sin\theta)^2}\right), \tag{2.5}$$

where V_c is the clearance volume, B is the bore, l is the connecting rod length, and a is the crank throw (stroke/2). The values for most of these parameters can be found in Table 2.1.

Integrating equation (2.4) results in the heat release Q as a function of θ. However, rewriting equation (2.4) (by noting that $d(pV)/d\theta = pdV/d\theta + Vdp/d\theta$) as

$$\frac{dQ}{d\theta} = \frac{1}{\gamma - 1}\frac{d(pV)}{d\theta} + p\frac{dV}{d\theta}, \tag{2.6}$$

is advantageous, because, upon integration, we can evaluate the first term analytically without the need to numerically differentiate the pressure data, resulting in a cleaner signal when noise is present [85]. Because we only sample the pressure measurement discretely, we compute Q as a finite sum rather than a continuous integral

$$Q_i = \frac{1}{\gamma - 1}[p_i V_i - p_0 V_0] + \sum_{j=0}^{i} p_j (\Delta V)_j. \tag{2.7}$$

Combustion only occurs near top dead center (TDC), so to reduce the calculation time, equation (2.7) is only computed from -45 to 45 crank angle degrees (CAD) after TDC. CA50 is then the crank angle position θ_{CA50} where

$$Q_{50\%} = \frac{1}{2}(Q_{max} - Q_{min}). \tag{2.8}$$

Figure 2.8 demonstrates graphically how $CA50$ is determined. In addition this figure shows $CA10$ and $CA90$; $CA1$ can be calculated similarly. Therefore by measuring the in-cylinder pressure and with knowledge of cylinder volume as a function of crank angle equation (2.5), both equation (2.7) and equation (2.8) can be used to calculate $CA50$.

2.7 Control of Combustion Timing

Cylinder-by-cylinder control is essential for satisfactory operation. Because HCCI is very sensitive to temperature changes, even small temperature differences between cylinders (even just a few degrees C) can cause unsatisfactory performance. These temperature differences invariably exist in multi-cylinder engines due to slight differences in compression ratio, intake and exhaust processes, or coolant variations between cylinders.

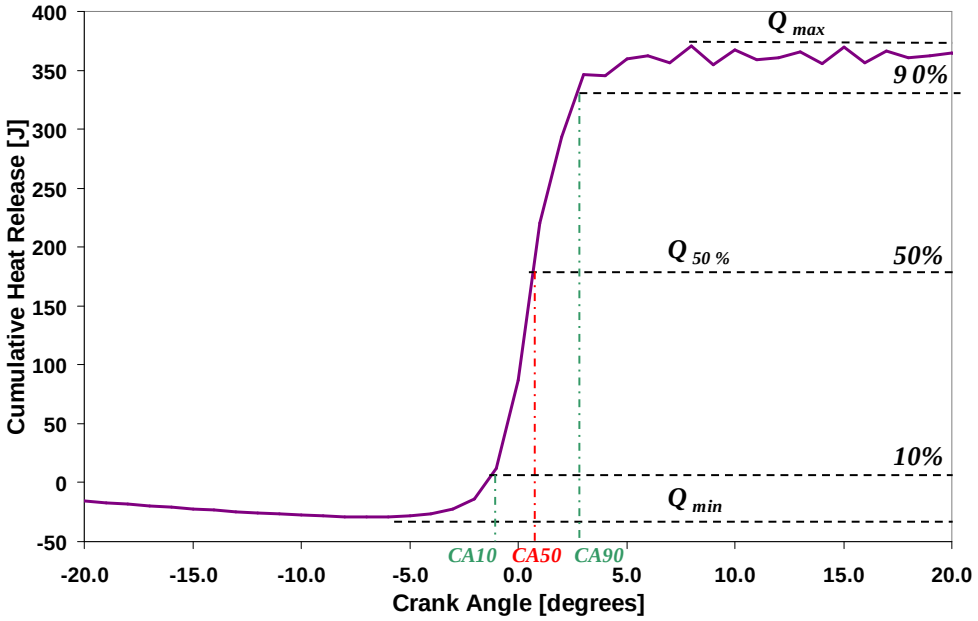

Figure 2.8: Cumulative heat release as a function of crank angle, showing the crank angle degree at which 10%, 50%, and 90% of the fuels heat has been released during the engine cycle.

Temperature variability has a strong effect on cylinder pressure. Figure 2.9 shows pressure as a function of crank angle for the engine without cylinder-by-cylinder control. Each line is the result of averaging 200 engine cycles during steady state operation of the engine. The engine coolant path from cylinder 6 to cylinder 1 in the inline six cylinder engine determines the relative temperature of each cylinder, affecting ignition. Cylinder 6 is first to be cooled by incoming water from the radiator and is therefore coldest and would be last to ignite, all other factors being the same. Cylinder 1 is at the end of the cooling passage and is hottest, igniting earliest.

The unbalanced combustion suggested by Figure 2.9 is inefficient because cylinders do not fire at the optimum time. Hot cylinders that ignite early produce a sudden and violent combustion that may damage the engine. Late-burning cylinders generate high emissions of hydrocarbons and carbon monoxide due to incomplete

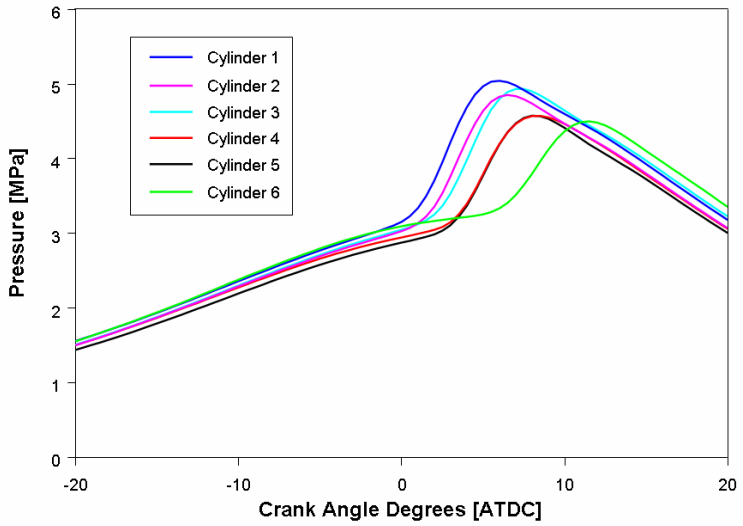

Figure 2.9: Pressure as a function of crank angle (zero is at top dead center) for the six cylinders of the Caterpillar 3406 HCCI engine without feedback control of combustion timing.

combustion.

The dual manifold control system implemented on the Caterpillar engine addresses this problem by detecting cylinder-to-cylinder differences in combustion timing and independently adjusting the intake temperature of each cylinder. Mixing valves in each of the six cylinders (Figure 2.6) compensate for the natural variability in cylinder-to-cylinder temperature and produce consistent combustion in all cylinders (Figure 2.10).

Automatic control of the mixing valves is achieved using servo motors. The combustion timing is calculated based on the measured pressure signal from each cylinder, and the mixing valve position is then scheduled by the control algorithm to yield the desired combustion timing.

This chapter is based on material as it appears in
D. L. Flowers, J. Martinez-Frias, F. Espinosa-Loza, N. J. Killingsworth, S. M. Aceves, R. Dibble, M. Krstic, and A Bining, "Development and Testing of a 6-Cylinder HCCI Engine for Distributed Generation," *In Proceedings of ASME ICEF*

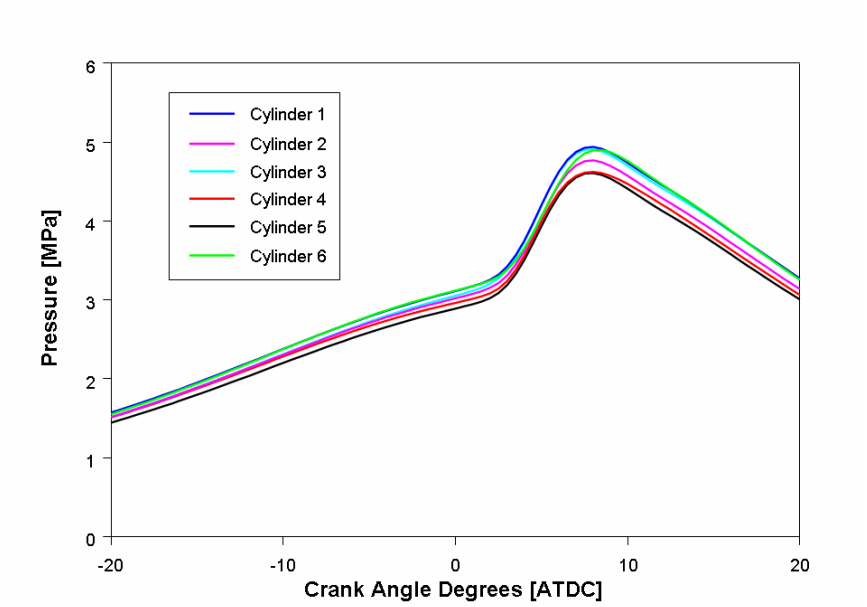

Figure 2.10: Pressure as a function of crank angle (zero is at top dead center) for the six cylinders of the Caterpillar 3406 HCCI engine after implementation of cylinder by cylinder feedback control of combustion timing.

– *2005*,Ottawa, Canada, pp. 465–473, 2005.

Chapter 3

HCCI Engine Modeling for Control

In this chapter a controls-oriented model of HCCI engine combustion for single stage fuels is presented. We formulate the model for both natural gas and high-octane gasoline fuel. In the following section we generate an ignition line from a zero-dimensional model of HCCI combustion with detailed chemistry, where the ignition line is used to model autoignition. Subsequently, we lay out all the equations that describe the compression, ignition, heat release, expansion and exhaust blowdown within the cylinder during an engine cycle. The model is then compared to the detailed chemical kinetic model. The developed equations are combined to create a state-space model. The end result is a cycle-by-cycle model of an HCCI engine. We derive a nonlinear feedforward controller based on this model and simulate it on a zero-dimension model with detailed chemical kinetics. Finally, we generate an ignition line for gasoline-fueled HCCI and validate the model against experimental engine data.

3.1 Ignition Correlation

The key to HCCI engine operation is the autoignition process, therefore correctly modeling the autoignition is the most crucial aspect of an HCCI engine model. Autoignition is controlled by chemical kinetics and is thus a complex

phenomenon. The use of a detailed chemical mechanism requires the solution of hundreds of differential equations, which is computationally intensive. As a result, simpler modeling schemes are often used, such as an integrated Arrhenius rate equation. This method defines combustion as the point at which the integral of a function of in-cylinder temperature, pressure, and concentration of specific species reaches some critical value [48]. However, the integrated Arrhenius equation requires solving for the upper limit of the integral.

We propose a simpler solution to modeling autoignition, correlating ignition to the point when a threshold, which is a function of in-cylinder temperature T_{cyl} and pressure p_{cyl}, is exceeded. It was found in a paper by Aceves et al. [2] that a $\log(p_{cyl})$ versus $\log(T_{cyl})$ map can be used to visualize ignition and that for many fuels, ignition falls on a line within this map. However, in this work we found that a line in p_{cyl} versus T_{cyl} space was appropriate to characterize ignition.

In this section we will outline the generation of a map and the use of this map to determine an ignition line. To generate the map we use a single-zone detailed chemical kinetic (CK) model of HCCI combustion during the closed portion of the engine cycle. The CK model is described in more detail in Appendix A. The CK model treats the in-cylinder gas mixture as perfectly homogenous, such that all thermodynamic properties, such as temperature, pressure, and species concentration are independent of location within the cylinder. This type of model only takes into account the bulk gas in the middle of the engine cylinder and does not account for the volume of gas lying within crevices of the engine. Neglecting the gas within the crevices causes an underprediction of unburned hydrocarbons, thus this type of model is not useful for the prediction of emissions. Nevertheless, single-zone CK models have been found to provide a good estimate of the start of combustion, [3], with minimal computational time.

The CK model is run with a chemical mechanism that includes species up to C4 chemistry [20] and the chemical kinetics are solved using Cantera [27]. The natural gas composition used for the simulations is given in the upper half of Table 3.1. The simulations are run for all combinations of the conditions listed in the lower half of Table 3.1, disregarding simulations in which CA50 is outside the range of

Table 3.1: Simulation Conditions

Fuel Blend	CH_4	C_2H_6	C_3H_8	C_4H_{10}				
mol %	94	4	1	1				
RPM	1300	1500	1800	2100				
p_{intake} atm	1	1.5	2	2.5	3	3.5	4	
T_{intake} K	410	420	430	440	450	460	470	480
ϕ	0.25	0.3	0.35	0.4	0.45			

[-5, 10] crank angle degrees (CAD) after top dead center (ATDC). Additionally, the runs at 1300 RPM include $p_{intake} = [0.9, 1.1, 1.2]$ atm.

The engine parameters for the simulations correspond to the experimental HCCI engine outlined in Chapter 2. This engine has a hot and cold manifold similar to the schematic in Figure 3.1 allowing individual control of the intake charge temperature for each cylinder.

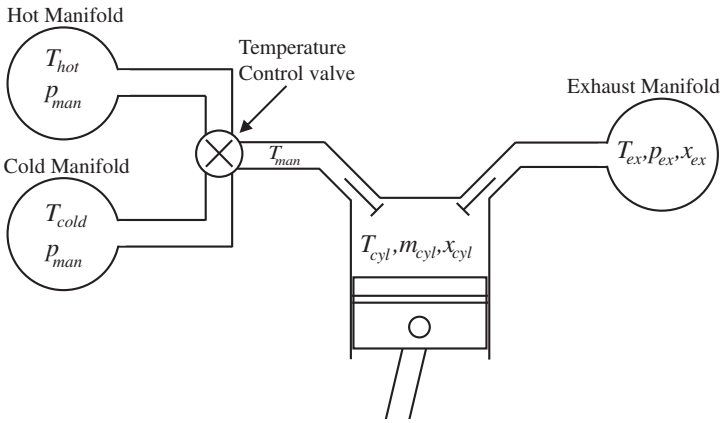

Figure 3.1: Schematic of engine. The intake charge temperature is controlled using a valve to regulate the amount of intake charge that comes from the hot and cold manifolds.

For each run of the CK model the crank angle degree in which one percent heat release occurs (CA1) is determined and the motored pressure and temperature is noted. The motored pressure and temperature are the pressure and temperature that would occur in the engine in the absence of all chemical reactions. Figure 3.2 (a) is a plot of the motored temperature versus motored pressure at which CA1 occurs. In Figure 3.2 (b) the pressure has been divided by p_{intake}^n , where $n = 0.8$

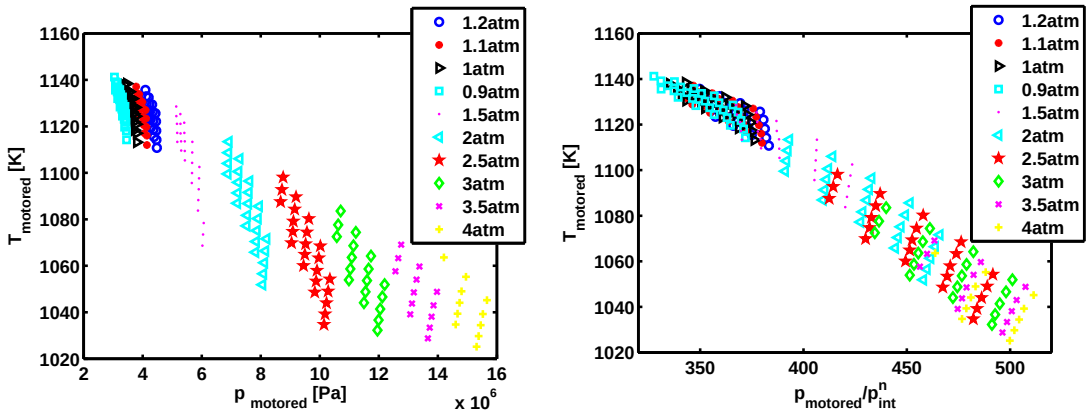

(a) (b)

Figure 3.2: Motored temperature versus motored pressure at which one percent heat release occurs at 1300 RPM (a). Normalizing the pressure by p_{intake}^{n} with $n = 0.8$ in (b) causes data to collapse on to roughly a single line.

and was found by trial and error, normalizing the motored pressure in this manner causes the data points for a given RPM to collapse onto roughly a single line. Each data point corresponds to a simulation of the CK HCCI model. We choose CA1 because it is essentially the point in the cycle at which chemistry becomes important and the in-cylinder pressure and temperature begin to deviate from the motored pressure and temperature.

A line is fit to the data plotted in Figure 3.3 for each RPM resulting in an ignition line

$$T_{cyl}(\theta_{SOC}) = b_1 \frac{p_{cyl}(\theta_{SOC})}{p_{man}^{n}} + b_2, \tag{3.1}$$

where θ_{SOC} is the crank angle of start of combustion (SOC). The slope b_1 is almost constant with RPM resulting in parallel lines in Figure 3.3 while the constant b_2 increases with RPM. This shift is expected because as the RPM increases so does the speed of the piston, whereas the chemical time scale of the reacting gas is fixed. This type of ignition model requires that CA1 occurs before TDC, which is typically the case. However this model might not suffice for engines with very late combustion timing.

Additionally, these simulations are used to determine a correlation for the burn duration defined as $\Delta\theta = \theta_{CA50} - \theta_{CA1}$. Figure 3.4 shows the burn duration as a

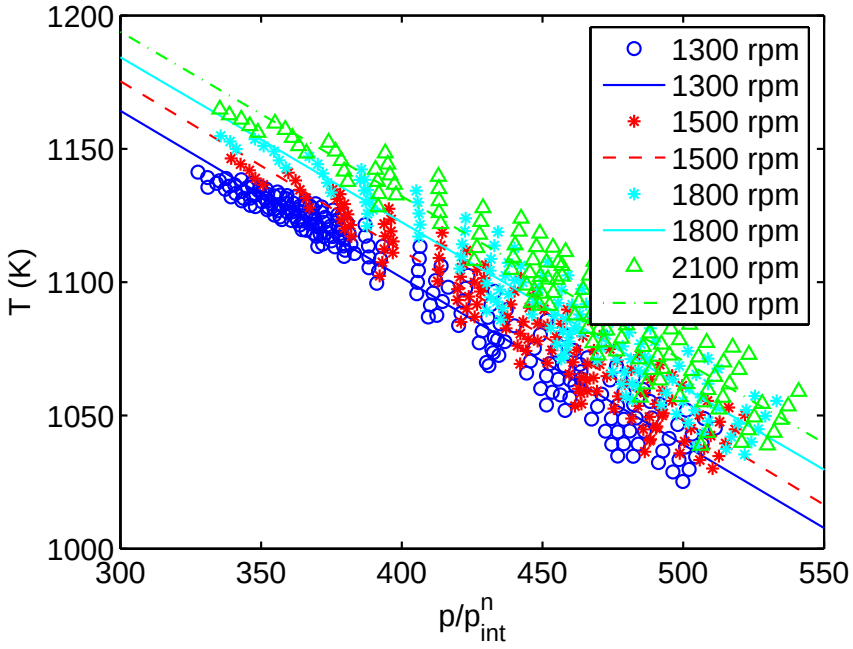

Figure 3.3: Motored temperature versus normalized motored pressure at which one percent heat release occurs for multiple speeds. Ignition lines plotted are least squares fits to the data for each speed.

function of CA1 for the conditions given in Table 3.1. We can see from this plot that the linear fit,

$$\Delta\theta(k) = b_3\theta_{SOC}(k) + b_4, \tag{3.2}$$

does not change much with RPM, so we use a single line. There is little change in burn duration with RPM because at higher RPM ignition occurs at higher temperatures, as we can see from Figure 3.3, thus the chemistry is faster and compensates for the increase in piston speed. In an actual engine the burn duration is longer than found here due to inhomogeneity of species and temperature within the cylinder.

3.2 HCCI Cycle Model

The model provides an estimate of the combustion timing as well as the properties of the the residual gas left in the cylinder at the end of cycle k. The combustion

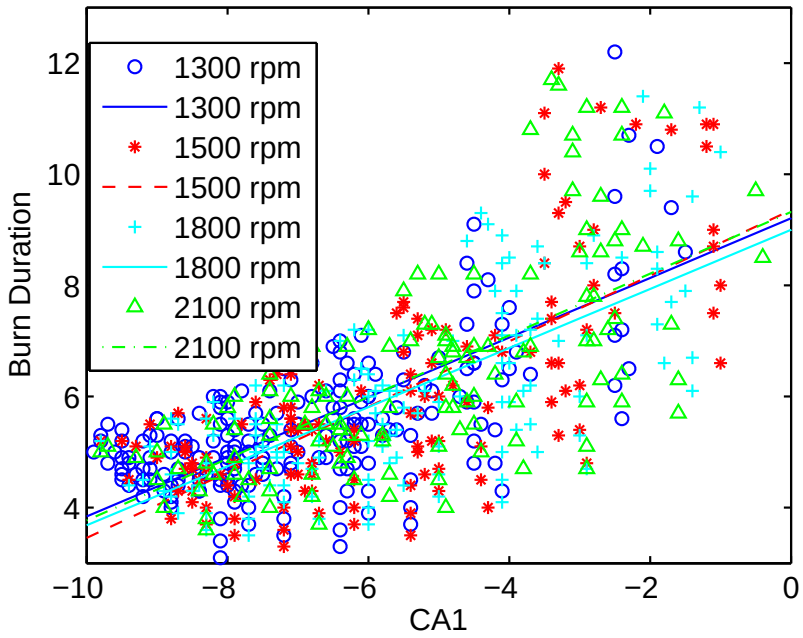

Figure 3.4: Burn duration versus the crank angle at which one percent heat release occurs and linear fit of data at each engine speed.

timing is the variable we are trying to control and the residual gas influences the next cycle $k+1$. The notation used in the following equations corresponds to the schematic of the engine presented in Figure 3.1.

First we separate the closed portion of the cycle, which occurs from intake valve closing (IVC) to exhaust valve opening (EVO), into three phases: IVC to start of combustion (SOC), SOC to the end of combustion, and expansion of the gases to EVO. Furthermore, we will model exhaust blowdown and stroke from EVO to exhaust valve closing (EVC). The result is an algebraic relationship between the gas properties at IVC and both the combustion timing and the in-cylinder gas properties at EVC.

3.2.1 Temperature Control

We control the temperature of the intake charge and ultimately the combustion timing by regulating the portion of intake charge that comes from the hot and cold manifolds (see Figure 3.1). A valve is used to control the ratio β of mass flow from

the hot and cold manifolds. Thus the overall intake manifold temperature is

$$T_{man}(k) = (1 - \beta(k))T_{hot}(k) + \beta(k)T_{cold}(k). \tag{3.3}$$

3.2.2 In-cylinder Mixing

The total mass of gas in the cylinder m_{cyl} is found using the ideal gas law at IVC,

$$m_{cyl}(k) = \frac{p_{man}(k)V_{IVC}}{RT_{IVC}(k)}, \tag{3.4}$$

and is the sum of the mass of the fresh charge and the mass of residual gas trapped from the previous cycle m_{res}. The specific gas constant $_{R=R_u/M}$ is the universal gas constant divided by the molecular weight of the gas mixture. m_{res} is determined using the ideal gas law at EVC,

$$m_{res}(k) = \frac{p_{EVC}(k-1)V_{EVC}}{RT_{EVC}(k-1)}. \tag{3.5}$$

In this equation, k indicates variables of the current engine cycle as a function of the previous cycle $(k-1)$. The temperature of the in-cylinder gases at IVC is found from the mass weighted temperature of the fresh charge and residual gases,

$$T_{IVC}(k) = \frac{m_{cyl}(k) - m_{res}(k)}{m_{cyl}(k)}T_{man}(k) + \frac{m_{res}(k)}{m_{cyl}(k)}T_{EVC}(k-1). \tag{3.6}$$

The air to fuel ratio in the cylinder AFR_{cyl} considering the additional air contained in the residual gas is,

$$AFR_{cyl}(k) = (1 - i_{cyl})(1 + AFR_{man}(k))\frac{m_{cyl}(k)}{m_{cyl}(k) - m_{res}(k)} - 1, \tag{3.7}$$

where AFR_{man} is the air to fuel ratio of the intake charge. We keep track of the mass of the species we assume to be unreactive $m_{y,i}$ at location y such as N_2, CO_2, and H_2O using an inert gas fraction $i_y = m_{y,i}/m_y$, where m_y is the total mass of gas at location y. The inert gas fraction in the cylinder is,

$$i_{cyl} = i_{EVC}(k-1)\frac{m_{res}(k)}{m_{cyl}(k)}. \tag{3.8}$$

Note that i_y is not the residual gas fraction, it does not include the unused air (composed of oxygen and nitrogen) after combustion in lean mixtures or the nitrogen in the fresh charge.

3.2.3 IVC to SOC

The in-cylinder gases undergo a polytropic compression from IVC until SOC. Therefore during this phase the in-cylinder gas temperature T_{cyl} and pressure p_{cyl} are,

$$T_{cyl}(k,\theta) = T_{IVC}(k)\left(\frac{V(\theta_{IVC})}{V(\theta)}\right)^{n_c-1}, \tag{3.9}$$

$$p_{cyl}(k,\theta) = p_{IVC}(k)\left(\frac{V(\theta_{IVC})}{V(\theta)}\right)^{n_c}, \tag{3.10}$$

where the polytropic exponent n_c is assumed to be constant and is chosen such that the motored pressure trace matches that of the CK model, which includes temperature dependent specific heats and heat transfer. The in-cylinder pressure at intake valve closing p_{IVC} is assumed to be equal to the manifold pressure p_{man}. The cylinder volume is found from the slider crank equation [33]

$$V(\theta) = V_c + \frac{\pi B^2}{4}\left(l + a - a\cos\theta - \sqrt{l^2 - (a\sin\theta)^2}\right), \tag{3.11}$$

the parameters from this equation can be found in Table 2.1.

3.2.4 SOC to CA50

The start of combustion occurs when the in-cylinder temperature T_{cyl} and pressure p_{cyl} lie on the ignition line equation (3.1) and θ_{SOC} is the argument of $T_{SOC}(\theta)$ when the ignition line is crossed. T_{SOC} and p_{SOC} are found from (3.9)-(3.10) with (3.11) evaluated at θ_{SOC}. It is assumed that the fuel reacts instantaneously at the crank angle where 50% of the heat is released (CA50). CA50 occurs $\Delta\theta$ after the start of combustion θ_{SOC} and the combustion duration is found from equation (3.2). The in-cylinder pressure and temperature adhere to equations (3.9) and (3.10) until,

$$\theta_{CA50} = \theta_{SOC} + \Delta\theta, \tag{3.12}$$

at which,

$$T_{CA50} = T_{bc} + \Delta T, \tag{3.13}$$

where T_{bc} is the in-cylinder gas temperature before combustion found from equation (3.9) evaluated at θ_{CA50}. The temperature rise due to combustion is,

$$\Delta T(k) = \frac{\eta_c Q_{LHV}}{c_v} \frac{1 - i_{cyl}(k)}{1 + AFR_{cyl}(k)}, \tag{3.14}$$

where the combustion efficiency η_c accounts for incomplete combustion and is assumed to be constant, Q_{LHV} is the lower heating value of the fuel, and c_v is the specific heat at constant volume of the in-cylinder gas. The pressure after combustion θ_{CA50} can be found using the ideal gas law.

3.2.5 CA50 to EVO

The gas then undergoes a polytropic expansion until the exhaust valve opens, the in-cylinder pressure and temperature at EVO are,

$$T_{EVO}(k) = T_{CA50}(k) \left(\frac{V(\theta_{CA50})}{V(\theta_{EVO})} \right)^{n_e - 1}, \tag{3.15}$$

$$p_{EVO}(k) = p_{CA50}(k) \left(\frac{V(\theta_{CA50})}{V(\theta_{EVO})} \right)^{n_e}. \tag{3.16}$$

3.2.6 Exhaust Blowdown

At exhaust valve opening it is assumed that the gas undergoes an adiabatic expansion from the pressure at EVO p_{EVO} down to the exhaust manifold pressure and there is a drop in temperature ΔT_{ex} due to heat loss,

$$T_{EVC}(k) = T_{EVO}(k) \left(\frac{p_{EVC}(k)}{p_{EVO}(k)} \right)^{(n_e - 1)/n_e} + \Delta T_{ex}. \tag{3.17}$$

3.2.7 Residual Gas State

The inert gas fraction assuming complete combustion is,

$$i_{EVC}(k) = \left(\frac{1 + AFR_{stoich}}{1 + AFR_{cyl}(k)} \right) (1 - i_{cyl}(k)) + i_{cyl}(k), \tag{3.18}$$

where AFR_{stoich} is stoichiometric air to fuel ratio.

3.3 Results and Discussion

The natural gas HCCI engine model presented in this chapter is compared to the detailed chemical kinetic model outlined in Appendix A. Figure 3.5 shows the error in CA50, $e_{CA50} = \theta_{CA50,0D} - \theta_{CA50,SM}$ between the zero-dimension model and the simple model presented here. Each circle is the average difference in CA50, e_{CA50}, for a fixed intake pressure p_{intake} spanning the range of intake temperatures T_{intake} and equivalence ratios ϕ in Table 3.1 at 1300 RPM. The error bars show the standard deviation for each fixed intake pressure.

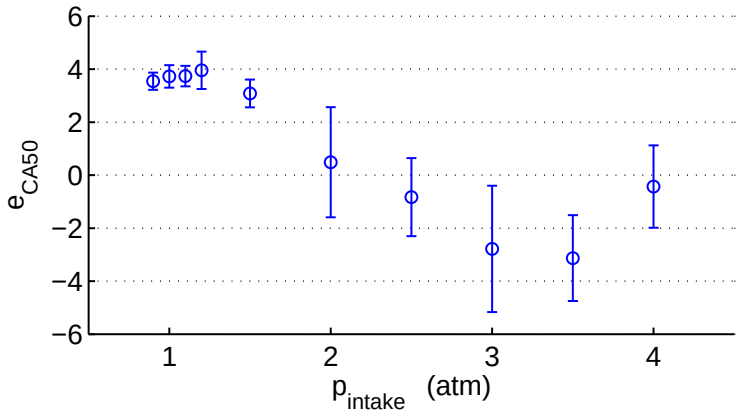

Figure 3.5: Average error between CA50 predicted by the detailed chemical kinetic model and the simple model for 1300 RPM and various T_{intake} and ϕ plotted versus p_{intake}. The error bars indicate the standard deviation.

Figure 3.5 shows that there is consistently three to four degrees of bias error in CA50 between the models around atmospheric intake pressure. As the intake pressure increases the average error decreases; however, the standard deviation increases. The simple model predicts CA50 early at low intake pressures and late for higher intake pressures. In some cases for higher RPM and intake pressures the simple model does not predict ignition. This discrepancy occurs because the model does not accurately predict the motored pressure over the whole range of intake pressures. The polytropic exponent during compression n_c is picked so that the motored pressure matches that of the detailed chemical kinetic model at an intake pressure of 2.5 atm and an intake temperature of 435 K. Because n_c is fixed the simple model overpredicts the motored pressure and temperature at low

intake pressures and underpredicts these at higher intake pressures. This error is due to two reasons, at higher intake pressures less temperature is required to ignite the mixture so the accompanying intake temperature at high intake pressures is typically lower, which necessitates a larger polytropic exponent n_c. Secondly, at higher intake pressures there is more mass in the cylinder while the surface area is the same so proportionally there is less heat transfer per mass of gas.

Furthermore, an increase in the standard deviation is due to using a single line to approximate the variation present in the data for the ignition line in Figure 3.3 and in the correlation for the burn duration in Figure 3.4. This scatter occurs in part because the ignition line (3.1) is not a function of the equivalence ratio. If the engine were expected to operate over a smaller range of intake pressures we anticipate that this model will provide better results. For example, naturally aspirated automobile engines typically operate at $p_{intake} \cong 1\ atm$, this condition is easier to model.

To improve the performance of the model over the range of intake pressures it is possible to compensate for the errors in the motored pressure by adjusting the ignition line. By requiring the line to pass through a point corresponding to an intake pressure of 2.5 atm (the midpoint intake pressure in this study) and rotating it clockwise about this point the modified ignition line will require more pressure and temperature for ignition than the original ignition line at low intake pressures and less at higher intake pressures. Figure 3.6 shows the modified ignition line for 1300 RPM. Figure 3.7 presents the error in CA50 when the modified ignition line is used for all RPM and conditions listed in Table 3.1. We can see from Figure 3.7 that the mean error in CA50 is closer to zero and the standard deviation is within two CAD for low intake pressures except for $p_{intake} = 1.1$ atm and well within 4 CAD at higher intake pressures. With this modification ignition is predicted for all cases.

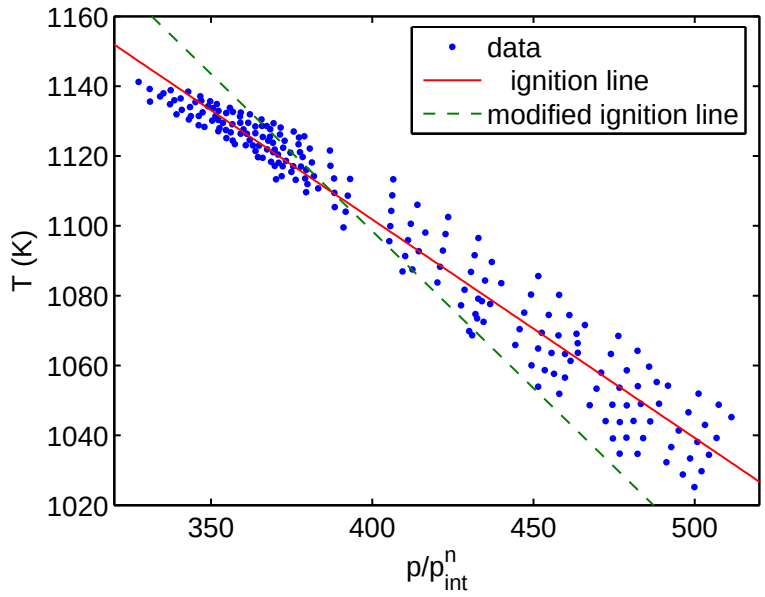

Figure 3.6: Motored temperature versus normalized motored pressure at which one percent heat release occurs. Solid red is the ignition line and the dashed green line is the modified ignition line.

3.4 Control Formulation

Equations (3.1)-(3.18) are combined to form one relation between the conditions at IVC and EVC. It is assumed that the exhaust manifold pressure p_{ex} is constant, which is close to reality except when the engine is turbocharged. First, we insert (3.9) and (3.10) into (3.1) and arrive at

$$T_{IVC}(k)\left(\frac{V(\theta_{IVC})}{V(\theta_{soc})}\right)^{n_c-1} = b_1 p_{man}^{(1-n)}(k)\left(\frac{V(\theta_{IVC})}{V(\theta_{soc})}\right)^{n_c} + b_2, \tag{3.19}$$

we then solve equation (3.19) for θ_{soc}

$$\theta_{soc} = f(T_{IVC}(k), p_{man}(k), V(\theta_{IVC}), b_1, b_2). \tag{3.20}$$

The in-cylinder temperature at the end of the cycle

$$T_{EVC}(k) = \Bigg[T_{IVC}(k)\left(\tfrac{V_{IVC}}{V_{CA50}}\right)^{n_c-1} + \tfrac{c_1}{1+AFR_{man}(k)}\left(1-\tfrac{c_2}{p_{man}(k)}\tfrac{T_{IVC}(k)}{T_{EVC}(k-1)}\right)\Bigg]^{\frac{1}{n_e}}\left(T_{IVC}(k)\tfrac{p_{EVC}}{p_{man}(k)}\tfrac{V_{CA50}}{V_{IVC}}\right)^{\frac{(n_e-1)}{n_e}}, \tag{3.21}$$

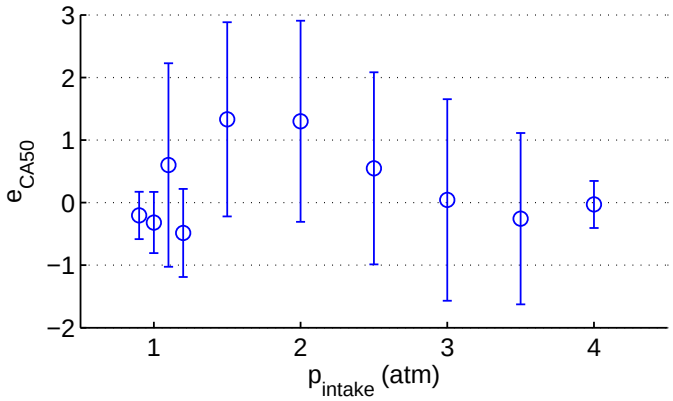

Figure 3.7: Average error between CA50 predicted by the CK model and the simple model using the modified ignition line for various T_{intake}, ϕ, and RPM, plotted versus p_{intake}. The error bars indicate the standard deviation.

depends on the current value of several parameters, and on the exhaust temperature from the past cycle $T_{EVC}(k-1)$. The in-cylinder temperature at IVC

$$T_{IVC}(k) = \frac{(1-\beta)T_{hot}(k) + \beta T_{cold}(k)}{1 - \frac{c_2}{p_{man}(k)}\left(1 - \frac{(1-\beta)T_{hot}(k)+\beta T_{cold}(k)}{T_{EVC}(k-1)}\right)}, \tag{3.22}$$

appears in (3.21) multiple times. The constants appearing in equations (3.21) and (3.22) are $c_1 = \eta_c Q_{LHV}/c_v$ and $c_2 = p_{EVC}V_{EVC}/V_{IVC}$.

The inert gas fraction does not appear in the control formulation of the simple model, because it cancels out when the equation for AFR_{cyl} (3.7) is substituted into the equation for ΔT (3.14). Finally, the state-space model is,

$$\begin{aligned} x&=T_{EVC}, \\ u&=\beta, \\ d&=[T_{hot} \quad T_{cold} \quad p_{man} \quad AFR_{man}]^T, \\ y&=CA50. \end{aligned}$$

where x is the state, u is the control input, d is made up of the measured disturbances, and y is the measured output. We desire to regulate CA50, which can be calculated as,

$$CA50(k) = (1+b_3)\theta_{soc} + b_4. \tag{3.23}$$

3.5 Model-Based Control

Due to the simplicity of this HCCI engine model we can use it to construct a feedforward controller. And because the model is first order we can construct a dead beat controller in which we can go to the desired setpoint in one time step. The control signal is constructed by determining the desired θ_{soc} based on equation (3.23). The volume at CA50 can then be determined using the slider crank equation (3.11) which allows us to determine T_{IVC} using equation (3.19). Finally, we can determine the required manifold temperature (temperature control valve position β) when we either measure directly or estimate the residual gas temperature, using equation (3.22). The residual gas temperature can be estimated using equation (3.21). Figure 3.8 shows a block diagram of the feedforward control scheme. The controller requires the manifold pressure, the residual gas temperature and the desired combustion timing. Additionally integral compensation is used to eliminate steady state errors which invariably exist due to modeling errors and disturbances.

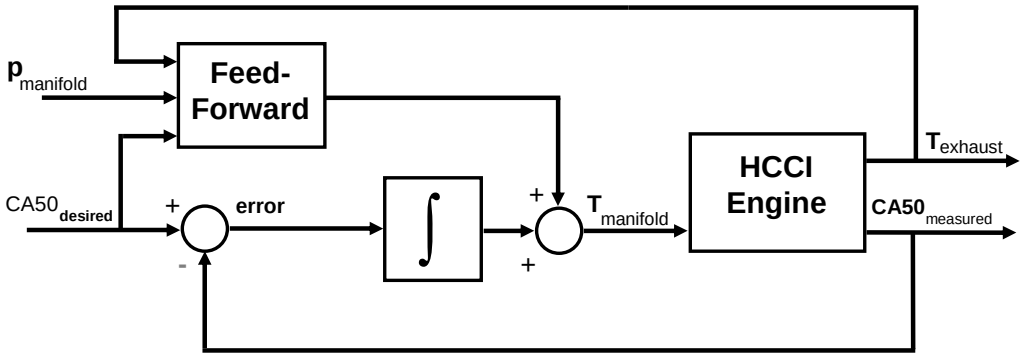

Figure 3.8: Block diagram of model based feedforward plus integral controller implementation on HCCI engine.

The controller is simulated using Matlab Simulink using the CK model with detailed chemical kinetics explained in Appendix A, except this model includes the capture of hot residual gas from the previous cycle. Figure 3.9 shows that

the feedforward controller is able to instantaneously make changes to the manifold temperature to arrive at a combustion timing near the desired value, and the integral controller is able to compensate for the modeling errors within a few engine cycles. This model is therefore very promising for control of an HCCI engine during speed and load transients.

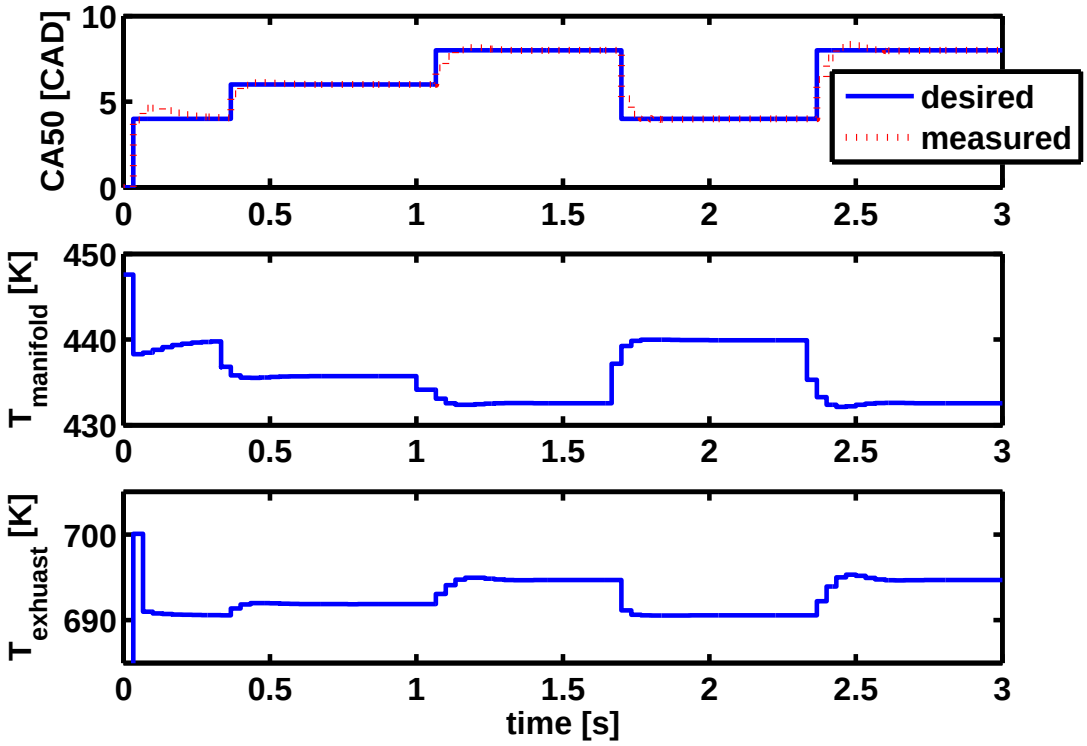

Figure 3.9: Simulations of CK HCCI engine model with model based feedforward controller plus integral action. The top plot shows the controller's ability to track the combustion timing. The manifold temperature is quickly adjusted by the controller during step changes in the combustion timing and that the integral controller gives zero steady state error.

3.6 Gasoline Model

The model is now extended to high-octane gasoline fueled HCCI engine combustion by deriving an ignition line for this fuel. High octane gasoline exhibits little low temperature heat release and ignition occurs at high temperatures, similar to

natural gas, making this type of model valid.

3.6.1 Ignition Line

The CK model is run with a chemical mechanism for iso-octane [21] and the chemical kinetics are solved using Cantera [27]. The engine parameters for the simulations correspond to a single cylinder automotive size HCCI engine [90]. The engine has a compression ratio of 15.2:1, a bore of 89 mm, and a stroke of 105.8 mm. Additionally, the temperature of the intake mixture going into the engine can be controlled. Simulations were run for various combinations of conditions: the intake pressure at both 0.8 and 1 atm, intake temperature ranging from 420 to 475 K, equivalence ratios of 0.2, 0.3, and 0.4, and at 1500, 2500, and 3500 RPM. Simulations in which CA50 is outside the range of [-5, 10] CAD ATDC were discarded.

For each run of the CK model the crank angle degree in which 1% heat release occurs, CA1, is determined and the motored pressure and temperature is noted. Figure 3.10 is a plot of the motored temperature versus motored pressure divided by p_{intake}^{n}, with $n = 0.8$. Each data point corresponds to a simulation of the CK HCCI model.

A line is fit to the data plotted in Figure 3.10 for each RPM resulting in an ignition line

$$T_{cyl}(\theta_{SOC}) = b_1 \frac{p_{cyl}(\theta_{SOC})}{p_{man}^{n}} + b_2. \tag{3.24}$$

The slope b_1 is almost independent with RPM, which results in parallel lines in Figure 3.10 while the constant b_2 increases with RPM.

3.6.2 Burn Duration

The burn duration in this case is found from experimental data from a single cylinder research HCCI engine [90], since the single-zone CK model is not able to capture the temperature and mixture stratification within the cylinder that influence the burn duration. The following equation

$$\Delta\theta(k) = b_{SOC}\theta_{SOC}(k) + b_{AFR}AFR_{cyl}(k) + b_5, \tag{3.25}$$

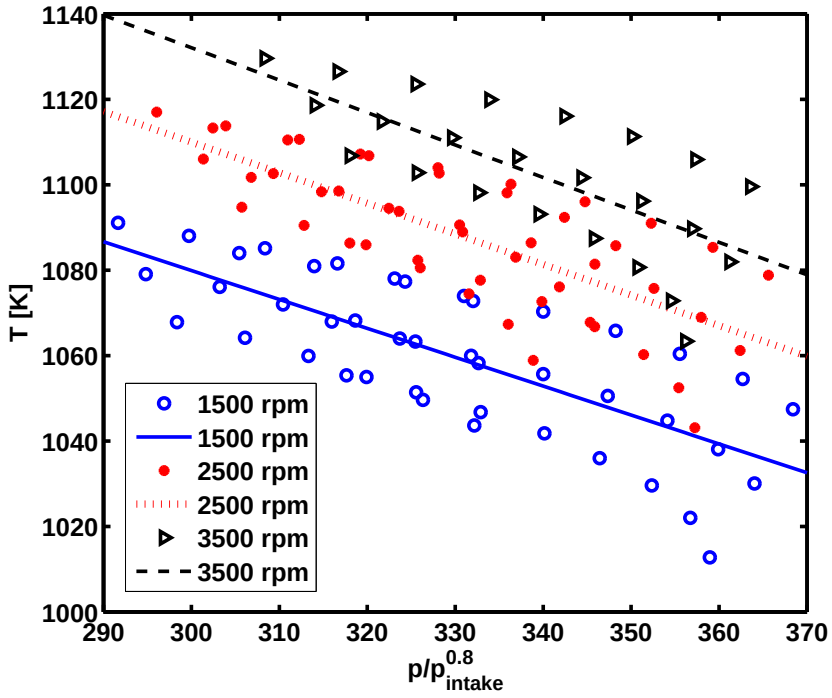

Figure 3.10: Motored temperature versus normalized motored pressure at which one percent heat release occurs for multiple speeds. Ignition lines plotted are least squares fits to the data for each speed.

is fit to the experimental data using the constants b_{SOC}, b_{AFR}, and b_5. Here in contrast to the natural gas model, we also added a second term to account for the effect of the air to fuel ratio (AFR) on the burn duration. An AFR closer to stoichiometric produces more heat and thus a shorter burn duration.

3.6.3 Comparison with Experimental Engine

The gasoline fueled HCCI engine model presented in this section is compared to pressure data from a single cylinder experimental HCCI engine [90]. The gas temperature at intake valve close in the engine differs from the manifold temperature due to heat transfer from the hot intake gas to the metal engine and because of the hot residual gas that stays in the cylinder and mixes with the fresh gas. Both of these effects change with the AFR. As the AFR decreases the relative amount of fuel increases, delivering more heat to the walls and increasing the burned gas

temperature and thus the residual gas temperature. Both of these effects advance the combustion phasing.

It was found by Dec & Sjöberg [22] that for single stage fuels (fuels without low temperature heat release) the stoichiometry has little effect on combustion phasing, but that the advancing combustion that occurs with a decrease in AFR is due to hotter residual gases and cylinder walls. Thus, the measured manifold temperature from the experiments was not used in the model, and the temperature at intake valve close was found using the procedure outlined in the paper by Sjöberg & Dec [76]. It is assumed in this procedure that the volume of gas inducted into the engine at a the same RPM is constant. Therefore, the volume of air inducted into the engine when it is motored with the intake air adjusted to the same temperature as the coolant can be compared to firing cases, since the former condition is easier to characterize. Using the ideal gas law for both the "base" motored case and the condition of interest the effective intake temperature is,

$$T_{in,effective} = T_{in,effective,base} \frac{m_{air,base}}{m_{air+fuel}} \frac{M_{air+fuel}}{M_{air}} \frac{p_{in}}{p_{in,base}}, \tag{3.26}$$

where $T_{in,effective,base}$ is the measured manifold temperature during motored operation. $m_{air,base}$ and $m_{air+fuel}$ are the mass of air inducted in the base case and the mass of fuel and air inducted in the case of interest. While $M_{air,base}$ and $M_{air+fuel}$ are the molecular weights of air in the base case and that of fuel and air mixture in the case of interest. And $p_{in,base}$ and p_{in} are the intake pressure in the base case and the case of interest, respectively.

Figure 3.11 plots pressure traces from the experimental engine [90] and the model outlined in this chapter at 1500 RPM. For the experiments the measured manifold intake temperature was held fixed while the AFR is swept, but for the model the effective intake temperature was found using equation (3.26) such that $T_{man} = T_{in,effective}$. Figure 3.11 shows that the simple model is able to capture the trend with varying AFR, and with only a few CAD of error in CA50.

Pressure traces with variation of the manifold temperature and a fixed AFR are plotted in Figure 3.12. The model predicts combustion fairly well for the cases with hotter manifold temperatures, but predicts late combustion for 136 and 138$°C$. The model fails to predict combustion for a manifold temperature of

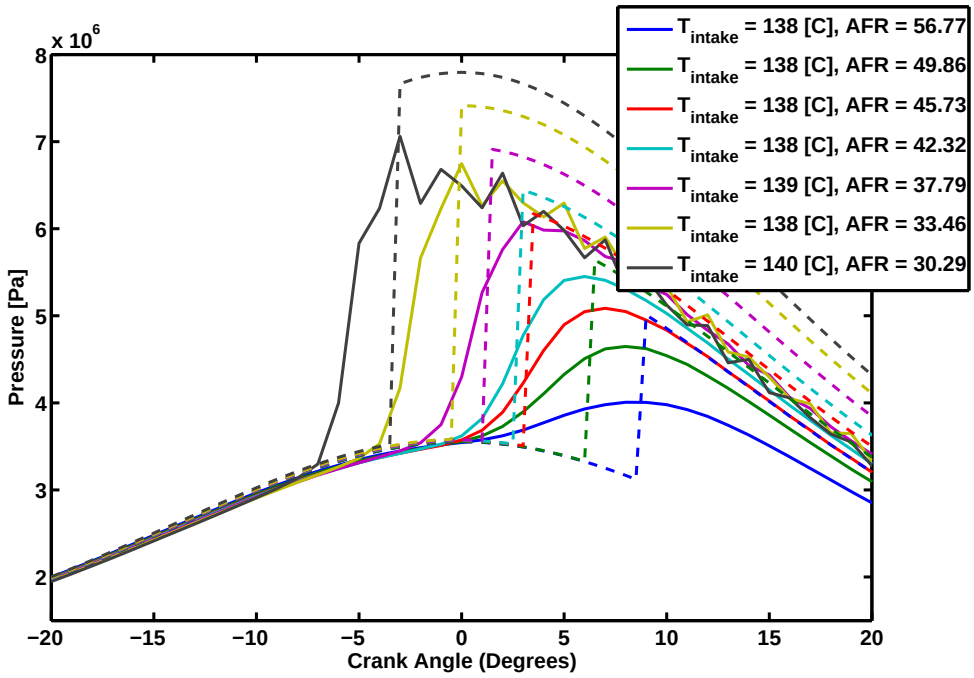

Figure 3.11: Pressure traces from experimental (solid) HCCI engine and the simple model (dashed) at 1500 RPM with a fixed intake temperature and sweep of the AFR.

$124°C$, however this operating point is rather unstable and would yield high CO and UHC so it is not a likely operating point.

3.7 Conclusions

We have presented a simple cycle-by-cycle model of an HCCI engine that relates the combustion timing $CA50(k)$ for the current cycle and in-cylinder temperature at EVC $T_{EVC}(k)$ to the past cycle's $T_{EVC}(k-1)$ and various measured parameters from the current cycle including the control variable $\beta(k)$. This model uses an ignition line derived in Section 3.1, which is a function of the motored in-cylinder pressure and temperature to predict the start of combustion. The simple model developed for natural gas fueled HCCI is compared to a CK model of HCCI combustion including detailed chemical kinetics and it is found that the simple model predicts ignition early at lower intake pressures and late for higher intake pressure,

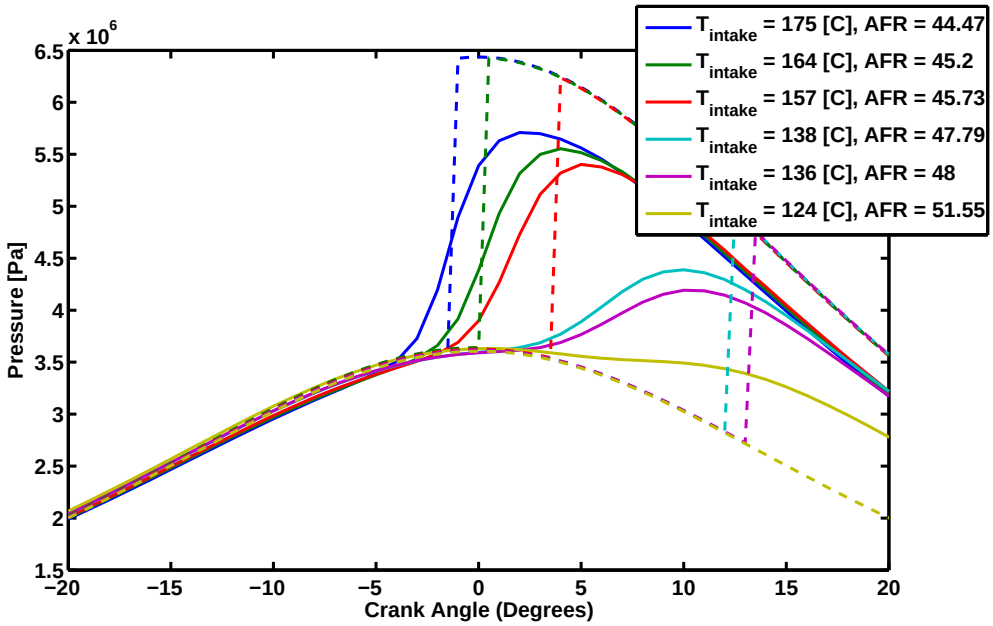

Figure 3.12: Pressure traces from experimental (solid) HCCI engine and the simple model (dashed) at 1500 RPM with a sweep of the intake temperature and a fixed AFR.

the ignition line is modified to correct for this discrepancy. After this modification the simple model is found to agree fairly well with the CK model over a range of simulation conditions. A model based controller was developed and found to give good transient performance when simulated on the detailed chemical kinetic model.

Furthermore, the model was adapted to predict combustion in a gasoline fueled HCCI engine with good results. The model was was compared to experimental data and found to predict the trends in ignition with both varying manifold temperature and air to fuel ratio.

This chapter is in part a reprint of the material as it appears in
N. J. Killingsworth, S. M. Aceves, D. L. Flowers, and M. Krstić, "A simple HCCI engine model for control," *In Proceedings of the IEEE International Conference on Control Applications*, Munich, Germany, October 2006.

N. J. Killingsworth, S. M. Aceves, D. L. Flowers, M. Janković, and M. Krstić, "A model of gasoline HCCI engine combustion for control," *In Proceedings of the 5th US Combustion Meeting*, San Diego, CA, 2007.

Chapter 4

Extremum Seeking

Typical control problems involve regulating the output of a system to a known setpoint. However, there are often cases where it is desirable to regulate the output to an optimal setpoint that is unknown or changing with time, where optimality is determined by the minimum or maximum of some cost function. These optimal setpoints are characterized by an extremum in the input-output map; a map that is often nonlinear. For such cases extremum seeking (ES), a nonmodel based online optimization method, can be used to find the optimal setpoint. Furthermore, extremum seeking is a powerful tool for determining optimal system parameters or control gains.

The first documented use of extremum seeking is Leblanc's 1922 application to electric railway systems [43]. In the 1950s and 1960s, extremum seeking was widely studied and used in applications in the former Soviet Union [17, 25, 41, 51, 50, 52] and by researchers in western countries [13, 23, 84, 88]. Interest in ES tapered off in the 1970's. However, of note is a review by Sternby [79] that appeared in 1979.

A proof showing stability of ES, which forces the estimate $\hat{\theta}(k)$ to converge to a local minimizer θ^* of the cost function $J(\theta)$ was shown in the late 1990s, in a paper by Krstic and Wang [42]. Shortly after, Rotea [67] and Walsh [87] published the first studies of multiparameter ES schemes. The availability of proofs shed light on the effect of the ES algorithm's design parameters on stability. Subsequently, ES has become a useful tool for real-time applications [9, 59, 60, 47, 91] as well as an active area of theoretical research [7].

Following is an overview of the ES algorithm, including a simplified explanation of how ES achieves convergence to the system's local optimizer. Then, we present the discrete ES equations. Finally an example of ES on a static quadratic cost function is shown.

4.1 How ES Works

Extremum seeking is a gradient based optimization method. ES differs from standard gradient based optimization algorithms in the manner it obtains the gradient information. The standard gradient optimization method is gradient descent

$$\theta(k+1)=\theta(k)-\gamma\nabla J(\theta(k)), \tag{4.1}$$

where γ is the step size and $\gamma<0$ can be used to when a maximizer rather than a minimizer is desired. Gradient descent relies on the principle that a function $J(\theta)$ decreases fastest along the negative of the gradient of J at θ, $\nabla J(\theta(k))$. The gradient descent method requires that the gradient is known, whereas ES does not require any information about the gradient or map.

As shown in Figure 4.1, ES estimates the gradient $\nabla J(\theta(k))$ by sinusoidally perturbing (with the signals $\alpha_i\cos(\omega_i k)$) the input parameters $\theta(k)$ of the system, where k is the iteration of the ES algorithm. The gradient is determined by highpass filtering (with $\frac{z-1}{z+h}$) the cost function signal $J(\theta(k))$ to remove the slow portion of the signal and then by demodulating the output by multiplication with a sinusoidal signal of the same frequency as the perturbation signal. This procedure estimates the gradient by isolating the portion of the cost function signal $J(\theta(k))$ that arises due to perturbation of the input signal. The gradient information is then used to modify the input parameters in the next iteration, specifically, the gradient estimate is integrated ($\frac{1}{z-1}$), yielding a new parameter estimate $\hat{\theta}(k)$, which converges to the optimizer θ^*. The integrator performs both the adaptation function and acts as a lowpass filter.

Here we give an intuitive argument that explains the convergence of ES. For simplicity we consider the single-parameter case in which the system input $\theta(k)$ and the estimate $\hat{\theta}(k)$ of the optimal input θ^* are scalar and only one probing

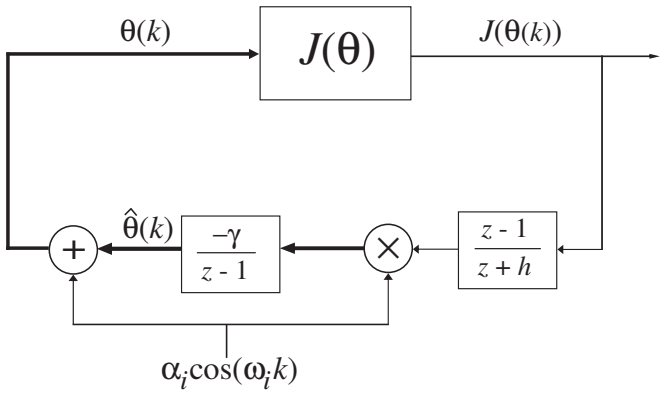

Figure 4.1: Discrete extremum seeking scheme. The input parameters $\theta(k)$ are perturbed by the signal $\alpha_i \cos(\omega_i k)$. The output of the cost function $J(\theta(k))$ is then highpass filtered, demodulated, and finally lowpass filtered to yield new input parameters.

signal $\alpha\cos(\omega k)$ is used (see Figure 4.1). We also assume a quadratic cost function $J(\theta)$ of the form

$$J(\theta) = J^* + \frac{J''}{2}(\theta^* - \theta)^2 \tag{4.2}$$

where the second derivative of the cost function with respect to θ, J'' is positive. The purpose of ES is to minimize $J(\theta)$ namely to find $\hat{\theta} = \theta^*$ such that $J(\theta) = J^*$. Let

$$\tilde{\theta} \triangleq \theta^* - \hat{\theta}, \tag{4.3}$$

denote the estimation error. Therefore substituting

$$\theta^* - \theta = \tilde{\theta} - \alpha\cos(\omega k)$$

into (4.2) yields,

$$J(\theta) = J^* + \frac{J''}{2}\Big(\tilde{\theta} - \alpha\cos(\omega k)\Big)^2. \tag{4.4}$$

Expanding this expression and then using the basic trigonometric identity $2\cos^2(\omega k) = 1 + \cos(2\omega k)$, we get

$$J = J^* + \frac{J''}{2}\tilde{\theta}^2 - \alpha\tilde{\theta}J''\cos(\omega k) + \frac{\alpha^2 J''}{2}\cos(\omega k)^2, \tag{4.5}$$

$$= J^* + \frac{\alpha^2 J''}{4} + \frac{\alpha^2 J''}{4}\cos(2\omega k) - \Big(\alpha J''\cos(\omega k)\Big)\tilde{\theta} + \frac{J''}{2}\tilde{\theta}^2. \tag{4.6}$$

The term $\frac{J''}{2}\tilde{\theta}^2$ is then omitted since it is quadratic in $\tilde{\theta}$ and we focus on local analysis only. The role of the "washout" high-pass filter $\frac{z-1}{z+h}$ in Figure 4.1 is to filter out the DC component (the first two terms of equation (4.6)) of the output signal $J(\theta(k))$. Note that the complex variable z is found using the z-transform, which is analogous to the Laplace transform in continuous time analysis. Thus,

$$\frac{z-1}{z+h}[J] \approx \frac{\alpha^2 J''}{4}\cos(2\omega k) - \left(\alpha J'' \cos(\omega k)\right)\tilde{\theta}\,. \tag{4.7}$$

This signal is then "demodulated" by multiplying equation (4.7) by $\alpha\cos(\omega k)$ yielding

$$\alpha\cos(\omega k)\frac{z-1}{z+h}[J] \approx \frac{\alpha^3 J''}{4}\cos(\omega k)\cos(2\omega k) - \left(\alpha^2 J'' \cos^2(\omega k)\right)\tilde{\theta}. \tag{4.8}$$

The last term $\alpha^2 J'' \cos^2(\omega k)\tilde{\theta}$ contains a DC component with gradient information that can be more readily seen by applying the trigonometric identities $2\cos(\omega k)\cos(2\omega k) = \cos(3\omega k) + \cos(\omega k)$ and $2\cos^2(\omega k) = 1 + \cos(\omega k)$, which gives

$$\alpha\cos(\omega k)\frac{z-1}{z+h}[J] \approx -\frac{\alpha^2 J''}{2}\tilde{\theta} + \frac{\alpha^3 J''}{8}\left(\cos(\omega k) + \cos(3\omega k)\right) - \frac{\alpha^2 J''}{2}\tilde{\theta}\cos(2\omega k). \tag{4.9}$$

The higher frequency terms with $\cos(\omega k), \cos(2\omega k)$, and $\cos(3\omega k)$ are attenuated by the integrator $\frac{1}{z-1}$, which behaves like a low pass filter, and are thus omitted. Therefore, the estimate is

$$\hat{\theta} \approx \frac{\gamma}{z-1}\left[\frac{\alpha^2 J''}{2}\tilde{\theta}\right]. \tag{4.10}$$

Using equation (4.3) and the fact that θ^* is constant

$$(z-1)[\tilde{\theta} - \theta^*] \approx -\gamma\left[\frac{\alpha^2 J''}{2}\tilde{\theta}\right], \tag{4.11}$$

$$\tilde{\theta}(k+1) - \tilde{\theta}(k) - \theta^* + \theta^* \approx -\gamma\left[\frac{\alpha^2 J''}{2}\tilde{\theta}(k)\right], \tag{4.12}$$

we arrive at,

$$\tilde{\theta}(k+1) \approx \left(1 - \frac{\gamma\alpha^2 J''}{2}\right)\tilde{\theta}(k)\,. \tag{4.13}$$

Hence, $\tilde{\theta}(k+1) < \tilde{\theta}(k)$ so the estimation error $\tilde{\theta}(k)$ decreases provided the adaptation gain γ and the probing amplitude α are chosen such that the positive quantity

$\frac{\gamma\alpha^2 J''}{2}$ is small. It is important to note that the perturbation frequency ω must be sufficiently high enough relative to to γ, α, h, and J'' for this analysis to hold true.

The complete proof of stability presented in [18] is considerably more involved, and is based on two-time-scale averaging [8] for the system

$$\tilde{\theta}(k+1)=\tilde{\theta}_k + \gamma\alpha\cos(\omega k)\left(e + \frac{J''}{2}\left(\tilde{\theta} - \alpha\cos(\omega k)\right)^2\right), \tag{4.14}$$

$$e(k+1)=-he(k) - (1+h)\frac{J''}{2}\left(\tilde{\theta} - \alpha\cos(\omega k)\right)^2, \tag{4.15}$$

where $e = J^* - \frac{1+h}{z+h}[J]$, with the assumption that γ and α are small. The proof guarantees exponential convergence of $J(\theta(k))$ to $J^* + O(\alpha^3)$.

Another intuitive point of view is to observe that the term $J''\tilde{\theta}$ in the signal equation (4.9) at the output of the multiplier is the gradient (derivative) of $J = J^* + \frac{J''}{2}\left(\tilde{\theta} - \alpha\cos(\omega k)\right)^2$ with respect to $\tilde{\theta}$ for $\alpha = 0$. Hence, the role of the additive probing term $\cos(\omega k)$ and the multiplicative term of the same form (along with the filtering effects of the washout filter and the integrator) is to estimate the gradient of J, which is then fed into the integrator, employing classical gradient-based optimization with step size γ (see equation (4.1)). While gradient-based methods usually require a model to determine the gradient, ES estimates the gradient in a non-model-based manner.

An interesting aspect of ES is the role of the signal $\cos(\omega k)$, which mimics amplitude modulation (AM) in analog communications. This similarity is not obvious since ES employs one addition and one multiplication block rather than two multipliers. The addition block is used because the nonlinearity $J(\theta)$ provides the effect of multiplication since its quadratic part generates a product of $\cos(\omega k)$ and $\tilde{\theta}$, which carries the gradient information discussed above. The modulation, demodulation, and filtering serve to extract the gradient information $J''\tilde{\theta}(k)$ from the signal $J(\theta(k))$.

4.2 ES Equations

The time-domain implementation of the multiparameter discrete-time ES algorithm in Figure 4.1 is

$$\zeta(k) = -h\zeta(k-1) + J(\theta(k-1)), \tag{4.16}$$

$$\hat{\theta}_i(k+1) = \hat{\theta}_i(k) - \gamma_i \alpha_i \cos(\omega_i k)[J(\theta(k)) - (1+h)\zeta(k)], \tag{4.17}$$

$$\theta_i(k+1) = \hat{\theta}_i(k+1) + \alpha_i \cos(\omega_i(k+1)), \tag{4.18}$$

where $\zeta(k)$ is a scalar and the subscript i indicates the i^{th} entry of a vector (note that ζ does not appear in Figure 4.1, but the use of this variable facilitates presenting the equations). γ_i is the adaptation gain, and α_i is the perturbation amplitude. Stability and convergence are influenced by the values of γ, α, and the shape of the cost function $J(\theta)$ near the minimizer. The modulation frequency ω_i is chosen such that $\omega_i = a^i\pi$, where a satisfies $0 < a < 1$. It is important that each probing signal ω_i is distinct, so that the effect of each individual signal can be determined by the algorithm. Additionally, the highpass filter $\frac{z-1}{z+h}$ is designed with $0 < h < 1$ and a cutoff frequency well below the modulation frequency ω_i.

4.3 Example

Here we present an example of the ES algorithm. Our goal is to find the minimizer for equation (4.2) with $J^* = 1$, $J'' = 2$, and $\theta^* = 5$. The ES algorithm in equations (4.16)-(4.18) are parameterized with $h = 0.5$ and $a = 0.64$. A range of adaptation gains $\gamma = 0.05, 0.1, 0.2$ with the perturbation amplitude $\alpha = 0.2$ were tried, with the results shown in Figure 4.2. We can see from this figure that convergence is achieved much more quickly as γ is increased; however, if this parameter is chosen too large stability is affected. And in Figure 4.3 we use $\gamma = 0.05$ and vary the perturbation amplitudes $\alpha = 0.2, 0.4, 0.6$. The rate of convergence increases as α is increased, but the magnitude of oscillation about the minimizer θ^* is greater due to the larger perturbation amplitude.

This chapter is in part a reprint of the material as it appears in

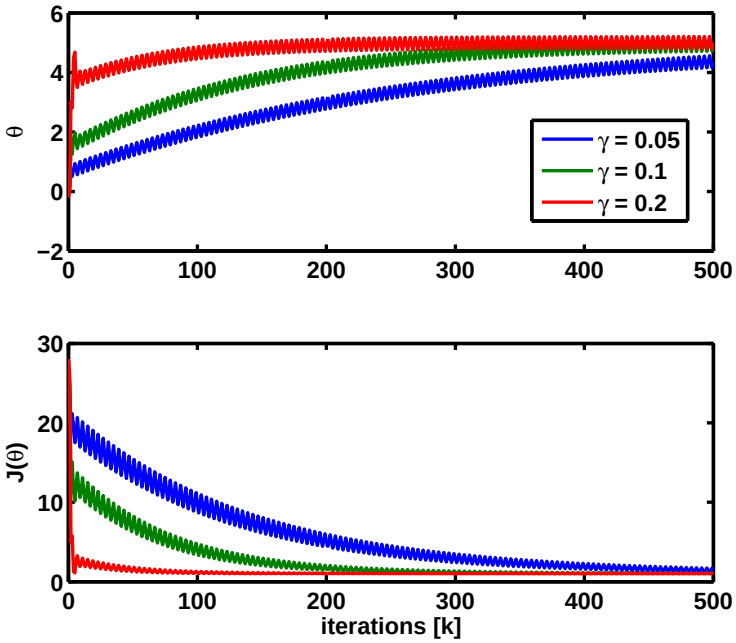

Figure 4.2: Response of the discrete extremum seeking scheme with variation in the adaptation gain γ.

N. J. Killingsworth and M. Krstić, "PID Tuning Using Extremum Seeking: Online, Model-Free Performance Optimization," *IEEE Control Systems Magazine*, vol. 26, no. 1, pp. 70–79, 2006.

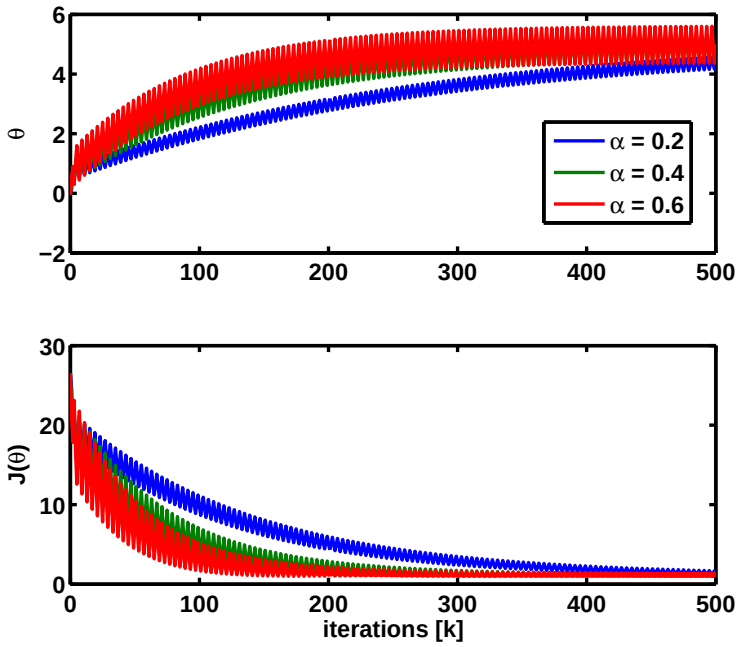

Figure 4.3: Response of the discrete extremum seeking scheme with variation in the perturbation amplitude α.

Chapter 5

Minimizing Fuel Consumption Via Extremum Seeking

Modern engines have an increasing number of inputs such as exhaust gas recirculation (EGR), variable cam timing, and spark timing to deal with increasingly stringent emissions and performance requirements. Engine control structures utilize a large number of look-up tables that depend on the engine speed and torque to schedule these inputs. The values that populate the look-up tables are typically found using mapping procedures; the engine is run on a dynamometer at steady state over the range of values for each input parameter to determine the optimal value of the input for each operating point [38]. The mapping time increases exponentially with the number of inputs [60].

Many design of experiment methodologies have been developed to handle this added complexity [53]. In particular, extremum seeking has been successfully used to speed up the mapping process by Popovic et al. [60]. They found that ES determines the same engine operating points as the standard mapping procedure in a fraction of the time. ES, a non-model-based optimization method, iteratively modifies the arguments (in this application: the engine parameters) of a cost function (which quantifies the engine performance and can include emissions performance) so that the output of the cost function reaches a local minimum or local maximum (as specified by the user).

In other work ES has also been used to continuously optimize engine perfor-

mance, such a setup can account for engine to engine variation in production, as well as for changes that occur on a specific engine due to use. Draper and Li [23] studied the continuous maximization of the torque of a SI engine. Similarly, Scotson and Wellstead [70] used ES to continuously update the optimal spark timing values stored in a map, which is a function of speed and load, in the engine control unit (ECU). More recently Gäfvert et al. [26] coupled an ES controller to a standard linear feedback controller for minimizing the fuel consumption of a gasoline direct injection engine by effectively adjusting the air-to-fuel ratio of the engine.

We use a different form of ES [7] than is used in the works cited above to find the combustion timing setpoint that minimizes the fuel consumption of an experimental HCCI engine; an optimization performed while the engine is running. We implement a discrete version of ES that uses sinusoidal perturbations [7]. In the next section the form of the cost function used and how ES is applied to the problem of fuel minimization is described. Then we report the results of experimental combustion timing setpoint optimization for minimum fuel consumption on an experimental HCCI engine.

5.1 Fuel Minimization

For a given operating point, defined by the speed and torque requirement of the engine, there is a combustion timing that minimizes the fuel consumption. This optimal combustion timing balances the work extracted from the combusting gases, heat transfer losses, and combustion efficiency. When combustion begins before TDC, the combusting gases combined with decreasing cylinder volume results in high pressure and temperature impeding the piston motion. Additionally, early combustion yields high temperatures that lead to an increase in NO_x and even possibly engine damage due to excessive pressure and pressure rise rates. Early combustion timing also allows more time for heat transfer, so more of the input fuel energy is lost to the engine's cooling system. Conversely, as the combustion is retarded, the peak cylinder pressure and temperature decrease due to the motion of the retreating piston and the gas performs less work. Delaying the combustion

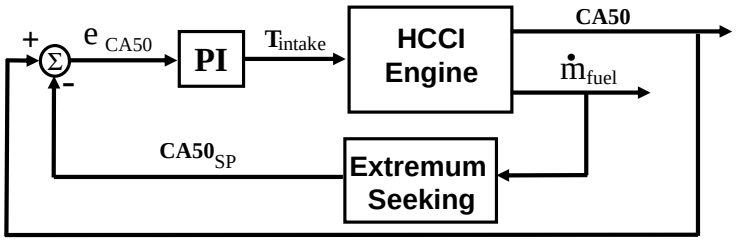

Figure 5.1: Block diagram of ES fuel minimization scheme. ES minimizes the measured fuel consumption of the HCCI engine by adjusting the combustion timing setpoint $CA50_{SP}$.

to later and later leads to incomplete combustion and possibly misfires. Therefore, some of the fuel's chemical energy fails to be released and is transported out the exhaust valve as unburned hydrocarbons and carbon monoxide. The tradeoffs in heat transfer, pressure rise rate, and combustion efficiency determine the optimal combustion timing.

5.1.1 Cost Function and Implementation

Figure 5.1 shows how ES is implemented on the experimental HCCI engine described in Chapter 2. A PI controller is used to control the combustion timing of the HCCI engine by adjusting the intake temperature while extremum seeking determines the combustion timing setpoint $CA50_{SP}$ that yields the minimum fuel consumption. The cost function minimized by ES consists of the fuel consumption averaged over 100 engine cycles,

$$J_{fuel}(\theta) \triangleq \frac{1}{n_f - n_0} \left(\sum_{n=n_0}^{n_f} \dot{m}_{fuel}(n, \theta) \right), \tag{5.1}$$

where n is the engine cycle, $\dot{m}_{fuel}(n, \theta)$ is the mass flowrate of fuel into the engine in [kg/s], and θ is the combustion timing setpoint. Here, the input parameter for

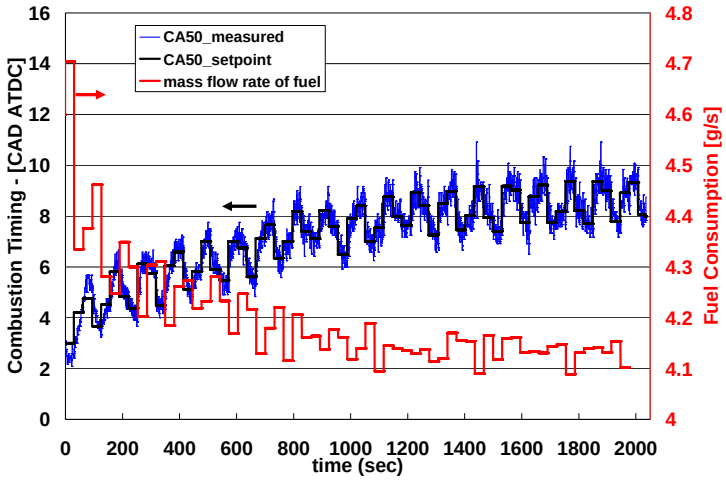

Figure 5.2: ES minimizes the fuel consumption by retarding the combustion timing from 3 to 8 CAD ATDC.

the cost function is defined as the 50% burn location, $\theta \triangleq CA50_{SP}$. The cost function $J_{fuel}(\theta)$ defined in (5.1) takes into account the fuel consumption over the interval $[n_0,n_f]$ after a delay of 200 engine cycles. This delay is intended to allow the combustion timing controller to get the engine to steady-state at the new combustion timing setpoint so that the cost is not distorted by transients while the engine stabilizes to to a new setpoint. With this delay included, ES executes every 300 engine cycles, and the cost function is evaluated for the last 100 cycles.

5.1.2 Experimental Setpoint Tuning

ES was applied to the experimental HCCI engine running at 1500 rpm. Figure 5.2 shows that ES delays the combustion timing to slightly later timing than 8 CAD ATDC, from an initial combustion timing of 3 CAD ATDC. As the combustion timing is delayed to this setpoint, fuel consumption is reduced; as can be seen on the right vertical axis of Figure 5.2.

The optimization process required around 50 iterations (approximately 30 minutes). The experiment was repeated in Figure 5.3 at the same operating point as

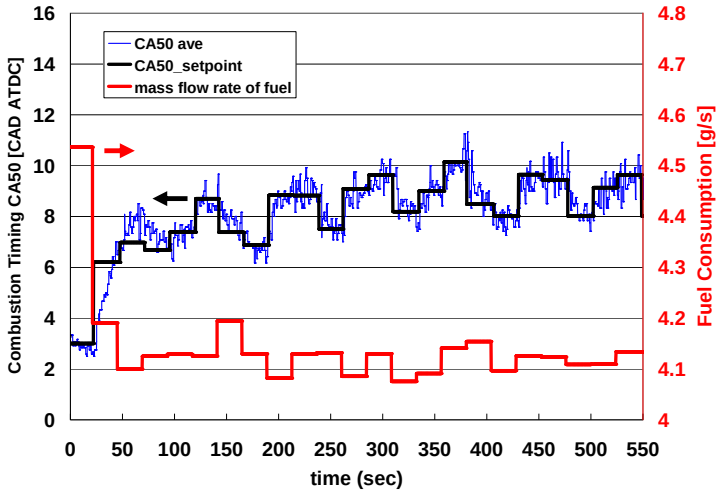

Figure 5.3: ES minimizes the fuel consumption by retarding the combustion timing from 3 to 8 CAD ATDC.

in Figure 5.2, but with a larger value of the adaptation gain, γ. ES finds the same minimum, but much more quickly (approximately 15 iterations or 10 minutes) with the larger gain. The total optimization time is also highly dependent on the wait time, n_0, and the the total number of cycles evaluated, $n_f - n_0$, in the cost function. As these parameters are reduced the amount of time for each iteration of ES is shorter.

5.2 Conclusions

ES has been shown to be a fast and effective method to map an HCCI engine. ES was used to determine combustion timing that yields the minimum fuel consumption. For engines undergoing slow transients during operation, ES can be used to continually update the optimal input parameters. This method can therefore be used on stationary engine-generator sets to minimize fuel consumption dynamically while the engine is running.

This chapter is in part a reprint of the material as it appears in

N. J. Killingsworth, S. M. Aceves, D. L. Flowers, F. Espinosa-Loza, and M. Krstić, "HCCI engine combustion timing control: optimizing gains and fuel consumption via extremum seeking," submitted to *IEEE Transactions on Control Systems Technology*, 2007.

Chapter 6

Extremum Seeking PID Tuning

Although proportional-integral-derivative (PID) controllers are widely used in the process industry, their effectiveness is often limited due to poor tuning. Manual tuning of PID controllers, which requires optimization of three parameters, is a time-consuming task. To remedy this difficulty, much effort has been invested in developing systematic tuning methods. Many of these methods rely on knowledge of the plant model or require special experiments to identify a suitable plant model. Reviews of these methods are given in [62] and the survey paper [63]. However, in many situations a plant model is not known, and it is not desirable to open the process loop for system identification. Thus a method for tuning PID parameters within a closed-loop setting is advantageous.

In relay feedback tuning [61],[46],[86], the feedback controller is temporarily replaced by a relay. Relay feedback causes most systems to oscillate, thus determining one point on the Nyquist diagram. Based on the location of this point, PID parameters can be chosen to give the closed-loop system a desired phase and gain margin.

An alternative tuning method, which does not require either a modification of the system or a system model, is unfalsified control [39], [68]. This method uses input-output data to determine whether a set of PID parameters meets performance specifications. An adaptive algorithm is used to update the PID controller based on whether or not the controller falsifies a given criterion. The method requires a finite set of candidate PID controllers that must be initially specified [39].

Unfalsified control for an infinite set of PID controllers has been developed in [68]; this approach requires a carefully chosen input signal [69].

Yet another model-free PID tuning method that does not require opening of the loop is iterative feedback tuning (IFT). IFT iteratively optimizes the controller parameters with respect to a cost function derived from the output signal of the closed-loop system, see [35]. This method is based on the performance of the closed-loop system during a step response experiment [45], [44].

In this chapter we present a method for optimizing the step response of a closed-loop system consisting of a PID controller and an unknown plant with a discrete version of extremum seeking (ES). Specifically, ES minimizes a cost function similar to that used in [45], [44], which quantifies the performance of the PID controller. ES, which is a non-model-based method, iteratively modifies the arguments (in this application the PID parameters) of a cost function so that the output of the cost function reaches a local minimum or local maximum.

In the next section we discuss the cost function and the form of the PID controller used in this work. We then outline how ES is used for PID tuning. We illustrate this technique through simulations comparing the effectiveness of ES to other PID tuning methods. Next, we address the importance of the choice of cost function and consider the effect of controller saturation. Furthermore, we discuss the choice of ES tuning parameters. Finally, we offer some conclusions.

6.1 Cost Function and PID Controllers

Extremum seeking is used to tune the parameters of a PID controller so as to minimize a given cost function. The cost function, which quantifies the effectiveness of a given PID controller, is evaluated at the conclusion of a step response experiment. We use the ISE (integral squared error) cost function

$$J(\theta) \triangleq \frac{1}{T - t_0} \int_{t_0}^{T} e^2(t, \theta) dt, \tag{6.1}$$

where the error $e(t,\theta) \triangleq r(t) - y(t,\theta)$ is the difference between the reference and the output signal of the closed-loop system, and

$$\theta \triangleq [K, T_i, T_d]^T \tag{6.2}$$

contains the PID parameters. The PID controller structure and the meaning of K, T_i, and T_d are given below.

The cost function $J(\theta)$ defined in (6.1) takes into account the error over the time interval $[t_0,T]$. By setting t_0 to approximate the time T_{peak} at which the step response of the closed-loop system reaches the first peak, the cost function $J(\theta)$ effectively places zero weighting on the initial transient portion of the response [45]. Hence, the controller is tuned to minimize the error beyond the peak time T_{peak} without constraints on the initial transient.

We use a standard PID controller

$$u(t)=K\left(e(t) + \frac{1}{T_i}\int_0^t e(\tau)d\tau + T_d\frac{dy(t)}{dt}\right), \tag{6.3}$$

with the exception that the derivative term acts on the measured plant output but not on the reference signal. This PID controller avoids large control effort during a step change in the reference signal. Figure 6.1 shows a block diagram of the closed-loop system, where G is the unknown plant. The controller is parameterized as

$$C_r(s) = K\left(1 + \frac{1}{T_i s}\right), \tag{6.4}$$

$$C_y(s) = K\left(1 + \frac{1}{T_i s} + T_d s\right), \tag{6.5}$$

and r, u, and y are the reference signal, control signal, and output signal, respectively.

6.2 Extremum Seeking Tuning Scheme

The cost function $J(\theta)$ should be understood as a mapping from the PID parameters K, T_i, and T_d to the tracking performance. ES seeks to tune the PID

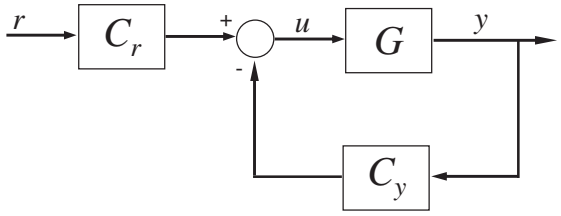

Figure 6.1: Closed-loop servo system. The output signal y of the unknown plant G is regulated to the reference signal r by the two-degree-of-freedom controller C_r and C_y.

controller by finding a minimizer of $J(\theta)$. However, since ES is a gradient method, the PID parameters found by ES are not necessarily a global minimizer of $J(\theta)$.

The overall ES PID tuning scheme is summarized in Figure 6.2. The step response experiment, which is contained within the dashed box, is run iteratively. The cost $J(\theta(k))$ is calculated at the conclusion of the step response experiment. The ES algorithm uses the value $J(\theta(k))$ of the cost function to compute new controller parameters $\theta(k)$. Another step function experiment is then performed with the new controller parameters, and the process continues iteratively.

The time-domain implementation of the discrete-time ES algorithm in Figure 4.1 is

$$\zeta(k) = -h\zeta(k-1) + J(\theta(k-1)), \tag{6.6}$$

$$\hat{\theta}_i(k+1) = \hat{\theta}_i(k) - \gamma_i \alpha_i \cos(\omega_i k)[J(\theta(k)) - (1+h)\zeta(k)], \tag{6.7}$$

$$\theta_i(k+1) = \hat{\theta}_i(k+1) + \alpha_i \cos(\omega_i(k+1)), \tag{6.8}$$

where $\zeta(k)$ is a scalar and the subscript i indicates the i^{th} entry of a vector. γ_i is the adaptation gain, and α_i is the perturbation amplitude. Stability and convergence

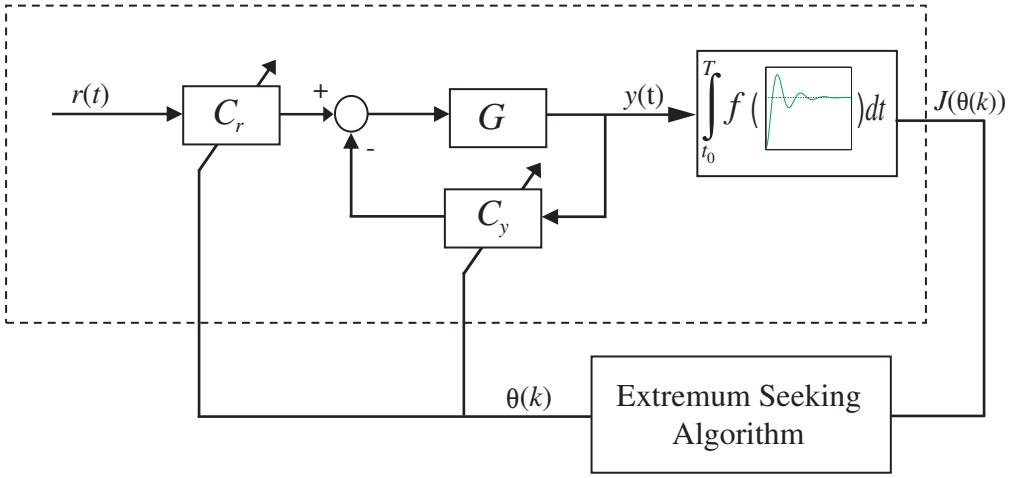

Figure 6.2: The overall extremum seeking PID tuning scheme. The ES algorithm updates the PID controller parameters $\theta(k)$ to minimize the cost function $J(\theta)$, which is calculated from a step response experiment carried out within the dashed box.

are influenced by the values of γ, α, and the shape of the cost function $J(\theta)$ near the minimizer, as explained in Chapter 4. The modulation frequency ω_i is chosen such that $\omega_i = a^i\pi$, where a satisfies $0 < a < 1$. Additionally, the highpass filter $\frac{z-1}{z+h}$ is designed with $0 < h < 1$ and a cutoff frequency well below the modulation frequency ω_i.

The PID tuning in this section comprises a novel hybrid application, where the plant dynamics are continuous time and the ES dynamics are discrete time.

6.3 Examples of Extremum Seeking PID Tuning

We now demonstrate ES PID tuning and compare this method with IFT and two classical PID tuning methods, namely, Ziegler-Nichols (ZN) tuning rules and internal model control (IMC). In particular, we use the ultimate sensitivity method

[64] version of the ZN tuning rules, which consists of a closed-loop experiment with only proportional feedback, where the feedback gain is increased to a critical value until the system begins to oscillate. PID parameters are then prescribed based on the critical gain K_c and the period T_c of oscillation to give the closed-loop system response approximately a quarter amplitude decay ratio, which corresponds to a damping ratio of about 0.2. The amplitude decay ratio is the ratio of two consecutive maxima of the error e after a step change of the reference signal. Specifically, the PID parameters given by ZN are $K = K_c/1.7, T_i = T_c/2$, and $T_d = T_c/8$.

Details of IMC can be found in [62], where the plant is assumed to have the form

$$G(s) = \frac{K_p}{1 + sT} e^{-sL}. \tag{6.9}$$

Based on (6.9), the PID parameters are chosen to be of the form $K = \frac{2T+L}{2K_p(T_f+L)}, T_i = T + L/2$, and $T_d = \frac{TL}{2T+L}$, where T_f is a design parameter that affects the tradeoff between performance and robustness. When the plant is unknown, a step response experiment can be used to obtain an estimate of the form (6.9) as explained in [62]. Although variations of IMC that can deal with alternative model structures are available in [66] and [37], these methods are not considered here. We note that ZN and IMC are derived for a PID structure with derivative action on both the reference signal and the output signal rather than the structure (6.4), (6.5), which does not have derivative action on the reference signal.

In [44] IFT, ZN, and IMC are applied to the models

$$G_1(s) = \frac{1}{1+20s}e^{-5s}, \tag{6.10}$$

$$G_2(s) = \frac{1}{1+20s}e^{-20s}, \tag{6.11}$$

$$G_3(s) = \frac{1}{(1+10s)^8}, \tag{6.12}$$

$$G_4(s) = \frac{1-5s}{(1+10s)(1+20s)}. \tag{6.13}$$

Notice that G_1 and G_2 have time delays, G_3 has repeated poles, and G_4 is non-minimum phase. We apply ES to (6.10)–(6.13) to facilitate comparison with the IFT, ZN, and IMC PID controllers found in [44].

The closed-loop systems are simulated using a time step of 0.01 s, and the time delays are approximated using a third-order Padé approximation to be consistent with [44]. The PID controller parameters given by ZN are used as a starting point for ES tuning. For all simulations the parameters a and h in the ES scheme (6.6)–(6.8) are set to 0.8 and 0.5, respectively.

6.3.1 Tuning for G_1

ES PID tuning is applied to G_1 in (6.10), which has a time delay of 5 s. For these simulations the cost function spans from $t_0 = 10$ s to $T = 100$ s, $\alpha = [0.1, 1, 0.1]^T$, $\gamma = [200, 1200, 200]^T$, and $\omega_i = a^i\pi$. Figure 6.3 shows that ES minimizes the cost function (6.1) with convergence in less than 10 iterations to PID parameters that produce a local minimum. ES achieves this step response by increasing the value of the integral time T_i to almost three times that given by the ZN tuning

Table 6.1: PID parameters for G_1. The PID parameters given by IFT (in [44]) and ES (in the present article) are similar. Both methods increase the integral time T_i markedly over ZN.

Tuning method	K	T_i	T_d
ZN	4.06	9.25	2.31
IMC	3.62	22.4	2.18
IFT	3.67	27.7	2.11
ES	3.58	27.8	2.15

rules, thereby reducing the influence of the integral portion of the controller, see Table 6.1. The performance of the PID parameters obtained from ES tuning is roughly equivalent to the IFT performance. This similarity is expected since both methods attempt to minimize the same cost function. Figure 6.3 shows that IFT and ES yield closed-loop systems with less overshoot and smaller settling times than ZN and IMC.

6.3.2 Tuning for G_2

For G_2, which is identical to G_1 except with a longer time delay of 20 s, we set $t_0 = 50$ s, $T = 300$ s, $\alpha = [0.06, 0.3, 0.2]^T$, $\gamma = [2500, 2500, 2500]^T$, and $\omega_i = a^i\pi$. Figure 6.4 shows that ES reduces the cost function by an order of magnitude in less than 10 iterations. Moreover, ES yields a closed-loop system whose step response is similar to that produced by IMC and IFT and thus has improved overshoot and settling time compared to ZN tuning. The PID parameters determined by the four tuning methods are presented in Table 6.2.

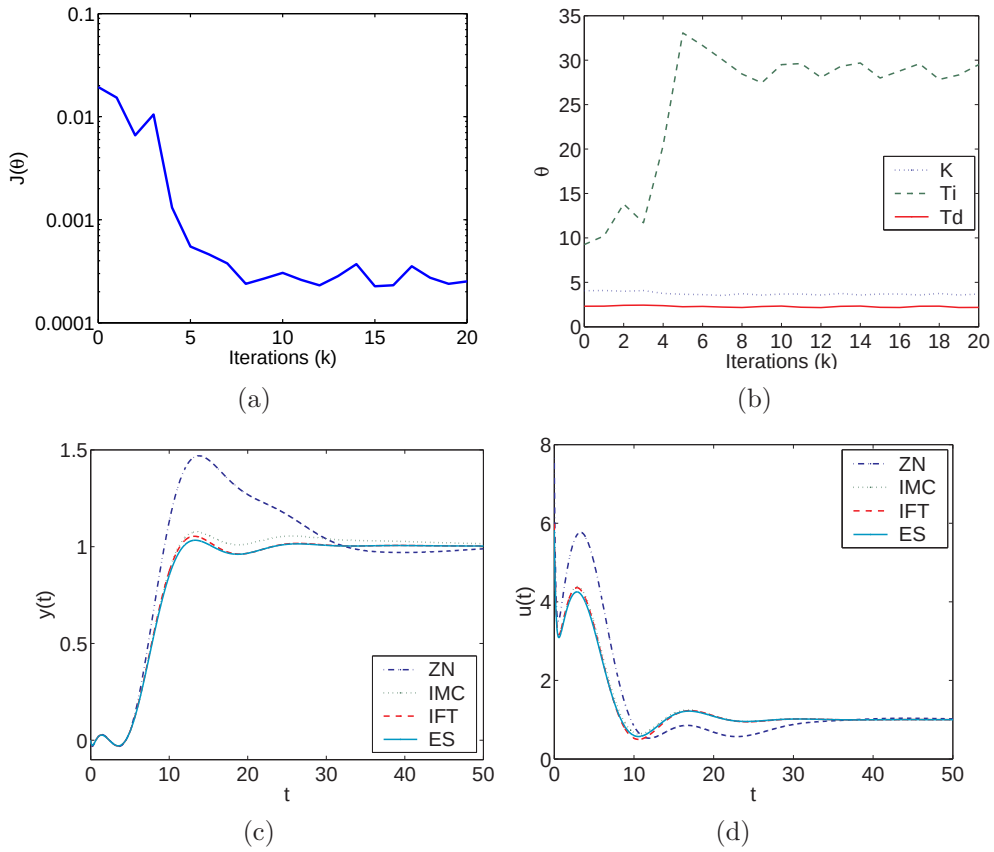

Figure 6.3: ES PID tuning of G_1 illustrated by (a) the evolution of the cost function and (b) the PID parameters during ES tuning of the closed-loop system with $G_1(s)$. The lower plots present (c) the output signal and (d) the control signal during step response experiments of the closed-loop systems with $G_1(s)$ and the PID controllers obtained from the four methods. ES reduces the cost function in (a) by increasing the integral time in (b), which produces a more favorable step response similar to that given by IFT in (c).

Table 6.2: PID parameters for G_2. Although ES and IFT yield different parameters, the resulting responses are similar, as shown in Figure 6.4.

Tuning method	K	T_i	T_d
ZN	1.33	31.0	7.74
IMC	0.935	30.5	6.48
IFT	0.930	30.1	6.06
ES	1.01	31.5	7.16

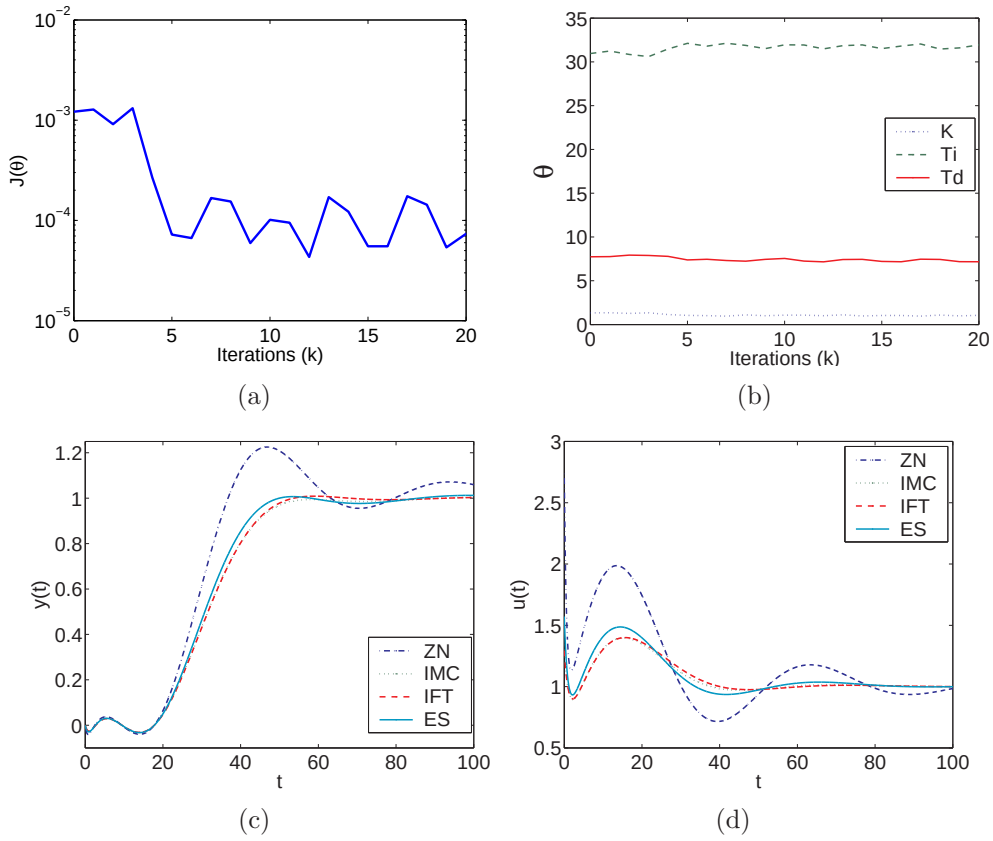

Figure 6.4: ES PID tuning of G_2 illustrated by (a) the evolution of the cost function and (b) the PID parameters during ES tuning of the closed-loop system with $G_2(s)$. The lower plots present (c) the output signal and (d) the control signal during step response experiments of the closed-loop systems with $G_2(s)$ and PID controller parameters obtained using the four methods. ES reduces the cost function in (a) after a few iterations and finds PID parameters in (b), which produce a step response similar to the IFT and IMC controllers in (c).

Table 6.3: PID parameters for G_3. IMC, IFT, and ES decrease the proportional gain K and the integral time T_i versus the parameters found using ZN. Furthermore, IMC reduces the derivative time T_d more so than IFT and ES.

Tuning method	K	T_i	T_d
ZN	1.10	75.9	19.0
IMC	0.760	64.7	14.4
IFT	0.664	54.0	18.2
ES	0.684	54.9	19.5

6.3.3 Tuning for G_3

For G_3 with a single pole of order eight we use $\alpha = [0.06, 1.1, 0.5]^T$, $\gamma = [800, 3500, 300]^T$, $\omega_1 = \omega_2 = a\pi$ (with $\alpha_2 \cos(\omega_2 k)$ replaced by $\alpha_2 \sin(\omega_2 k)$ in Figure 4.1), and $\omega_3 = a^3\pi$. Furthermore, the cost function accounts for the error from $t_0 = 140$ s to $T = 500$ s. Figure 6.5 shows that ES improves the step response behavior obtained by the ZN tuning rules, and returns a response that is similar to that achieved by IFT, however, with a smaller settling time than the IMC controller. Table 6.3 indicates that ES reduces the integral time T_i and controller gain K to reduce the value of the cost function. This plant, which is more challenging than G_1 and G_2, requires roughly 30 iterations for parameter convergence.

6.3.4 Tuning for G_4

The PID controller for the closed-loop system with nonminimum phase G_4 in (6.13) is tuned using ES. We set $t_0 = 30$ s, $T = 200$ s, $\alpha = [0.05, 0.6, 0.2]^T$, $\gamma = [2000, 10000, 2000]^T$, $\omega_1 = \omega_2 = a\pi$ (with $\alpha_2 \cos(\omega_2 k)$ replaced by $\alpha_2 \sin(\omega_2 k)$ in Figure 4.1), and $\omega_3 = a^3\pi$. Figure 6.6 shows that ES produces a step response

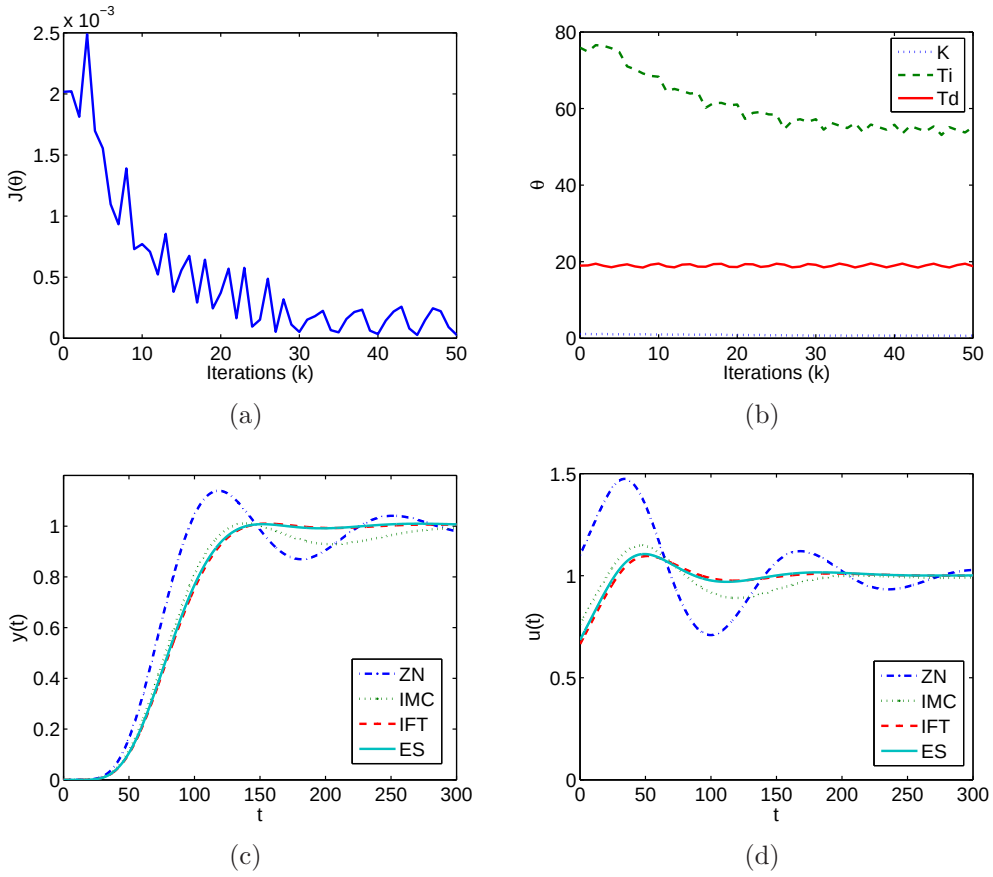

Figure 6.5: ES PID tuning of G_3 illustrated by (a) the evolution of the cost function and (b) the PID parameters during ES tuning of the closed-loop system with $G_3(s)$. The lower plots present (c) the output signal and (d) the control signal during step response experiments of the closed-loop systems with $G_3(s)$ and the PID controllers obtained by means of the four methods. ES reduces the cost function in (a), although not as quickly as for the other plants, by decreasing the integral time T_i in (b), which produces a more favorable step response in (c).

Table 6.4: PID parameters for G_4. IMC, IFT, and ES progressively decrease the influence of the integral term while increasing the effect of the derivative term.

Tuning method	K	T_i	T_d
ZN	3.53	16.8	4.20
IMC	3.39	31.6	3.90
IFT	3.03	46.3	6.08
ES	3.35	49.2	6.40

similar to IFT; both ES and IFT yield no overshoot and a smaller settling time than the ZN and IMC controllers. However, ES produces a slightly larger initial control signal than IFT. Table 6.4 shows that an increased integral time improves the system response.

6.4 Cost Function Comparison

The cost function dictates the performance of the PID controller obtained from ES. It is therefore important to choose a cost function that emphasizes the relevant performance aspects such as settling time, overshoot, and rise time. To illustrate the dependence of the optimal PID parameters θ^* on the cost function we use ES for plant $G_2(s)$ to minimize the ISE cost function (6.1) with $t_0 = 0$ and $t_0 = T_{peak}$ as well as the cost functions

$$IAE = \frac{1}{T}\int_0^T |e|dt, \tag{6.14}$$

$$ITAE = \frac{1}{T}\int_0^T t|e|dt, \tag{6.15}$$

$$ITSE = \frac{1}{T}\int_0^T te^2dt. \tag{6.16}$$

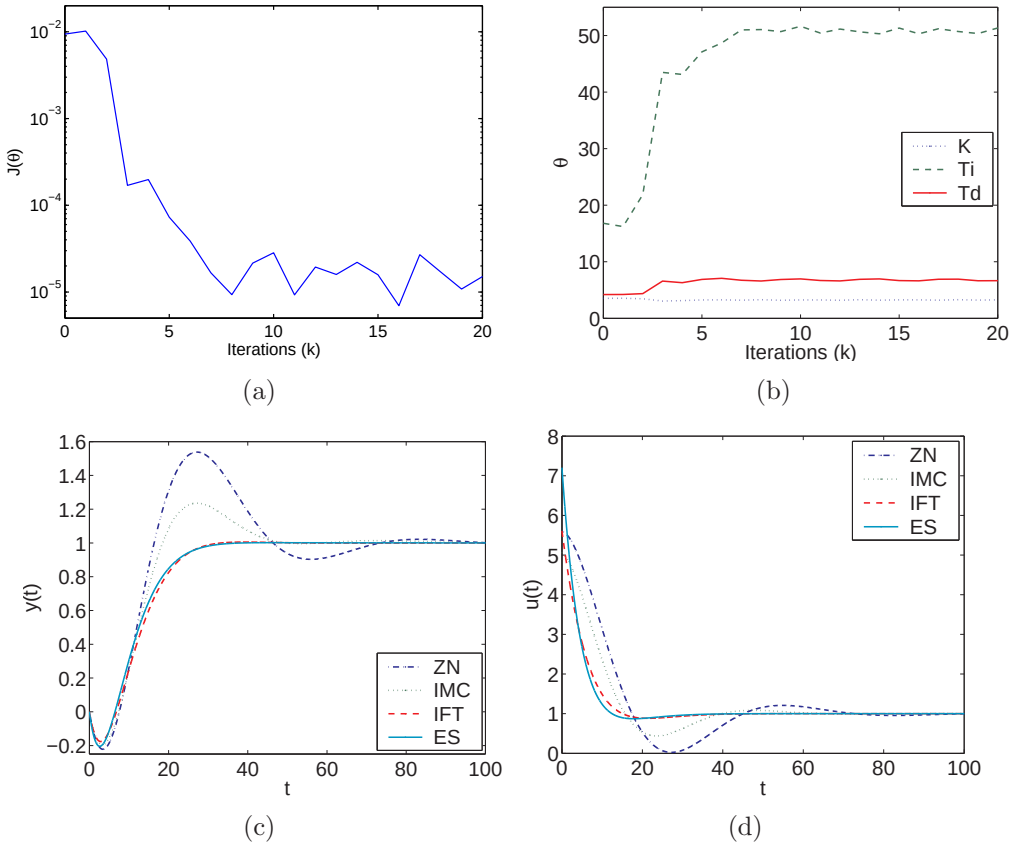

Figure 6.6: ES PID tuning of G_4 illustrated by (a) the evolution of the cost function and (b) the PID parameters during ES tuning of the closed-loop system with $G_4(s)$. The lower plots present (c) the output signal and (d) the control signal during step response experiments of the closed-loop systems with $G_4(s)$ and PID controllers obtained using the four methods. ES reduces the cost function in (a) by increasing the integral time T_i and the derivative time T_d in (b), which produces a more favorable step response similar to that found using IFT in (c).

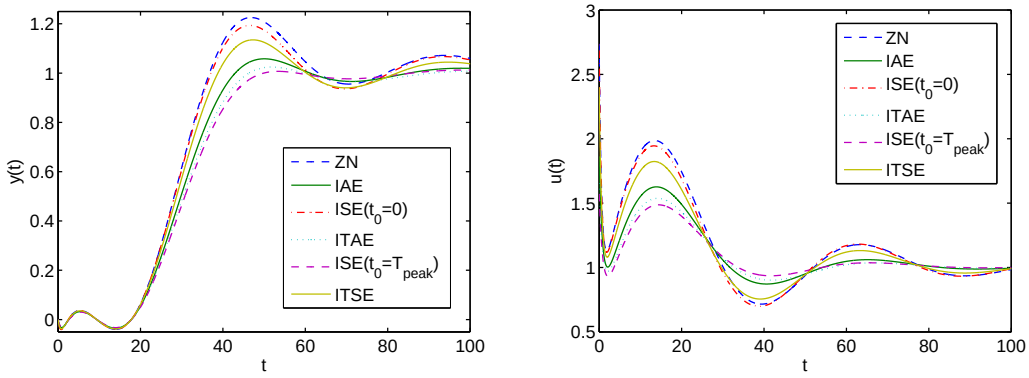

(a) (b)

Figure 6.7: The effect of the cost function illustrated by the output signal (a) and the control signal (b) during step response experiments of the closed-loop systems with $G_2(s)$ and PID controllers obtained using ES with various cost functions. The use of different cost functions in ES yield different step responses, with the Window cost function producing the best result.

Note that (6.15) and (6.16) involve a time-dependent weighting, which de-emphasizes the transient portion of the response. Figure 6.7 shows that ISE with $t_0 = T_{peak}$ produces a response with the smallest overshoot and fastest settling time. ITAE and IAE perform slightly worse than ISE with $t_0 = T_{peak}$, whereas ISE with $t_0 = 0$ and ITSE are similar to ZN in terms of overshoot and settling time. However, Figure 6.7 also indicates that using a cost function comprised of the squared error (ISE and ITSE) versus the absolute error (IAE and ITAE) decreases the time required for the output of closed-loop system to initially reach the setpoint.

Because of the flexibility of ES the cost function can be modified on the fly, allowing the PID parameters to be re-tuned whenever it is desirable to emphasize a different performance aspect. However, stability of ES must be maintained for the new cost function through the choice of the ES parameters.

6.5 Control Saturation

Many applications of PID control must deal with actuator saturation. Actuator saturation can result in integrator windup, in which the feedback loop becomes temporarily disconnected since the controller output is no longer affected by the feedback signal. During saturation the integral term grows while the error remains either positive or negative. Hence the integrator is slow to recover when the actuator desaturates.

To examine ES tuning in the presence of saturation, we apply ES with and without the tracking anti-windup scheme [62] depicted in Figure 6.8, which modifies the integral control signal using a feedback signal proportional to $\tilde{u}$ the difference between the requested control signal $u_{requested}$ and the actual control signal u_{actual} produced by the actuator. The tracking time constant T_t for the case of ES is set to $T_t = \sqrt{T_i T_d}$. For IMC this choice of T_t results in a slow controller response, and thus we use $T_t = 18$.

We compare ES and IMC in the presence of saturation with and without anti-windup. Figure 6.9 shows that overshoot is a problem for the IMC controller, whereas ES increases the integral time (see Table 6.5) to improve the performance of the controller. ES finds controller parameters that perform almost as well as the systems with anti-windup. However, for small changes in the reference signal the actuator will not saturate and the ES controller without anti-windup with its large integral time will give poor performance. Whereas the ES and IMC controllers with

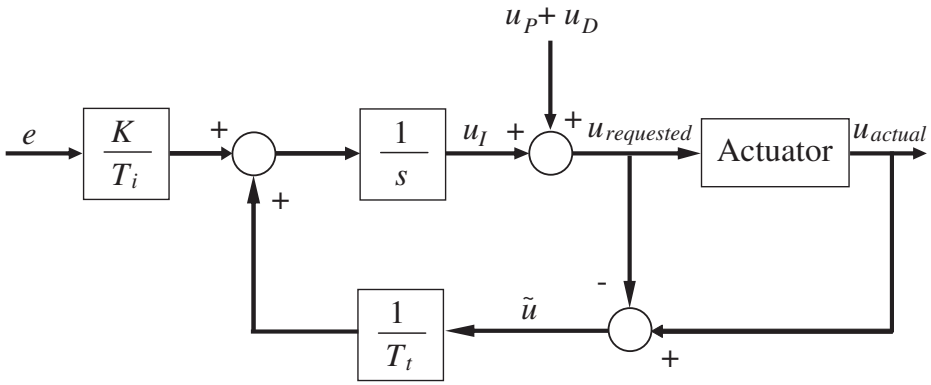

Figure 6.8: Tracking anti-windup scheme. The approach reduces integrator windup by feeding back the error signal $\tilde{u} = u_{actual} - u_{requested}$, which is the difference between the requested control signal $u_{requested}$ and the actual control signal u_{actual}.

Table 6.5: PID parameters for G_1 with saturation. ES without anti-windup increases the integral time to decrease the effect of integral windup, whereas ES with tracking can use a smaller integral time because of the anti-windup scheme.

Tuning method	K	T_i	T_d
IMC	3.62	22.4	2.18
ES	3.61	47.6	1.81
ES_{aw}	4.07	12.8	2.20

anti-windup yield good performance for small and large changes of the reference signal.

6.6 Selecting Parameters of ES Scheme

Implementation of ES requires the choice of several parameters, namely, the perturbation amplitudes α_i, adaptation gains γ_i, perturbation frequencies ω_i, and the parameter h in the highpass filter. However, it turns out that the minimizer found by ES is fairly insensitive to the ES parameters. To investigate this sensi-

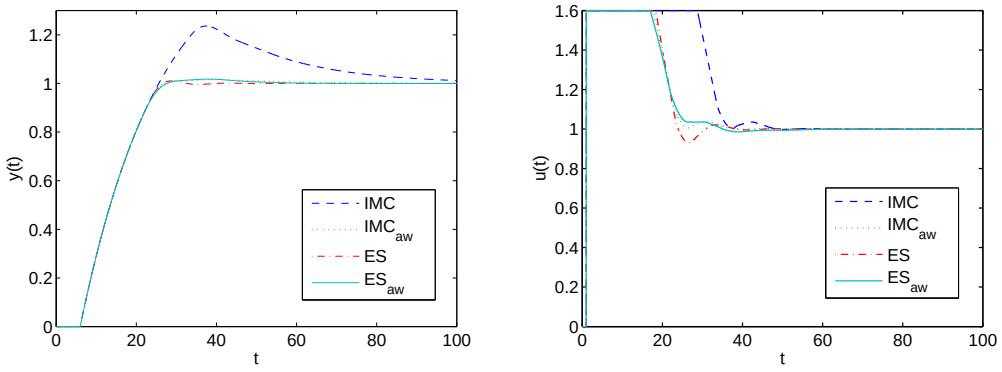

(a) (b)

Figure 6.9: The effect of actuator saturation illustrated by the output signal (a) and the control signal (b) during step response experiments of the closed-loop systems with $G_1(s)$, control saturation of 1.6, and PID controllers obtained using IMC and ES both with and without anti-windup. ES finds PID parameters that produce a step response with little overshoot even without the aid of anti-windup. Furthermore, the step response for ES without anti-windup is comparable to IMC and ES with anti-windup.

tivity, we use ES to tune the closed-loop system with G_2 in (6.11) while varying α and γ. The parameters h and ω_i are chosen to be $h = 0.5$ and $\omega_i = 0.8^i\pi$.

For the plant G_2, Figure 6.10 shows the evolution of the cost function during tuning with various ES parameters. Table 6.6 shows that ES yields almost identical PID parameters even though α is varied by 50 percent and γ is reduced by an order of magnitude. However, the convergence is slower due to the reduced perturbation amplitudes α_i and adaptation gains γ_i. The tradeoff between the speed of convergence and the domain of initial conditions that yield the minimizer θ^* is quantified in [83], where the authors demonstrate analytically the ability of ES to avoid getting trapped in local minima, when its parameters are chosen appropriately.

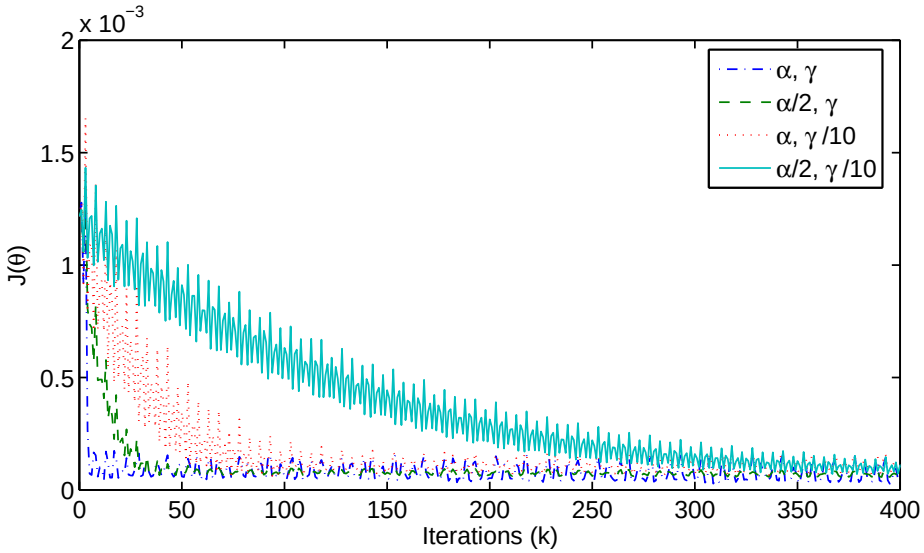

Figure 6.10: Sensitivity of ES to α and γ illustrated by the evolution of the cost function during ES tuning of the PID parameters for the plant $G_2(s)$ with various values of α and γ. In each case ES converges to a similar cost with slower convergence for reduced gains.

Table 6.6: PID Parameters for G_2 with different values of α and γ. ES arrives at similar PID parameters for reduced values of the perturbation amplitude α and the adaptation gain γ.

ES tuning parameters	K	T_i	T_d
α, γ	1.01	31.5	7.16
$\frac{\alpha}{2}, \gamma$	1.00	31.1	7.60
$\alpha, \frac{\gamma}{10}$	1.01	31.3	7.54
$\frac{\alpha}{2}, \frac{\gamma}{10}$	1.01	31.0	7.65

6.7 Comparison of Tuning Methods

ES and IFT use the same cost function and thus yield similar results. It is therefore interesting to compare how these methods minimize the cost function. Both methods are non-model-based and estimate the gradient of the cost function with respect to the controller parameters. The estimated gradient is then used in a gradient search scheme to find a local minimizer of the cost function. The difference lies in how these algorithms estimate the gradient. IFT uses signal information from three experiments including a special feedback experiment and assumes that the system is linear time-invariant to estimate the gradient. Although IFT is based on linear theory, the technique can be applied to nonlinear systems [34].

On the other hand, ES requires only one experiment per iterative gradient estimate and its derivation does not assume that the system is linear. ES uses simple filters along with modulation by sinusoidal signals to estimate the gradient. However, ES requires a choice of several design parameters, whereas IFT requires that only the step size be specified.

While both ES and IFT are more difficult to implement than ZN and IMC, ES and IFT often yield improved performance. For G_3, which has repeated poles, these benefits can be seen in Figure 6.5, as well as for the nonminimum phase plant G_4 in Figure 6.6. Additionally, ES outperforms IMC in the presence of control saturation as shown in Figure 6.9.

6.8 Conclusions

ES tunes PID controllers by minimizing a cost function that characterizes the desired behavior of the closed-loop system. This tuning method is demonstrated on four typical plants and found to give parameters that yield performance that is better than or comparable to that of other popular tuning methods. Additionally, ES produces favorable results in the presence of actuator saturation. The ES method thus has an advantage over model-based PID tuning schemes in applications that exhibit actuator saturation. However, since ES requires initial values of the PID parameters, the method can be viewed as a complement to another PID parameter design method. Furthermore, the ES cost function can be chosen to reflect the desired performance attributes.

This chapter is in part a reprint of the material as it appears in
N. J. Killingsworth and M. Krstić, "PID tuning using extremum seeking: online, model-free performance optimization," *IEEE Control Systems Magazine*, vol. 26, no. 1, pp. 70–79, 2006.

Chapter 7

Optimizing HCCI Engine Combustion Timing Controller Gains Via Extremum Seeking

A feedback controller is required to regulate the HCCI engine to a stable and efficient combustion timing setpoint. Numerous HCCI engine combustion timing control studies have successfully incorporated proportional integral derivative (PID) controllers. Furthermore, a wide variety of actuation methods effectively work with PID control. Olsson et al. [56] incorporated gain scheduled PID controllers to control the combustion timing of each cylinder of an experimental HCCI engine by regulating the octane number of fuel mixture going to each cylinder. In the work by Haraldsson et al. [31] a novel variable compression ratio engine controls the mean combustion timing of all five cylinders using a PID controller.

In the study by Haraldsson et al. [29], a fast thermal management (FTM) actuation system controls the combustion timing. The FTM system consists of a stream of ambient air and a hot stream of air that passes through an exhaust heat exchanger; the two streams are mixed to regulate the intake air temperature. The FTM system controls the mean combustion timing of all the engine cylinders [29], and later the cylinder individual combustion timing [36]. PID controllers are used with gains that depend on the engine speed. Haraldsson et al. [29] find that changes in RPM alter the amount of heat transfer and thus the wall temperature.

Agrell et al. [5] used a PI controller with the combustion timing averaged over five cycles as the feedback signal and the valve timing on a single-cylinder engine with variable valve timing as the output. They used one of two different valve strategies dependent on the operating conditions: one changed the inlet valve closing to vary the effective compression ratio, and the other strategy used negative valve overlap, which traps more residual gas, increasing the temperature of the charge. In subsequent work a feedforward controller was added to the PI controller [6]. The feedforward controller consists of an ignition model that is a nonlinear map covering a number of operating conditions and based on a knock integral [6].

Feedforward compensation was also used by Strandh et al. [80]. System identification was used to construct a model of the dual fuel HCCI engine mentioned previously [56]. This model is used to derive a first order feedforward filter. Comparing the performance of a PID controller with and without the feedforward filter,

the feedforward filter increases the bandwidth of the controller, allowing cycle-by-cycle control.

In summary, PID controllers with and without feedforward compensation effectively control the combustion timing of various HCCI engines, using numerous options for actuation. However, PID controllers require the tuning of their parameters. Moreover, the nonlinear nature of HCCI engines requires gain scheduling to achieve good performance over the whole operating range of the engine, further increasing the task of tuning. There are many published methods available to tune PID controllers [62]. However, most tuning methods require a model of the system to be controlled. Physics based models of HCCI engines tend to be overly complicated and most system identification approaches yield a linear model. Due to the nonlinear nature of HCCI engines, linear models are only valid near the operating point for which they are derived. Therefore, many linear models are required to span the operating range of an HCCI engine, which can be time intensive.

Nonmodel based tuning methods are thus desirable. One such method is iterative feedback tuning (IFT). IFT iteratively optimizes the controller parameters with respect to a cost function derived from the output signal of the closed-loop system [35]. Recently, IFT was effectively applied to tune the combustion timing control of an HCCI engine with variable valve timing [32]. However, tuning required two (three) experiments to be performed for each iteration for a one (two) degree of freedom controller. Thus, the tuning procedure is somewhat disjointed and the controller parameters are calculated off-line after these independent ex-

periments are conducted.

In contrast to off-line approaches we present an online method for optimizing the step response of the combustion timing by tuning the HCCI engine controller. Specifically, we use a discrete version of extremum seeking [7] to minimize a cost function that quantifies the performance of the controller. The cost is a function of the error between the actual and desired combustion timing. The controller parameters are updated online as the optimization takes place. Thus, this method does not require off-line calculations and greatly reduces the time to find optimal controller parameters. A previous study compared ES PID tuning with other leading PID tuning methods on an assortment of simulated plants showed that ES PID tuning produced similar or better performance than the other tuning methods [40].

In the next section we give a background of the extremum seeking algorithm used in this work. We then describe the experimental HCCI engine system. Next, we outline the procedure for using ES for controller parameter tuning, the form of the controller and the cost function used for combustion timing control. Then we report experimental PID tuning results. Finally, we present the use of ES to determine optimal combustion timing setpoints on an experimental HCCI engine.

7.1 Experimental Setup

A 14.6 liter Caterpillar 3406 natural gas spark ignition engine converted to run in HCCI mode is used in this work. This engine is described in detail in Chapter 2 and only some of its basic attributes will be recapped here.

A thermal management system controls the combustion timing of the engine on a cylinder-by-cylinder basis. The thermal management system controls the temperature of gases inducted into each cylinder, which in turn controls the autoignition process. Hot and cold streams of fuel and air are delivered to two separate manifolds. Each cylinder has a temperature mixing valve where cold intake charge is blended with the charge from the hot manifold, regulating intake temperature to each cylinder. Each temperature control valve is computer controlled using an electric servo motor. The length of the intake runners results in about a one cycle transport delay before a change in the valve input affects the intake mixture entering the cylinder. This thermal management system allows the intake temperature of each cylinder to be quickly adjusted for cylinder-by-cylinder control of the combustion timing.

The combustion timing feedback signal is derived from in-cylinder measurements of the pressure. A net heat release analysis of the pressure measurements determines the combustion timing in each cylinder [11]. We define the combustion timing to be the crank angle at which 50% of the heat has been released ($CA50$). The calculated combustion timing is used as a feedback, allowing control of the

combustion timing by means of the temperature control valves.

7.2 Combustion Timing Controller Tuning

In this section we will use ES to tune the combustion timing controller on the experimental engine. The controller parameter tuning occurs online (while the engine is running) such that a cost function is minimized. First, we will describe the form of the combustion timing controller. We use a PID controller, which compares the difference between the desired combustion timing setpoint $CA50_{sp}$ and the measured combustion timing $CA50_m$ of the HCCI engine and produces a control signal $u(t)$ to reduce the difference between them.

We use a standard PID controller with the exception that the derivative term acts on the measured output but not on the reference signal avoiding large control effort during a step change in the reference signal. We also investigate adding a feedforward term K_f to the PID controller. The form of the controller is,

$$u(t)=K_f r(t) + K\left(e(t) + \frac{1}{T_i}\int_0^t e(\tau)d\tau + T_d\frac{dy(t)}{dt}\right), \tag{7.1}$$

where the error $e(t) \triangleq r(t) - y(t)$ is the difference between the reference $r(t)$ and the measured output $y(t)$ signal of the closed-loop system. The Laplace transforms of the feedforward $C_r(s)$ and feedback $C_y(s)$ portions of the controller are

$$C_r(s) = K_f + K\left(1 + \frac{1}{T_i s}\right), \tag{7.2}$$

$$C_y(s) = K\left(1 + \frac{1}{T_i s} + T_d s\right). \tag{7.3}$$

7.2.1 Cost Function

Extremum seeking tunes the parameters of the combustion timing controller to minimize a given cost function. The cost function quantifies the performance of the controller; specifically, the controller's ability to track a square wave reference signal. We use a cost function based on the integrated squared error (ISE)

$$J(\theta) \triangleq \frac{1}{N}\left(\sum_{n=n_0}^{n_f} e^2(n,\theta) + \sum_{n=n_0+\delta}^{n_f+\delta} e^2(n,\theta)\right), \tag{7.4}$$

where n is the engine cycle, N is the total number of engine cycles evaluated, δ is the period of the square wave reference signal, and θ contains the controller parameters

$$\theta \triangleq [K_f, K, T_i, T_d]^T. \tag{7.5}$$

The cost function $J(\theta)$ defined in (7.4) accounts for the tracking error over the interval $[n_0,n_f]$ for two successive periods δ of the square wave reference signal. By setting n_0 to approximate the engine cycle n_{peak} at which the step response of the closed-loop system reaches the first peak or maximum, the cost function $J(\theta)$ places zero weighting on the initial transient portion of the response [45]. Hence, the controller is tuned to minimize the error beyond n_{peak} ignoring the initial transient.

Figure 7.1 shows an example of how the cost function $J(\theta(k))$ is evaluated in the experiment. The calculation of the cost uses only the data points within the

dashed box. We evaluate the cost only at the later combustion timing. Thus for a step from 6 to 10 crank angle degrees (CAD) after top dead center (ATDC), the cost is evaluated only for operation at 10 CAD ATDC. The sensitivity of the combustion timing becomes greater as combustion is delayed [57], [16]. So an optimal controller for going from CA50 = 6 to 10 CAD ATDC will be stable during the transition from 10 to 6 CAD ATDC whereas the opposite case will not necessarily result in stable operation. The cost is generated after two periods of the square wave, shown in Figure 7.1 with the downward pointing arrows.

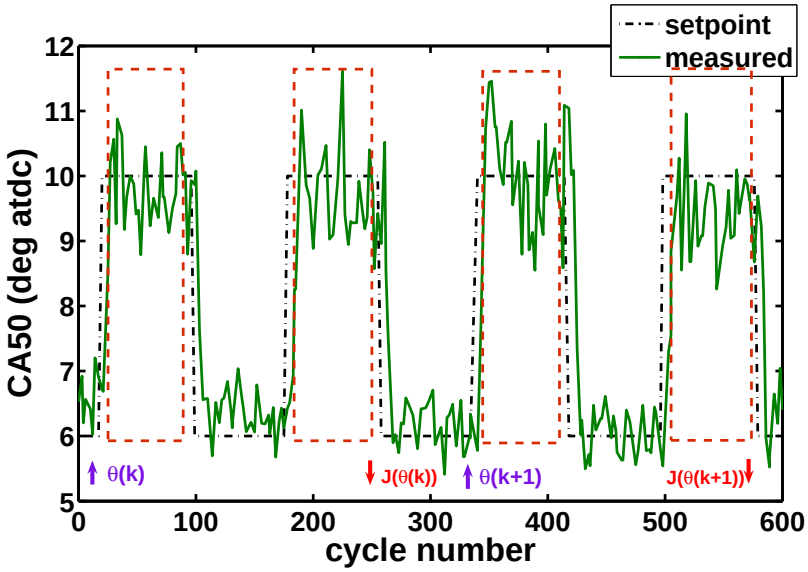

Figure 7.1: Timing of ES PID tuning scheme. The cost function J is calculated every two periods of the square wave reference signal. Additionally, the cost function is evaluated only at the later combustion timing as indicated by the dashed red box. The new PID parameters $\theta(k+1)$ are updated every two periods and after the cost $J(\theta(k))$ is calculated.

The cost function must have a sufficient signal to noise ratio such that ES can resolve the effect of the perturbation signal $\alpha_i \cos(\omega_i k)$. Evaluating the cost over two periods of the reference signal, rather than one, reduces the variance

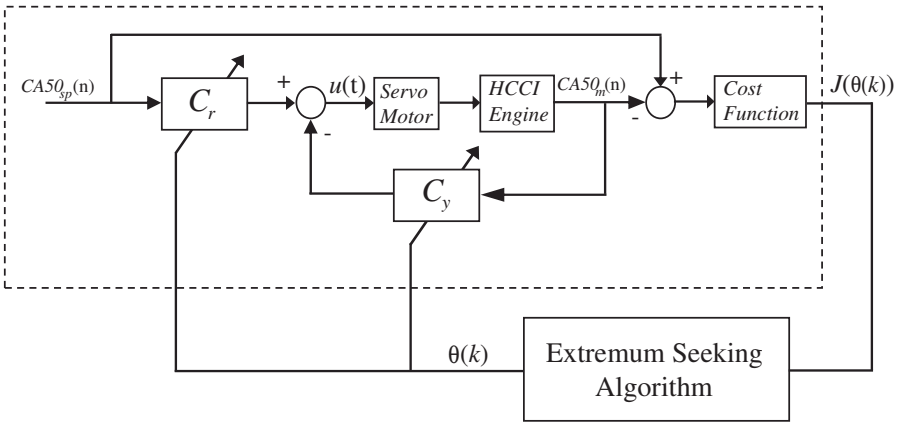

Figure 7.2: The overall extremum seeking PID tuning scheme including the dynamics of the temperature control valves and HCCI engine. The ES algorithm updates the controller parameters $\theta(k)$ to minimize the cost function $J(\theta)$, which is calculated from the response of the combustion timing controller to a square wave reference signal during continuous operation of the HCCI engine shown within the dashed box.

allowing the tracking behavior of the current controller to be seen more clearly. Additionally, to help isolate the effect of the current controller we low pass filter the measured combustion timing signal evaluated in the cost function. The plots, however, present the unfiltered combustion timing signal.

7.2.2 Experimental Controller Tuning

Figure 7.2 depicts the overall ES PID tuning scheme. The ES algorithm uses the value of the cost function at iteration k to compute new controller parameters for the next iteration $k+1$, as shown in Figure 7.1. The new controller is applied during the next two periods of the square wave reference signal. The process continues iteratively.

The combustion timing controller for cylinder one receives a square wave com-

bustion timing reference signal. All the other cylinders have a fixed combustion timing in an effort to keep the engine speed constant (changing the combustion timing produces a small change in the torque produced and can cause a disturbance in the engine speed). The one per revolution pulse from the camshaft encoder provides the timing signal for the square wave reference signal, which has a period of 160 engine cycles. Starting with a stable and conservative controller, we run at least four periods of the reference signal to generate initial conditions for the ES algorithm.

The engine was run at 1600 rpm with a load of 25 kW. For each period of the square wave reference signal the cost is evaluated from $n_0 = 10$ to $n_f = 70$ engine cycles, and for every experiment the parameters a and h in the ES scheme (4.16)–(4.18) are set to 0.7 and 0.5, respectively.

Figure 7.3 shows the ES tuning of a PI controller ($T_d = K_f = 0$). The initial PI controller is parameterized with $\theta = [0, 1, 0.1, 0]^T$ defined in (7.5). The ES perturbation frequency is $\omega = \pi[0, a^2, a, 0]^T$. Because $0 < a < 1$ the perturbation frequency of the integral time T_i is higher than for proportional gain K. Figure 7.3 shows the combustion timing (CA50) setpoint and the measured combustion timing. With the initial (untuned) controller parameters the PI controller is unable to regulate the combustion timing to the setpoint within a period of the squarewave reference signal. However, as ES tunes the controller parameters the controller adjusts the engine's inlet temperature fast enough to move from $CA50 = 6$ to 10 and back to 6 within 160 engine cycles. Greater overshoot occurs as the controller

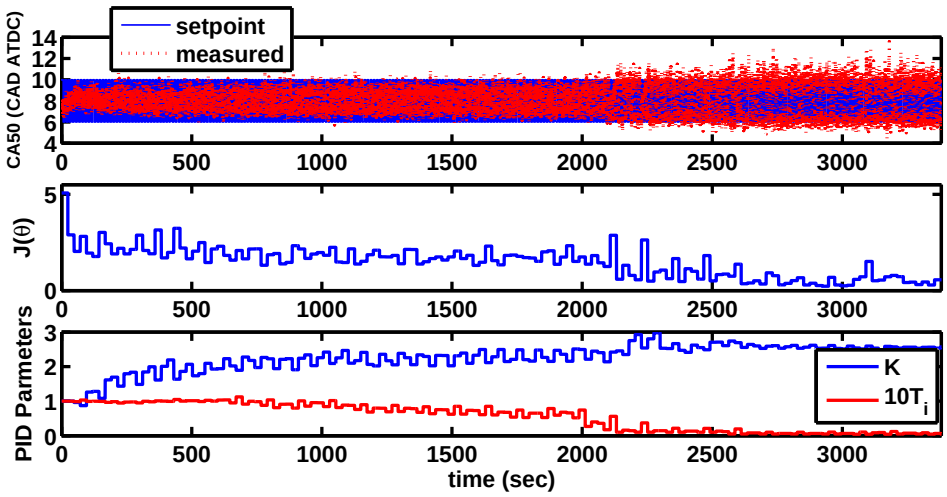

Figure 7.3: ES tuning of PI controller illustrated by tracking of the combustion timing with a square wave reference signal, evolution of the cost function, and the PI parameters during tuning.

becomes better tuned. This overshoot is because the natural variability in the ignition process is more pronounced at later combustion timings, which the improved controller is better able to achieve. This phenomenon can be seen in greater detail in Figure 7.1.

In this experiment the perturbation amplitude α and adaptive gain γ are conservative, and thus ES slowly reduces the cost function $J(\theta)$ by reducing the integral time T_i and by increasing the proportional gain K. These changes increase the effect of both the proportional and integral terms of the controller. For this case, the tuning algorithm converges in approximately 125 iterations of ES or 50 minutes. A better choice of the initial controller parameters will reduce the tuning time, because the initial parameters will likely be closer to the optimal parameters thus less adjustment will be needed, and the controller will be able to track a step change in the combustion timing more precisely so a shorter period of the

reference signal can be used. It would also be possible to decrease the tuning time by reducing the number of samples N evaluated in the cost function $J(\theta(k))$ as it becomes smaller. The minimum cost and the minimizer θ^* are listed in Table 7.1. Note that the perturbation amplitude α was reduced while the experiments were running, especially as the integral time T_i became smaller.

The derivative term was included in the tuning shown in Figure 7.4 with a perturbation frequency $\omega = \pi[0, a^2, a, a^3]^T$. The initial PID controller consists of the parameters $\theta = [0, 1, 0.08, 0.005]^T$. Similar to the previous experiment, ES increases the proportional gain K while decreasing the integral time T_i. Additionally, the derivative time T_d is decreased. Results in Table 7.1 show that the PID controller found using ES produces an identical minimum cost as was found with the PI controller. However, it should be noted that for these experiments the reference signal oscillates between 8 and 11 CAD ATDC rather than the 6 and 10 CAD ATDC used for the PI tuning shown in Figure 7.3, so direct comparison of their costs cannot be made. The results in Table 7.1 show that ES finds a small value of the derivative time T_d, so it appears that at this operating point the addition of the derivative term does not play a key role. Note that the PID parameters converge in around 15 minutes for this case. This tuning time decreases because larger values of the perturbation amplitude α and adaptive gain γ were used. Typically, increasing α and γ will increase the speed of convergence. However, when these parameters are too large the stability of ES can be affected [40].

Next we look at tuning an additional constant feedforward term K_f. The

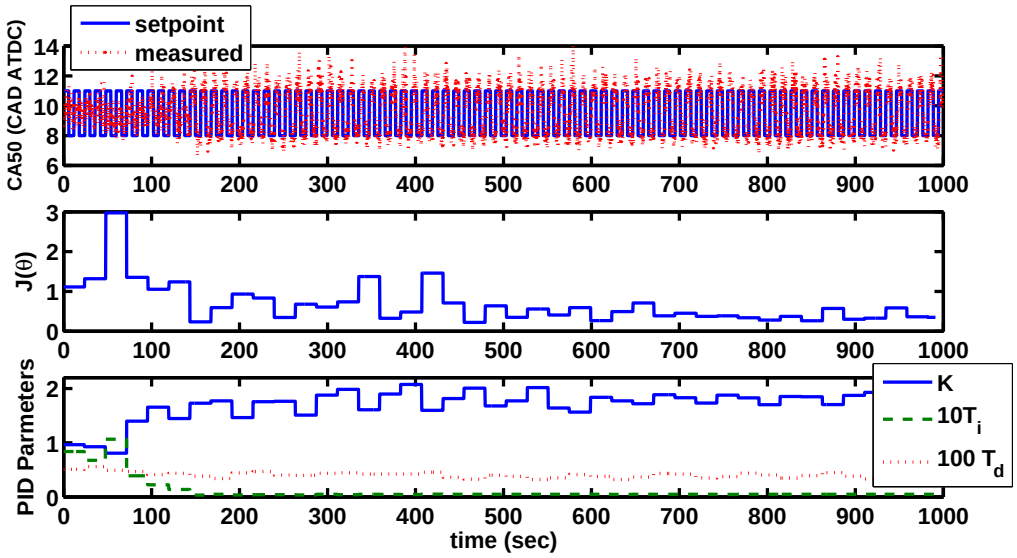

Figure 7.4: ES tuning of PID controller illustrated by tracking of the combustion timing with a square wave reference signal, evolution of the cost function, and the PID parameters during tuning.

initial controller used is $\theta = [0.1, 1, 0.1, 0]^T$ and the ES perturbation frequency is $\omega = \pi[a, a^3, a^2, 0]^T$. Figure 7.5 shows that in this case the feedforward term is quickly increased, while the other parameters stay relatively constant. Initially, the cost function fluctuates from a high value to a low value. This behavior occurs because the measured combustion timing does not track the reference signal well. The combustion timing becomes delayed occasionally and tracks the later part of the reference signal resulting in a lower cost, but then it becomes advanced and the cost goes up. Using a longer reference signal period will reduce this effect, but at the expense of longer tuning times. Furthermore, the artificial fluctuation in the cost function can be reduced if the tracking error during the earlier combustion timing is included in the cost.

Figure 7.6 shows a repeat of the experimental conditions from the previous run,

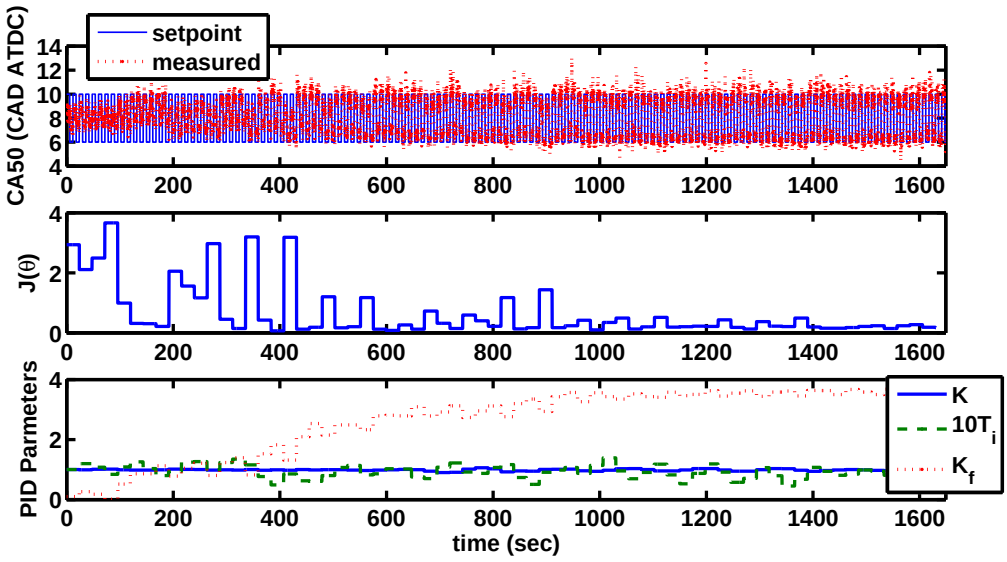

Figure 7.5: ES tuning of PI plus feedforward controller illustrated by tracking of the combustion timing with a square wave reference signal, evolution of the cost function, and the PI and feedforward parameters during tuning.

but this time ES finds a different local minimizer. Table 7.1 shows that a similar feedforward term K_f is found. However, both the proportional gain K and the integral time T_i are reduced. While the proportional gain is almost an order of magnitude smaller in this experiment versus the previous one, the integral gain $K_i = \frac{K}{T_i}$ is 4.83 for this experiment and 8.28 for the previous experiment. Thus, the integral gains for the two different controllers are closer in magnitude than the proportional gains. Also, notice that the reduction in the feedback controller gains K and K_i results in a reduced cost in Table 7.1 for this controller.

Figure 7.7 displays another run of ES tuning of a PI plus feedforward controller. This experiment is identical to the past two experiments shown, with the exception of the perturbation frequency. The ES perturbation frequency is $\omega = \pi[a^2, a^3, a, 0]^T$; therefore, the integral time T_i receives the highest frequency

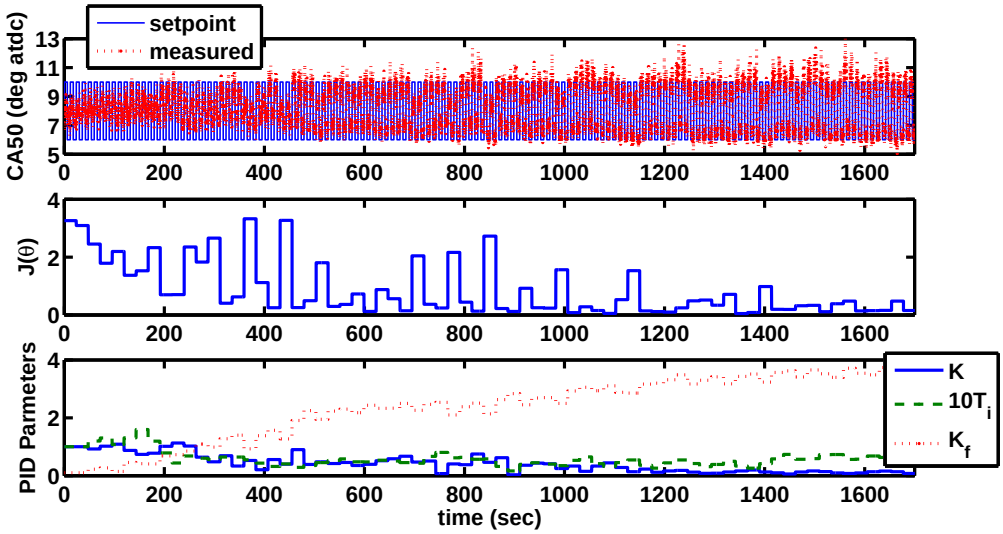

Figure 7.6: Repeat of ES tuning of PI plus feedforward controller (Figure 7.5) illustrated by tracking of the combustion timing with a square wave reference signal, evolution of the cost function, and the PI and feedforward parameters during tuning.

rather than the feedforward term K_f. The change in perturbation frequency results in the integral time T_i changing more quickly, and the discovery of a new local minimizer. The role of the feedforward gain K_f is reduced and the integral gain plays a more dominant role in the setpoint response of the controller. Figs. 7.5–7.7 indicate that there are multiple local minimizers of $J(\theta)$, and that either the feedforward term K_f or integral gain K_i can play a dominant role in the setpoint response. However, a large integral gain results in a larger high frequency gain and affects the steady state response. Therefore, a local minimizer with a large integral gain K_i tends to have a higher cost. We can see from these experiments the influence of picking the perturbation frequency for each parameter in θ. The input parameter with the highest frequency will be perturbed more often than the

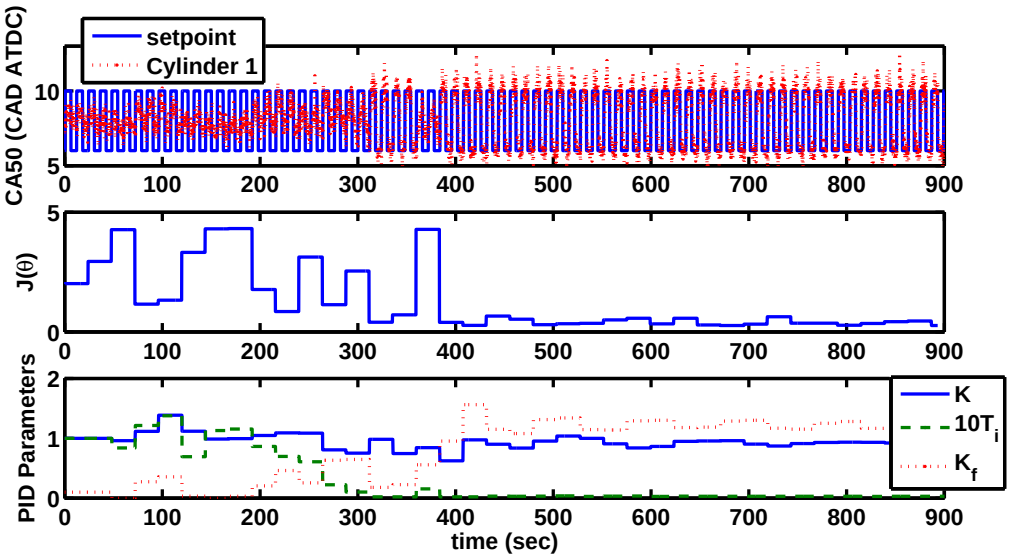

Figure 7.7: Repeat of ES tuning of PI plus feedforward controller with alternate perturbation frequency illustrated by tracking of the combustion timing with a square wave reference signal, evolution of the cost function, and the PI and feedforward parameters during tuning.

Table 7.1: ES Controller Tuning Results

Controller	Cost	K_f	K	T_i	T_d
PI (Fig. 7.3)	0.222	0	2.53	0.00500	0
PID (Fig. 7.4)	0.222	0	2.01	0.00501	0.00327
PI + FF (Fig. 7.5)	0.0965	3.56	0.942	0.114	0
PI + FF (Fig. 7.6)	0.0465	3.43	0.161	0.0333	0
PI + FF (Fig. 7.7)	0.265	1.26	0.923	0.00300	0

other input parameters, and assuming a gradient $\nabla J(\theta(k))$ is generated because of the perturbation, this input parameter will also be modified more often. In short, the choice of perturbation frequency affects how ES navigates the controller parameter space.

7.2.3 Disturbance Rejection

The formulation of the square wave reference signal and the cost function (7.4) used for ES tuning emphasizes the controller's setpoint response. The setpoint response of the combustion timing controller is important during the transition between low and high loads because these conditions require different combustion timings. At low loads an early combustion timing will be desirable to minimize CO and UHC emissions, whereas at higher loads a later combustion timing will minimize NO_x and the pressure rise rate. Furthermore, the combustion timing that yields the maximum brake torque will change with load and speed.

However, the disturbance rejection of the controller is also important during speed and load transients. This fact makes a case for using a controller with feedforward compensation. The feedforward term can be used to handle the setpoint changes, while the feedback portion need not be so aggressive and can better deal with disturbance rejection.

Disturbance rejection will now be studied to test the versatility of PI versus PI plus feedforward controllers. Both experiments shown in Figure 7.8 have a CA50 setpoint of 8 CAD ATDC, while the load is changed from 21 kW to 25 kW and back to 21 kW. The load change can be seen in the RPM. As the load is increased the RPM falls off; inversely, as the load is decreased the RPM increases. In plot (a) of Figure 7.8 the PI controller found in the experiment depicted in Figure 7.3 is used. Comparing plot (a) to plot (b), which illustrates the use of the PI plus

feedforward controller from Figure 7.7, we can see that the use of the feedforward term allows the feedback part of the controller to better reject disturbances. The measured combustion timing differs at times from the setpoint by more than two CAD in plot (a). In addition, the standard deviation exceeds 1 especially after the load change. In Contrast, in plot (b) of Figure 7.8 the PI plus feedforward controller keeps the combustion timing well within ±2 CAD of the setpoint and the standard deviation less than 1.

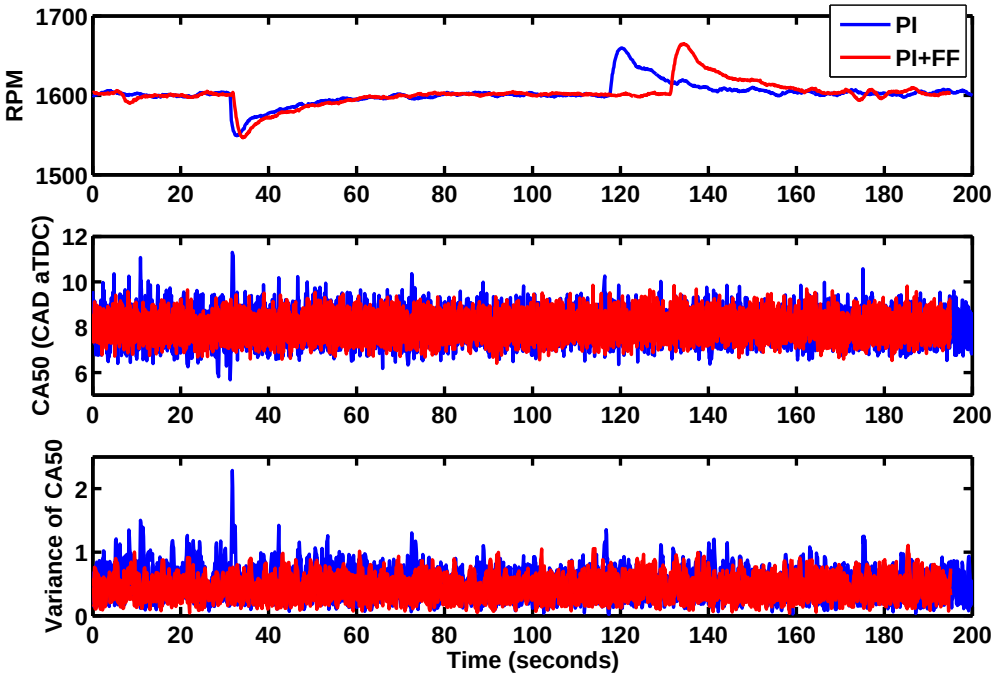

Figure 7.8: Load disturbance with (a) PI and (b) PI plus feedforward combustion timing controller. The plots present the RPM, tracking of the CA50 setpoint = 8 CAD ATDC, and the standard deviation of combustion timing during load disturbance.

7.3 Conclusions

Extremum seeking tuning is an effective method to tune PI, PI plus feedforward, and PID controllers and does so in a timely fashion. The PI plus feedforward controller provides good setpoint response in addition to disturbance rejection when compared with a PI controller. Gain scheduling is needed for HCCI controllers; extremum seeking can effectively populate the controller parameters for gain scheduling to span the loads and speeds that define an engine's operating range.

This chapter is in part a reprint of the material as it appears in
N. J. Killingsworth, S. M. Aceves, D. L. Flowers, F. Espinosa-Loza, and M. Krstić, "HCCI engine combustion timing control: optimizing gains and fuel consumption via extremum seeking," submitted to *IEEE Transactions on Control Systems Technology*, 2007.

Chapter 8

Conclusions and Future Work

8.1 Conclusions

HCCI engines are a promising technology that can help reduce some of our energy problems in the near term. However, control remains a challenge because HCCI engines do not have a direct means to control the combustion timing. Due to the inherent control difficulties of HCCI engines, their introduction for distributed power generation provides an intelligent first step for a future in automotive applications.

We have demonstrated the conversion process of a natural gas spark ignition engine genset to run HCCI mode in Chapter 2. A real-time control system has been developed, which controls the engine's combustion timing on a cylinder-by-cylinder basis using a novel dual intake manifold. Such a system is implementable in production and is a logical first step for HCCI engines.

Controls oriented models are necessary to help elucidate the system dynamics and to be used in the derivation of control laws. Such a model of HCCI engine combustion is developed in Chapter 3. The complexity of the model is kept low to allow the use of this model in the development of feedforward control algorithms. This simplicity is achieved through the use of an ignition line that is a function of in-cylinder motored temperature and pressure to capture start of combustion. A feedforward controller based on this model is demonstrated on a zero dimensional model of an HCCI engine incorporating detailed chemical kinetics and shows promise. This model is valid for fuels with little low temperature heat release and is demonstrated for both a natural gas and high-octane gasoline fueled HCCI engine.

A non-model based method of speeding up the engine mapping process is demonstrated in Chapter 5 using extremum seeking. Specifically, we experimentally show the use of ES to minimize the fuel consumption of an HCCI engine by determining the optimal combustion timing.

An online model based method of tuning PID controller gains using extremum seeking is presented in Chapter 6. This tuning method is demonstrated on a series of four process models and compared to three widely used PID tuning methods. Extremum seeking tuning is found to yield controllers that provide similar if not better performance than the other tuning methods. This method is demonstrated experimentally to tune the combustion timing controller of an HCCI engine in Chapter 7. Moreover, ES is used to tune a PI controller plus a constant feedforward term for improved setpoint response. ES proves to be a quick means to determine

optimal PID parameters while the engine is running. PID controllers are widely used across many industries, thus this tuning method has applicability to many processes and industries.

8.2 Future Work

Although the work presented in this thesis has made important steps towards achieving the ultimate goal of the use of HCCI engines in automobiles there is still much work to be done to make this a reality. I believe the most important next step regarding this work is to demonstrate the model based controller presented in Chapter 3 on an experimental HCCI engine. The model based controller performed well on a zero-dimension simulation of the HCCI engine but there are many processes that occur in practice that the model does not address. Such a controller holds the promise of enabling HCCI engines to operated in the transient conditions required of automotive applications.

Furthermore, this HCCI engine model can be extended to Diesel like fuels, which exhibit low temperature heat release. Some means of predicting timing and the amount of energy released in the first low temperature reaction would be needed. The model from Chapter 3 could also likely be adapted to capture spark assisted HCCI engine combustion. Heat release due to flame propagation would need to be included and the ignition line could be used to predict the point of autoignition of the end gas. This model could therefore also be used to predict

knock in conventional spark ignition engine applications. Another extension that could be made to the model is to include the effects of a variable valve timing (VVT) system, such that the effective compression ratio and the amount residual gases trapped are accounted for.

Another need is to incorporate emissions constraints into the setpoint tuning work in Chapter 5. Real-time measurements of NO_x, CO, and UHC could be added to the cost function $J(\theta)$ directly or a Lagrangian multiplier approach could be used, such that if a particular emission exceeds its limit its weight within the cost function is increased until the emissions levels are brought below requirements. Including emissions into the optimization process reduces the degrees of freedom making the fuel minimization process more difficult to achieve.

In both Chapters 6 and 7 the extremum seeking PID tuning scheme optimized the setpoint response of the controller. However, ES PID tuning can be setup to emphasize other performance attributes of the controller while tuning, such as disturbance rejection. The performance of HCCI engine combustion timing controller during step changes in load while holding constant combustion timing could be used to tune the controller for disturbance rejection. This scheme would require the ability to computer control the load such that repeatable conditions occur.

Appendix A

Single-Zone Combustion Model

In this appendix a single-zone combustion model with detailed chemical kinetics (CK) is presented. Because HCCI engine combustion is governed by the chemical reactions taking place in the engine combustion chamber this type of model has been found to do a good job of predicting start of combustion. The chemical kinetics based engine model treats the in-cylinder gas mixture as perfectly homogenous, such that all thermodynamic properties, such as temperature, pressure, and species concentration are independent of location within the cylinder. This type of model only takes into account the bulk gas in the central core of the combustion chamber and does not account for the volume of gas in the crevices and the boundary layer of the combustion chamber. Hydrocarbons and carbon monoxide are known to evolve from the boundary later and crevices, thus this type of model is not useful for predicting emissions of hydrocarbons and carbon monoxide. Nevertheless, single-zone chemical kinetics based engine models have been found to provide a

good estimate of the start of combustion, [3], with minimal computational time.

This model consists of solving the conservation equations for the individual species mass fractions Y_i and conservation of energy

$$\frac{dY_i}{dt} = \frac{\omega_i M_i}{\rho} \quad i = 1, \dots N_s, \tag{A.1}$$

$$\rho V c_v \frac{dT}{dt} = -p\frac{dV}{dt} - \sum_{i=1}^{N_s} (\omega_i M_i u_i) + \dot{Q}_{ht}, \tag{A.2}$$

where ω_i is the species molar production term, M_i is the molecular mass, and u_i is the specific internal energy of species i. N_s is the total number of species in the mixture, ρ is the mixture density, c_v is the specific heat at constant volume, T is the temperature, and p is the pressure. The cylinder volume is found from the slider-crank equation [33],

$$V(\theta) = V_c + \frac{\pi B^2}{4}\left(l + a - a\cos\theta - \sqrt{l^2 - (a\sin\theta)^2}\right). \tag{A.3}$$

The parameters for the slider-crank equation can be found in Table 2.1.

Heat transfer to the walls is included as

$$\dot{Q}_{ht} = h_c A\left(T - T_w\right). \tag{A.4}$$

where A is the cylinder surface area, which changes with crank angle and T_w is the cylinder wall temperature. The heat transfer coefficient h_c is found using Woschni's correlation [33]

$$h_c = 129.8 B^{-0.2} P^{0.8} T^{-0.55} w^{0.8}. \tag{A.5}$$

The average gas velocity is defined as,

$$w = C_1 S_p + C_2 \frac{V_d T_{ref}}{P_{ref} V_{ref}}(P - P_{mot}), \tag{A.6}$$

where V_d is the displaced cylinder volume, T_{ref}, p_{ref}, and V_{ref} are the temperature, pressure and volume of the working fluid at the reference state, respectively, usually corresponding to the inlet conditions. S_p is the mean piston speed, and C_1 and C_2 are constants dependent on the stroke of the engine. The in-cylinder pressure p is found using the using the ideal gas law. The motored pressure p_{mot} is determined for a cycle where chemical reactions are "frozen," that is, not allowed to occur. The Cantera software package [27] is used to determine the species' molar production terms, defined as

$$\omega_i = \sum_{j=1}^{N_f} \left(\upsilon_{ij}^{''} - \upsilon_{ij}^{'} \right) q_j, \tag{A.7}$$

$$q_j = k_{fj}(T) \prod_{i=1}^{N_s} \left(\rho \frac{Y_i}{M_i} \right)^{\upsilon_{ij}^{'}} - k_{rj}(T) \prod_{i=1}^{N_s} \left(\rho \frac{Y_i}{M_i} \right)^{\upsilon_{ij}^{''}}, \tag{A.8}$$

where j is the index of the chemical reaction

$$\sum_{i=1}^{N_s} \upsilon_{ij}^{'} X_i \Leftrightarrow \sum_{i=1}^{N_s} \upsilon_{ij}^{''} X_i. \tag{A.9}$$

$\upsilon_{ij}^{'}$ and $\upsilon_{ij}^{''}$ are the stoichiometric coefficients for the forward and backward stages, respectively, q_j is the rate-of-progress variable for the j^{th} reaction and X_i is the chemical symbol for species i. Parameters $k_{fj}(T)$ and $k_{rj}(T)$ are the reaction rate coefficients determined using the Arrehenius chemical kinetic rate expression

$$k_j(T) = A_i T^{\beta_j} e^{\frac{-E_j}{R_u T}}, \tag{A.10}$$

where A_j is the pre-exponential factor, β_j is the temperature exponent, E_j is the activation energy for the j^{th} reaction. These parameters are defined by the chemical mechanism used, such as in [21]. R_u is the universal gas constant.

Bibliography

[1] S. M. Aceves, D. L. Flowers, J. Martinez-Frias, F. Espinosa-Loza, M. Christensen, B. Johansson, and R. P. Hessel. Analysis of the effect of geometry-generated turbulence on HCCI combustion by multi-zone modeling. *SAE Paper 2005-01-2134*, 2005.

[2] S. M. Aceves, D. L. Flowers, J. Martinez-Frias, F. Espinosa-Loza, W. J. Pitz, and R. Dibble. Fuel and additive characterization for HCCI combustion. *SAE Paper 2003-01-1814*, 2003.

[3] S. M. Aceves, D. L. Flowers, J. Martinez-Frias, J. R. Smith, R. Dibble, M. Au, and J. Girard. HCCI combustion: analysis and experiments. *SAE Paper 2001-01-2077*, 2001.

[4] E. I. Administration. http://www.eia.doe.gov/, 2006.

[5] F. Agrell, H. E. Ångstrom, B. Eriksson, J. Wikander, and J. Linderyd. Integrated simulation and engine test of closed-loop HCCI control by aid of variable valve timings. *SAE Paper 2003-01-0748*, 2003.

[6] F. Agrell, H. E. Ångstrom, B. Eriksson, J. Wikander, and J. Linderyd. Control of HCCI during transients by aid of variable valve timings through the use of model based non-linear compensation. *SAE Paper 2005-01-0131*, 2005.

[7] K. Ariyur and M. Krstic. *Real-Time Optimization by Extremum Seeking Feedback*. Wiley-Interscience, Hoboken, N.J, 2003.

[8] E.-W. Bai, L.-C. Fu, and S. Sastry. Averaging analysis for discrete time and sampled data adaptive systems. *IEEE Transactions on Circuits and Systems*, 35:137–148, 1988.

[9] A. Banaszuk, S. Narayanan, and Y. Zhang. Adaptive control of flow separation in a planar diffuser. In *41st Aerospace Sciences Meeting & Exhibit*, Reno, NV, 2003.

[10] J. Bengtsson, M. Gäfvert, and P. Strandh. Modeling of HCCI engine combustion for control analysis. In *Conference in Decision and Control (CDC 2004)*, Bahamas, Jan. 2004.

[11] J. Bengtsson, P. Strandh, R. Johansson, P. Tunestål, and B. Johansson. Closed-loop combustion control of homogeneous charge compression ignition (HCCI) engine dynamics. *International Journal of Adaptive Control and Signal Processing*, 18:167–179, Jan. 2004.

[12] J. Bengtsson, P. Strandh, R. Johansson, P. Tunestål, and B. Johansson. Multi-output control of a heavy duty HCCI engine using variable valve actuation and model predictive control. *SAE Paper 2006-01-0873*, Apr. 2006.

[13] P. F. Blackman. Extremum-seeking regulators. In J. H. Westcott, editor, *An Exposition of Adaptive Control*. The Macmillan Company, New York, NY, 1962.

[14] M. Canova, R. Garcin, S. Midlam-Mohler, Y. Guezeneec, and G. Rizzoni. A control – oriented model of combustion process in a HCCI diesel engine. In *Procedings of American Control Conference*, pages 4446–4451, Portland, OR, 2005.

[15] C. J. Chiang and A. G. Stefanopoulou. Control of thermal ignition in gasoline engines. In *Procedings of American Control Conference*, pages 3847–3852, Portland, OR, 2005.

[16] C. J. Chiang and A. G. Stefanopoulou. Stability analysis in homogeneous charge compression ignition HCCI engines with high dilution. *IEEE Transactions on Control Systems Technology*, 15(2):209–219, 2007.

[17] P. I. Chinaev. In P. I. Chinaev, editor, *Self-Tuning Systems Handbook*. Naukova Dumka, Kiev, 1969.

[18] J. Y. Choi, M. Krstic, K. B. Ariyur, and J. S. Lee. Extremum seeking control for discrete-time systems. *IEEE Transactions on Automatic Control*, 47:318–323, 2002.

[19] M. Christensen and B. Johansson. Homogeneous charge compression ignition with water injection. *SAE Paper 1999-01-0182*, 1999.

[20] H. J. Curran. Private communication. National University of Ireland, Galway, 2006.

[21] H. J. Curran, P. Gaffuri, W. J. Pitz, and C. K. Westbrook. A comprehensive modeling study of iso-octane oxidation. *Combustion and Flame*, 129:253–280, 2002.

[22] J. E. Dec and M. Sjöberg. Isolating the effects of fuel chemistry on combustion phasing in an HCCI engine and the potential of fuel stratification for ignition control. *SAE Paper 2004-01-0557*, 2004.

[23] C. Draper and Y. Li. *Principles of Optimizing Control Systems*. ASME, New York, NY, 1954.

[24] O. Erlandsson. *Thermodynamic Simulation of HCCI Engine Systems*. PhD thesis, Department of Heat and Power Engineering, Lund Institute of Technology, Lund University, Sweden, 2002.

[25] A. A. Feldbaum. *Computers in Automatic Control Systems*. Fizmatgiz, Moscow, 1959.

[26] M. Gäfvert, K.-E. årzén, and L. M. Pedersen. Simple linear feedback and extremum seeking control of gdi engines. In *Procedings of Seoul 2000 FISITA World Automotive Congress*, Seoul, Korea, June 2000.

[27] D. Goodwin. An open-source, extensible software suite for cvd process simulation. In M. Allendorf, F. Maury, and F. Teyssandier, editors, *Proceedings of CVD XVI and EuroCVD Fourteen*, pages 155–162. Electrochemical Society, 2003.

[28] G. Haraldsson, J. Hyvönen, P. Tunestål, and B. Johansson. HCCI combustion phasing in a multi cylinder engine using variable compression ratio. *SAE Paper 2002-01-2858*, 2002.

[29] G. Haraldsson, J. Hyvönen, P. Tunestål, and B. Johansson. HCCI closed-loop combustion control using fast thermal management. *SAE Paper 2004-01-0943*, 2004.

[30] G. Haraldsson, J. Hyvönen, P. Tunestål, and B. Johansson. Transient control of a multi-cylinder HCCI engine during a drive cycle. *SAE Paper 2005-01-0153*, 2005.

[31] G. Haraldsson, P. Tunestål, B. Johansson, and J. Hyvönen. HCCI combustion phasing with closed-loop combustion control using variable compression ratio in a multi cylinder engine. *SAE Paper 2003-01-1830*, 2003.

[32] C. C. Hernández. HCCI timing control using iterative feedback tuning. Master's thesis, Department of Electrical Engineering, KTH, Stockholm, Sweden, 2006.

[33] J. B. Heywood. *Internal Combustion Engine Fundamentals*. McGraw-Hill, 1988.

[34] H. Hjalmarsson. Control of nonlinear systems using iterative feedback tuning: theory and applications. In *Proceedings of the American Control Conference*, pages 2083–2087, Philadelphia,PA, 1998.

[35] H. Hjalmarsson, M. Gevers, S. Gunnarsson, and O. Lequin. Iterative feedback tuning: theory and applications. *IEEE Control Systems Magazine*, 18(4):26–41, 1998.

[36] J. Hyvönen, G. Haraldsson, and B. Johansson. Balancing cylinder-to-cylinder variations in a multi-cylinder VCR-HCCI engine. *SAE Paper 2004-01-1897*, 2004.

[37] A. Isaksson and S. Graebe. Analytic pid parameter expressions for higher order systems. *Automatica*, 35(6):1121–1130, 1999.

[38] M. Jankovic and S. Magner. Optimization and scheduling for automotive powertrains. In *Procedings of American Control Conference*, pages 4054–4059, Boston,MA, 2004.

[39] M. Jun and M. Safonov. Automatic pid tuning: An application of unfalsified control. In *Proc. of IEEE International Symposium on CACSD*, pages 328–333, Hawaii, HI, 1999.

[40] N. J. Killingsworth and M. Krstić. PID tuning using extremum seeking: Online, model-free performance optimization. *IEEE Control Systems Magazine*, 26(1):70–79, 2006.

[41] A. A. Krasovskii. *Dynamics of Continuous Self-Tuning Systems*. Fizmatgiz, Moscow, 1963.

[42] M. Krstić and H.-H. Wang. Design and stability analysis of extremum seeking feedback for general nonlinear systems. *Automatica*, 36(2):595–601, 2000.

[43] M. Leblanc. Sur l'électrification des chemins de fer au moyen de courants alternatifs de fréquence élevée. *Revue Générale de l'Electricité*, 1922.

[44] O. Lequin, E. Bosmans, and T. Triest. Iterative feedback tuning of pid parameters: comparision with classical tuning rules. *Control Eng. Practice*, 11(9):1023–1033, 2003.

[45] O. Lequin, M. Gevers, and T. Triest. Optimizing the settling time with iterative feedback tuning. In *Proc. of the 14th IFAC world congress*, pages 433–437, Beijing, P.R. China, 1999.

[46] A. Leva. Pid autotuning algorithm based on relay feedback. In *IEEE Proc.-D Control Theory and Applications*, volume 140, pages 328–338, Beijing, P.R. China, 1993.

[47] Y. Li, M. A. Rotea, G. T.-C. Chiu, L. G. Mongeau, and I.-S. Paek. Extremum seeking control of a tunable thermoacoustic cooler. *IEEE Transactions on Control Systems Technology*, 13:527– 536, 2005.

[48] J. C. Livengood and P. C. Wu. Correlation of autoignition phenomena in internal combustion engines and rapid compression machine. In *Proceedings of the Fifth International Symposium on Combustion*, pages 347–356, Ottawa, Canada, 1955.

[49] J. Martinez-Frias, S. M. Aceves, D. L. Flowers, J. R. Smith, and R. Dibble. HCCI engine control by thermal management. *SAE Paper 2000-01-2869*, 2000.

[50] S. M. Meerkov. Asymptotic methods for investigating a class of forced states in extremal systems. *Automation and Remote Control*, 12:1916–1920, 1967.

[51] S. M. Meerkov. Asymptotic methods for investigating quasistationary states in continuous systems of automatic optimization. *Automation and Remote Control*, 11:1726–1743, 1967.

[52] S. M. Meerkov. Asymptotic methods for investigating stability of continuous systems of automatic optimization subjected to disturbance action. *Avtomatika i Telemekhanika*, 12:14–24, 1968.

[53] D. Montgomery. *Design and Analysis of Experiments*. John Wiley & Sons, NY, NY, 5th edition, 2001.

[54] M. Noguchi, Y. Tanaka, T. Tanaka, and Y. Takeuchi. A study on gasoline engine combustion by observation of intermediate reactive products during combustion. *SAE Paper 790840*, 1979.

[55] J. Olsson, O. Erlandsson, and B. Johansson. Experiments and simulation of a six-cylinder homogeneous charge compression ignition (HCCI) engine. *SAE Paper 2000-01-2867*, 2001.

[56] J. Olsson, P. Tunestål, and B. Johansson. Closed-loop control of an HCCI engine. *SAE Paper 2001-01-1031*, 2001.

[57] J. Olsson, P. Tunestål, B. Johansson, S. Fiveland, R. Agama, M. Willi, and D. Assanis. Compression ratio influence on maximum load of a natural gas fueled HCCI engine. *SAE Paper 2002-01-0111*, 2002.

[58] S. Onishi, S. H. Jo, K. Shoda, P. D. Jo, and S. Kato. Active thermo-atmosphere combustion (ATAC)- a new combustion process for internal combustion engines. *SAE Paper 790501*, 1979.

[59] K. Peterson and A. Stefanopoulou. Extremum seeking control for soft landing of an electromechanical valve actuator. *Automatica*, 40:1063–1069, 2004.

[60] D. Popovic, M. Jankovic, S. Magner, and A. Teel. Extremum seeking methods for optimization of variable cam timing engine operation. *IEEE Transactions on Control Systems Technology*, 14(3):398–407, May 2006.

[61] K. Åström and T. Hägglund. Automatic tuning of simple regulators with specifications on phase and amplitude margins. *Automatica*, 20(5):645–651, 1984.

[62] K. Åström and T. Hägglund. *PID Controllers: Theory, Design and Tuning*. Instrument Society of America, Research Triangle Park, NC, second edition, 1995.

[63] K. Åström, T. Hägglund, C. Hang, and W. Ho. Automatic tuning and adaptation for pid controllers – a survey. *Control Engineering Practice*, 1(4):26–41, 1993.

[64] K. Åström and B. Wittenmark. *Computer Controlled Sytems: Theory and Design*. Prentice–Hall, Upper Saddle River, NJ, third edition, 1997.

[65] D. J. Rausen, A. G. Stefanopoulou, J. M. Kang, J. A. Eng, and T. W. Kuo. A mean-value model for control of homogenous charge compression ignition (HCCI) engines. *Journal of Dynamic Systems, Measurement, and Control*, 127(3):355–362, 2005.

[66] D. Rivera and M. Morari. Control relevant model reduction problems for siso h_2, h_∞, and μ-controller synthesis. *International Journal of Control*, 46(2):505–527, 1987.

[67] M. A. Rotea. Analysis of multivariable extremum seeking algorithms. In *Procedings of American Control Conference*, pages 433–437, Chicago, IL, 2000.

[68] M. Saeki. Unfalsified control approach to parameter space design of pid controllers. In *Proc. of the 42nd IEEE Conference on Decision and Control*, pages 786–791, Maui, HI, 2003.

[69] M. Saeki, A. Takahashi, O. Hamada, and N. Wada. Unfalsified parameter space design of pid controllers for nonlinear plants. In *Proc. of IEEE International Symposium on CACSD*, pages 1521–1526, Taipei, Taiwan, 2004.

[70] P. G. Scotson and P. E. Wellstead. Self-tuning optimization of spark ignition automotive engines. *IEEE Control Systems Magazine*, pages 94–101, April 1990.

[71] G. M. Shaver and J. C. Gerdes. Cycle-to-cycle control of HCCI engines. In *Proceedings of the 2003 ASME International Mechanical Engineering Congress and Exposition*, Washington, DC, 2003. IMECE2003-41966.

[72] G. M. Shaver, J. C. Gerdes, P. Jain, P. A. Caton, and C. F. Edwards. Modeling for control of HCCI engines. In *Procedings of American Control Conference*, pages 749–754, Denver, CO, 2003.

[73] G. M. Shaver, J. C. Gerdes, and M. Roelle. Physics-based closed-loop control of phasing, peak pressure, and work output in HCCI engines utilizing variable valve actuation. In *Procedings of American Control Conference*, pages 150–155, Boston, MA, 2004.

[74] G. M. Shaver, J. C. Gerdes, M. J. Roelle, P. A. Caton, and C. F. Edwards. Dynamic modeling of residual-affected homogenous charge compression ignition engines with variable valve actuation. *Journal of Dynamic Systems, Measurement, and Control*, 127(3):374–381, 2005.

[75] G. M. Shaver, M. Roelle, and J. C. Gerdes. Decoupled control of combustion timing and work output in residual-affected HCCI engines. In *Procedings of American Control Conference*, pages 3871–3876, Portland, OR, 2005.

[76] M. Sjöberg and J. Dec. An investigation of the relationship between measured intake temperature bdc temperature and combustion phasing for premixed and DI HCCI engines. *SAE Paper 2004-01-1900*, 2004.

[77] J. S. Souder. *Closed-Loop Control of a Multi-Cylinder HCCI Engine*. PhD thesis, University of California, Berkeley, 2004.

[78] J. S. Souder, P. Mehresh, J. K. Hedrick, and R. W. Dibble. A multi-cylinder HCCI engine model for control. In *Proceedings of the 2004 ASME International Mechanical Engineering Congress and Exposition*, Anaheim, CA, 2004. IMECE2004-61966.

[79] J. Sternby. A review of extremum control–an area for adaptive control? Technical Report WA2-A, Department of Automatic Control, Lund Institute of Technology, April 1979.

[80] P. Strandh, J. Bengtsson, R. Johansson, P. Tunestål, and B. Johansson. Cycle-to-cycle control of a dual-fuel HCCI engine. *SAE paper 2004-01-0941*, 2004.

[81] P. Strandh, M. Christensen, J. Bengtsson, R. Johansson, A. Vressner, P. Tunestål, and B. Johansson. Ion current sensing for HCCI combustion feedback. *SAE Paper 2003-01-3216*, 2003.

[82] F. Sun, X. Chen, D. S.-K. Ting, and A. Sobiesiak. Modeling operation of HCCI engines fueled with ethanol. In *Procedings of American Control Conference*, pages 1003–1009, Portland, OR, 2005.

[83] Y. Tan, D. Nešić, and I. Mareels. On non-local stability properties of extremum seeking control. *Automatica*, 42(6):889–903, 2006.

[84] H. S. Tsien. *Engineering Cybernetics*. McGraw-Hill, New York, NY, 1954.

[85] P. A. Tunestal. *The Use of Cylinder Pressure for Estimation of the In-Cylinder Air/Fuel Ratio of an Internal Combustion Engine*. PhD thesis, Department of Mechanical Engineering, University of California, Berkeley, 2000.

[86] A. Voda and I. Landau. A method for the auto-calibration of pid controllers. *Automatica*, 31(1):41–53, 1995.

[87] G. C. Walsh. On the application of multi-parameter extremum seeking control. In *Procedings of American Control Conference*, pages 411–415, Chicago, IL, 2000.

[88] D. J. Wilde. *Optimum Seeking Methods*. Prentice Hall, Englewood Cliffs, NJ, 1964.

[89] G. M. R. L. Withrow. Motion pictures of engine flames correlated with pressure cards. *SAE Transactions*, 42(5):185–204, 1938.

[90] J. Yang, T. Culp, and T. Kenney. Development of a gasoline engine system using HCCI technology - the concept and test results. *SAE Paper 2002-01-2832*, 2002.

[91] X. T. Zhang, D. M. Dawson, W. Dixon, and B. Xian. Extremum seeking nonlinear controllers for a human exercise machine. In *Procedings of the 2004 IEEE. Conference on Decision and Control*, pages 3950–3955, Atlantis, Bahamas, 2004.

[92] J. Zhao, T. Asmus, D. Assanis, J. Dec, J. Eng, and P. Najt, editors. *Homogeneous Charge Compression Ignition (HCCI) Engines: Key Research and Development Issues*, volume SAE PT-94. SAE International, 2003.